

Aus dem  
LIFE-Zentrum  
Labor für Tumorummunologie  
Labor der Ludwig-Maximilians-Universität München



**Differential expression of CSCs biomarkers in renal cell carcinoma stem cells after a combined treatment with phytochemicals and immune checkpoint inhibitors**

Dissertation  
zum Erwerb des Doctor of Philosophy (Ph.D.) an der Medizinischen Fakultät der  
Ludwig-Maximilians-Universität München

vorgelegt von  
Chen Lyu

aus  
Jilin / China

Jahr  
2024

---

Mit Genehmigung der Medizinischen Fakultät der  
Ludwig-Maximilians-Universität München

Erstes Gutachten: Priv. Doz. Dr. Heike Pohla  
Zweites Gutachten: Prof. Dr. Alexander Buchner  
Drittes Gutachten: Prof. Dr. Michael Staehler  
Viertes Gutachten: Prof. Dr. Volker Vielhauer

Dekan: Prof. Dr. med. Thomas Gudermann

Tag der mündlichen Prüfung: 11.03.2024

# Affidavit



## Affidavit

LYU, Chen

\_\_\_\_\_  
Surname, first name

\_\_\_\_\_  
Street

\_\_\_\_\_  
Zip code, town, country

I hereby declare, that the submitted thesis entitled:

Differential expression of CSCs biomarkers in renal cell carcinoma stem cells after a combined treatment with phytochemicals and immune checkpoint inhibitors

.....

is my own work. I have only used the sources indicated and have not made unauthorised use of services of a third party. Where the work of others has been quoted or reproduced, the source is always given.

I further declare that the dissertation presented here has not been submitted in the same or similar form to any other institution for the purpose of obtaining an academic degree.

03.07.2024 , Planegg

place, date

Chen LYU

*Signature doctoral candidate*

# Confirmation of congruency



LUDWIG-  
MAXIMILIANS-  
UNIVERSITÄT  
MÜNCHEN

Promotionsbüro  
Medizinische Fakultät



**Confirmation of congruency between printed and electronic version of the doctoral thesis**

LYU, Chen

\_\_\_\_\_  
Surname, first name

\_\_\_\_\_  
Street

\_\_\_\_\_  
Zip code, town, country

I hereby declare, that the submitted thesis entitled:

Differential expression of CSCs biomarkers in renal cell carcinoma stem cells after a combined treatment with phytochemicals and immune checkpoint inhibitors

.....

is congruent with the printed version both in content and format.

03.07.2024 , Planegg  
place, date

Chen LYU

*Signature doctoral candidate*



# Table of content

<b>Affidavit</b> .....	<b>3</b>
<b>Confirmation of congruency</b> .....	<b>4</b>
<b>Table of content</b> .....	<b>5</b>
<b>List of abbreviations</b> .....	<b>6</b>
<b>List of publications</b> .....	<b>9</b>
<b>Your contribution to the publications</b> .....	<b>10</b>
1.1 Contribution to paper I .....	10
1.2 Contribution to paper II .....	10
1.3 Contribution to paper III .....	10
<b>2. Introductory summary</b> .....	<b>11</b>
2.1 Renal cell carcinoma (RCC) .....	11
2.1.1 RCC treatment strategy .....	12
2.1.2 Immune checkpoint inhibitors (ICIs) and RCC .....	13
2.2 Cancer stem cells (CSCs) .....	15
2.2.1 CSCs and drug resistance .....	15
2.2.2 CSCs markers .....	16
2.3 Phytochemicals (PTCs) .....	22
2.3.1 EGCG .....	23
2.3.2 Shikonin .....	24
2.3.3 Apigenin .....	25
2.3.4 Wogonin .....	27
<b>3. Paper I</b> .....	<b>30</b>
<b>4. Paper II</b> .....	<b>57</b>
<b>5. Paper III</b> .....	<b>84</b>
<b>References</b> .....	<b>108</b>
<b>Acknowledgements</b> .....	<b>116</b>

## LIST OF ABBREVIATIONS

### List of abbreviations

2D	Two-dimensional
3D	Three-dimensional
7-AAD	7-aminoactinomycin D
ABC	ATP-binding cassette
ABCG2	ATP binding cassette subfamily G member 2
ADP	Adenosine diphosphate
ALDH1	Aldehyde dehydrogenase 1
APCs	Antigen-presenting cells
ATP	Adenosine triphosphate
bFGF	Basic fibroblast growth factor
ccRCC	clear cell renal cell carcinoma
CDC6	Cell division cycle 6
CDK4	Cyclin-dependent kinase 4
COX-2	Cyclooxygenase 2
CSCs	Cancer stem cells
CTLA-4	Cytotoxic T-lymphocyte-associated antigen 4
CXCR4	C-X-C Motif Chemokine Receptor 4
EGCG	Epigallocatechin-3-gallate
EGF	Epidermal growth factor
EMT	Epithelial-to-mesenchymal transition
ERK	Extracellular-signal-regulated kinase
EZH2	Enhancer of Zeste 2
HIF-1 $\alpha$	Hypoxia-inducible factor-1 $\alpha$
HR	Hazard ratio
IC50	The half-maximal inhibitory concentration
ICAM-1	Intercellular adhesion molecule 1
ICIs	Immune checkpoint inhibitors
IFN- $\gamma$	Interferon-gamma
IL	Interleukins

## LIST OF ABBREVIATIONS

KIRC	Kidney renal clear cell carcinoma
MAPK	Mitogen activated protein kinase
MHC	Major histocompatibility complex
MLTC	Mixed lymphocyte tumor cell culture
MMP-2	Matrix metalloproteinase-2
mRNAsi	mRNA expression-based stemness index
mTOR	Mammalian target of rapamycin
NF- $\kappa$ B	Nuclear factor kappa-light-chain-enhancer of activated B cells
NO	Nitric oxide
Nrf2	Nuclear factor erythroid 2-related factor 2
NSCLC	Non-small cell lung cancer
ORR	Objective response rate
OS	Overall survival
PBMCs	Peripheral blood mononuclear cells
PBS	Phosphate-buffered saline
PD-L1	Programmed death ligand-1
PFS	Progression-free survival
PI3K	Phosphatidylinositol 3-kinase
PTCs	Phytochemicals
qRT-PCR	Quantitative real-time polymerase chain reaction
RCC	Renal cell carcinoma
ROS	Reactive oxygen species
STAT1	Signal transducer and activator of transcription 1
TCGA	The Cancer Genome Atlas
TCR	T cell receptor
TGF- $\beta$	Transforming growth factor beta
TH1	T helper 1
TICs	Tumor initiating cells
TILs	Tumor-infiltrating lymphocytes
TKIs	Tyrosine kinase inhibitors
TME	Tumor microenvironment

## LIST OF ABBREVIATIONS

TPA	Tetradecanoylphorbol-13-acetate
VCAM-1	Vascular cell adhesion molecule 1
VEGF	Vascular endothelial growth factor

## List of publications

### Publications related to the thesis:

1. **Lyu C**, Stadlbauer B, Wang L, Buchner A, Pohla H: Identification of a novel combination treatment strategy in clear cell renal cell carcinoma stem cells with shikonin and ipilimumab. *Front Immunol.* 2023, 14:1186388.
2. **Lyu C**, Wang L, Stadlbauer B, Noessner E, Buchner A, Pohla H: Identification of EZH2 as Cancer Stem Cell Marker in Clear Cell Renal Cell Carcinoma and the Anti-Tumor Effect of Epigallocatechin-3-Gallate (EGCG). *Cancers (Basel)* 2022, 14(17):4200.
3. **Lyu C**, Wang L, Stadlbauer B, Buchner A, Pohla H: A Pan-Cancer Landscape of ABCG2 across Human Cancers: Friend or Foe? *Int J Mol Sci.* 2022, 23(24):15955.

### Other publications:

1. Wang L, **Lyu C**, Stadlbauer B, Buchner A, Noessner E, Pohla H. Berbamine targets cancer stem cells and reverses cabazitaxel resistance via inhibiting IGF2BP1 and p-STAT3 in prostate cancer. *The Prostate* 2023, Oct 12.doi: 10.1002/pros.24632.
2. Werner M, **Lyu C**, Stadlbauer B, Schrader I, Buchner A, Stepp H, Sroka R, Pohla H: The role of Shikonin in improving 5-aminolevulinic acid-based photodynamic therapy and chemotherapy on glioblastoma stem cells. *Photodiagnosis Photodyn Ther* 2022, 39:102987.
3. Wang L, Liu Y, **Lyu C**, Buchner A, Pohla H: Diagnostic and Prognostic Role of miR-192 in Different Cancers: A Systematic Review and Meta-Analysis. *Biomed Res Int* 2021, 2021:8851035.
4. Wang L, Stadlbauer B, **Lyu C**, Buchner A, Pohla H: Shikonin enhances the antitumor effect of cabazitaxel in prostate cancer stem cells and reverses cabazitaxel resistance by inhibiting ABCG2 and ALDH3A1. *Am J Cancer Res* 2020, 10:3784-3800.
5. **Lyu C**, Liu S, Xia J, et al. The mechanism of dietary protein modulates bone metabolism via alterations in members of the GH/IGF axis. *Current Protein and Peptide Science* 2019, 20(2):115-124.
6. **Lyu C**, Li W, Liu S, et al. Systematic review on the efficacy and safety of immune checkpoint inhibition in renal cell carcinoma. *Future oncology* 2018, 14(21):2207-2221.

## Your contribution to the publications

### 1.1 Contribution to paper I

Identification of a novel combination treatment strategy in clear cell renal cell carcinoma stem cells with shikonin and ipilimumab.

Chen Lyu was responsible for performing and analyzing the experiments, organizing the database, conducting statistical analysis, drafting the manuscript, and addressing the questions raised by the journal reviewers.

### 1.2 Contribution to paper II

Identification of EZH2 as Cancer Stem Cell Marker in Clear Cell Renal Cell Carcinoma and the Anti-Tumor Effect of Epigallocatechin-3-Gallate (EGCG).

Chen Lyu was responsible for designing the study, performing and analyzing the experiments, organizing the databases, conducting the statistical analyses, drafting the manuscript, and addressing the reviewers' questions.

### 1.3 Contribution to paper III

A Pan-Cancer Landscape of ABCG2 across Human Cancers: Friend or Foe?

With the exploration of the knowledge of *ABCG2* genes in our project, its intriguing mechanisms have heightened our interest in studying not limited in RCC. Thus, Chen Lyu designed this study, organized the databases, and performed the experiments and statistical analyses. Also, drafting the manuscript and responding to the reviewers' questions were performed by Chen Lyu.

## 2. **Introductory Summary**

Renal cell carcinoma (RCC) is a kind of kidney tumor that is distinguished by its tendency to stay undetected until late stages, resulting in a large rise in fatality rates. Immune checkpoint inhibitors have demonstrated potential in treating advanced RCC, either replacing or supplementing therapies with tyrosine kinase inhibitors (TKIs), with objective response rates varying from 42% to 71% for each combination regimen [1]. Not all patients respond to these therapies, only a few people with the median progression-free survival (PFS) varying from 11.6 to 15.4 months, followed by the therapy-resistance, which highlights the need for novel treatment strategies [2].

Recent studies have focused on the function of cancer stem cells (CSCs) in the development and progression of RCC, as these cells are thought to be resistant to traditional cancer therapies and contribute to tumor relapse. CSCs are a small subset of cells seen within malignancies that possess self-renewal and differentiation capabilities and are successful of initiating and sustaining tumor growth. CSCs have been recognized in more than a few cancers, together with RCC, and are related with in favorable outcomes. Therefore, figuring out CSC-specific biomarkers and growing treatments focused on these cells is necessary for enhancing affected person outcomes.

One possible method for concentrated on CSCs in RCC is via the use of phytochemicals (PTCs), which are naturally happening compounds discovered in plants. PTCs have been proven to have anti-cancer properties, and some have been proven to mainly target CSCs. Therefore, there is developing amount of research in creating phytochemical-based treatment strategies for RCC that especially target CSCs.

The goal of this thesis was to uncover new phytochemicals that originate from conventional herbs that target RCC CSCs, and combination with other treatments such as immune checkpoint inhibitor for enhancing the efficacy of present treatment strategies and creating new remedies for RCC. Various techniques, including viability, proliferation, migration, invasion, and apoptosis assays, have been utilized to identify promising candidate phytochemicals. Because of its exceptional ability to efficiently suppress CSCs, shikonin was chosen as the most promising and favorable partner for combination treatment with immune checkpoint inhibitors. Then, potential mechanisms of shikonin and ipilimumab involved in regulating T cell subpopulations and potential immunotherapeutic targets were investigated. Furthermore, figuring out biomarkers such as VCMA1 that predict response to immune checkpoint inhibitor remedy will permit for the improvement of personalized therapy plans for RCC patients.

### 2.1 **Renal cell carcinoma (RCC)**

Renal cell carcinoma (RCC) is the most common kidney cancer, with an approximately 79,000 new cases and 13,920 deaths in the United States in 2022 [3, 4]. In addition, the clinical situation of patients with RCC can be challenging due to the asymptomatic nature of early-stage RCC. Most cases are detected incidentally on imaging studies performed for other reasons, such as abdominal pain or trauma. Patients with advanced disease have mostly symptoms such as flank pain, hematuria, and weight loss. RCC patients diagnosed at early stages would have a

more favorable prognosis compared to those presenting with advanced-stage RCC. The classification of RCC is defined by the dimensions and specific site of the primary tumor as well as the presence and extent of metastasis. In T1, the tumor is limited to the kidney and measures 7 centimeters or smaller. Then, T2 indicates a tumor larger than 7 centimeters that is still confined to the kidney. Moreover, in T3, cancer has migrated to neighboring lymph nodes, the renal vein or vena cava, the fat encompassing the kidney, or the membrane of fatty tissue around the tissues that collect urine. In some cases, the primary tumor can be of any size. Finally, in T4, the cancer has expanded beyond the layer of fatty tissue around the kidney and has entered neighboring tissues, indicating that it has evolved to an advanced and severe level. This might include the adrenal glands, located above the kidney, as well as neighboring lymph nodes. Furthermore, cancer cells have the ability to reach distant areas inside the body, harming key organs such as bones, liver, lungs, and even the brain [4] (Figure 1A). Clear cell renal cell carcinoma (ccRCC), the most prevalent subgroup of renal cell carcinoma (RCC), accounts for 70-85% of cases and demonstrates a wide range of clinical characteristics. These might range from sluggish and painless development to aggressive and widespread metastases. Almost 30% of patients with ccRCC develop metastases during their follow-up period [5, 6].

### **2.1.1 RCC treatment strategy**

The selection of a treatment strategy for advanced RCC takes into account diverse factors, including the tumor's stage and molecular attributes, the patient's overall health, and the range of available therapeutic options [7]. At the present, the preferred form of care for patients with localized RCC is surgical resection, with partial nephrectomy being the preferred approach for tumors measuring  $\leq 4$  cm, and radical nephrectomy for tumors  $>4$  cm in size or tumors that involve the renal sinus or perinephric fat [8]. Data from large retrospective studies indicate that partial nephrectomy has been correlated with better overall survival than radical nephrectomy in individuals with tumors  $\leq 4$  cm in size [9]. A comprehensive meta-analysis of data pooled from 14 independent studies, including a substantial cohort of 40,768 patients, has revealed that partial nephrectomy was connected to lower risk of overall mortality and cardiovascular events compared to radical nephrectomy, particularly in patients with pre-existing chronic kidney disease or cardiovascular disease [10]. Furthermore, for patients with locally advanced or metastatic RCC, systemic therapy is the preferred treatment approach. Traditionally, cytokine therapy with interleukin 2 (IL-2) and interferon-gamma (IFN  $-\gamma$ ) was the mainstay of systemic treatment for RCC. However, the development of targeted therapies that inhibit the vascular endothelial growth factor (VEGF) pathway, a critical signaling cascade involved in angiogenesis and tumor growth regulation, can be effectively achieved through the use of tyrosine kinase inhibitors (TKIs) like sunitinib, pazopanib, and axitinib, and agents that inhibit the mammalian target of rapamycin (mTOR) pathway, such as everolimus and temsirolimus. Furthermore, immunotherapies have revolutionized the treatment of advanced RCC [11, 12] (Figure 1B).

However, the efficacy of these treatment modalities has been limited to advanced RCC, where the disease is often refractory to standard therapy, resulting in a poor prognosis. For instance, only 10-20% advanced RCC patients' response to chemotherapy, and the median survival time is about 6-9 months [13]. Similarly, the response rates to TKIs such as sorafenib, range from 25% to 40% [14]. Moreover, the duration of response to these agents is limited, with most patients experiencing disease progression within a year of treatment initiation [15]. The limited efficacy of traditional treatments for advanced RCC has underscored the need for new therapeutic approaches.



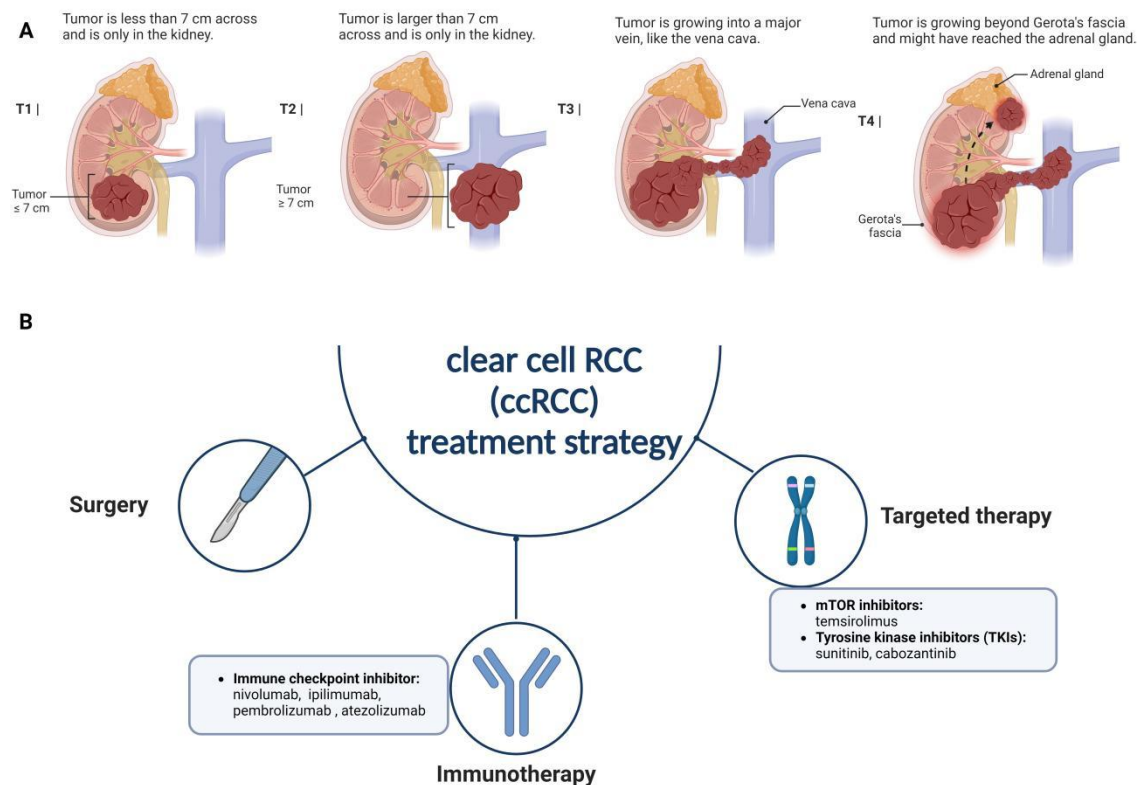
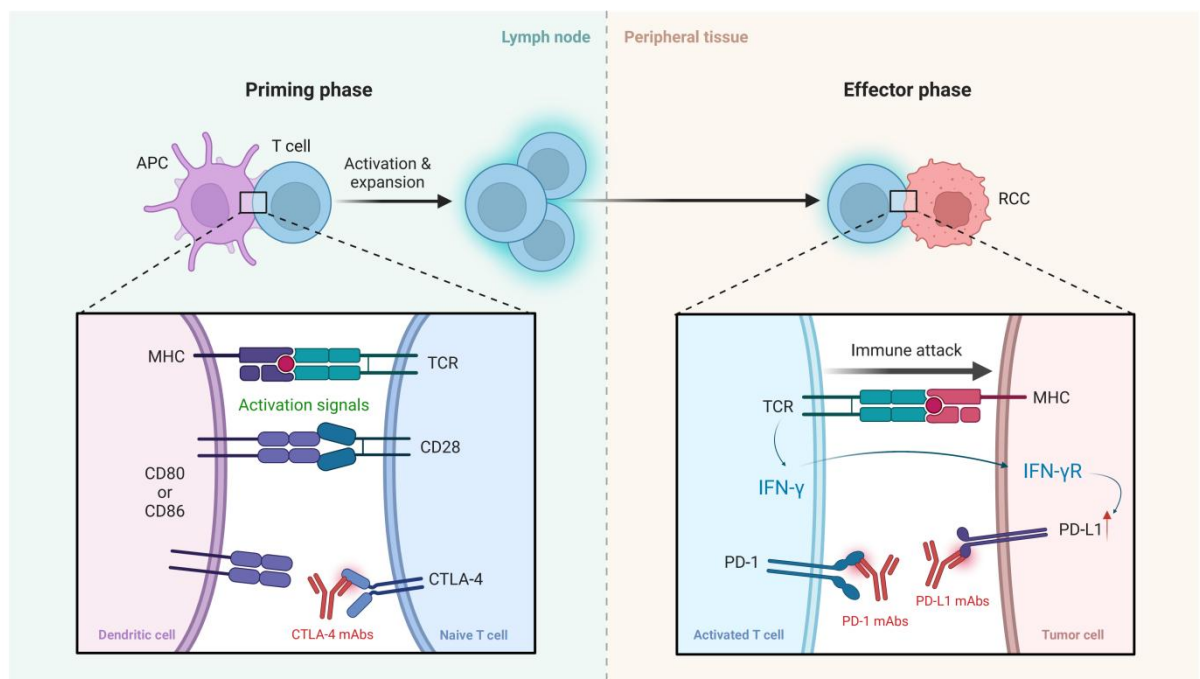


**Figure 1. RCC stage and treatment strategy.** A. The RCC status during T1 and T2 has remained confined within the kidney. Cancers in T3 have either infiltrated into surrounding major veins or nearby lymph nodes. RCC in T4, often known as advanced or metastatic cancer, indicates that the illness has progressed beyond the kidney and into other parts of the body. This might encompass distant lymph nodes or other organs, indicating a more serious and extensive disease. B. RCC treatment strategy including category of treatments and first to third line approved drugs for RCC (Figure created with BioRender.com).

### 2.1.2 Immune checkpoint inhibitors (ICIs) and RCC

The treatment landscape for metastatic renal cell carcinoma (RCC) has witnessed a notable paradigm shift in recent years, attributed to the availability of immune checkpoint inhibitors (ICIs) as therapeutic alternative. ICIs have been shown to be effective either as monotherapy or in combination with TKIs for the treatment of metastatic RCC [16]. Mechanistically, T cell priming is a critical and complicated phase in the adaptive immune response to the malignancies. The identification of processed tumor antigens, which are given to T cells by specialized antigen-presenting cells (APCs) that consist of monocytes and dendritic cells. The interaction between the T cell receptor (TCR) and a sophisticated assembly of major histocompatibility complex (MHC) molecules as well as tumor-derived peptide antigens results in this recognition. The recognition of these antigens by T cells in lymphoid tissues sets off a chain of events that culminates in the activation of both CD4<sup>+</sup> and CD8<sup>+</sup> T cells. Both CD4<sup>+</sup> and CD8<sup>+</sup> T cells require co-stimulation to become fully activated, which facilitates the interaction of CD28 on T cells with CD80 or CD86 on APCs. Furthermore, cytotoxic T-lymphocyte-associated antigen 4 (CTLA-4) is a co-inhibitory receptor presented on T cells that governs the modulation of CD4<sup>+</sup> T cell initiation and provides assistance to CD8<sup>+</sup> T cell initiation within lymphoid tissue. Within hours to days of activation, T cells initiate the secretion of the co-inhibitory receptor known as

programmed cell death 1 (PD-1), releasing it into their surrounding environment. In the tumor microenvironment (TME), CD4+ T helper 1 cells as well as CD8+ T cells produce IFN- $\gamma$ , which activates tumoricidal functions of macrophages and promotes antigen presentation by tumor cells. However, IFN- $\gamma$  also causes tumor cells and macrophages to express the immunological checkpoint protein programmed death ligand-1 (PD-L1), which binds to PD-1 on T cells as well as inhibits their activity. Therefore, by blocking the immune checkpoints CTLA-4, PD-L1 and PD-1, drugs can disrupt the immunosuppressive interactions between cancer cells and T cells, thereby restoring the T cells' ability to eliminate cancer cells expressing the corresponding antigen [17, 18]. For RCC, several ICIs have been developed for its treatment, for example, nivolumab and pembrolizumab which selectively target PD-1, as well as atezolizumab, avelumab, and durvalumab, which are designed to inhibit PD-L1, have exhibited remarkable and enduring responses, leading to significant improvements in progression-free survival (PFS) as demonstrated in various clinical trials [19-21] (Figure 2).



#### Immune checkpoint inhibitor in RCC:

PD-1 mAbs: pembrolizumab, nivolumab

PD-L1 mAbs: atezolizumab, durvalumab, avelumab

CTLA-4 mAbs: ipilimumab, tremelimumab

**Figure 2. The mechanism of ICI inhibitors effect.** Two signals control lymphocyte activation at the immunological synapse between resting T cells and APC. The binding to the TCR mediates the first. The second signal could be activation or inhibition in the instance of T cell-CD28 binding to co-stimulatory CD80/CD86. The latter mechanism occurs through the engagement of T cells with CTLA-4, which interacts with the same CD80/CD86 molecules found on APCs. CTLA-4 signaling regulates T cells by preventing naïve activation and clonal proliferation. Monoclonal antibodies that inhibit CTLA-4 function effectively restore CD28-mediated pro-activatory signaling, leading to robust and powerful anti-tumor T cell responses. Activated T cells in peripheral tissues can be deactivated by the binding of PD-L1 (or PD-L2, not depicted) produced by tumor cells, organ cells, or other immune cells to PD-L1. Meanwhile, IFN- $\gamma$  stands as the primary and widely recognized stimulus responsible for the induction of heightened expression of both PD-L1 and PD-L2. The anti-PD-1 or anti-PD-L1 blocking by monoclonal antibodies also could restore CD28 pro-activatory signaling and reinstates T lymphocyte responses that are beneficial against tumors. Below part shows the FDA-approved classes of immune checkpoint inhibitors in RCC. TCR, T-cell receptor; APC, Antigen Presenting Cells; MHC, Major Histocompatibility Complex; CTLA-4,

Cytotoxic T-Lymphocyte Antigen 4; PD-1, Programmed cell death protein 1; PD-L1, Programmed cell death-ligand 1; IFN- $\gamma$ , interferon-gamma (Figure created with BioRender.com).

## **2.2 Cancer stem cells (CSCs)**

Cancer stem cells (CSCs), also known as tumor initiating cells (TICs), are a distinct population of cells within a tumor that share features with normal stem cells and play an essential part in tumor formation and progression. These cells possess the ability of self-renewal indefinitely, differentiate into multiple lineages, and maintain their pluripotency, which contributes to the heterogeneity of tumors [22] (Figure 3A). The role of CSCs was first proposed in the 1960s, and breast cancer was the first solid tumor in which CSCs were discovered and later isolated. [23, 24]. The first 10 years of the twenty-first century saw a record-breaking rise in research dedicated to identify CSCs across a wide range of prevalent cancer categories. This time period witnessed an inflow of scientific research detailing the discovery of CSCs in a variety of common cancer types, including leukemia [25-27], breast cancer [23], colorectal cancer [28, 29], brain cancer [30], prostate cancer [31] and also in RCC [32]. Currently, in accordance with the CSC theory, the development of tumors inside malignancies is coordinated by relatively modest populations of tumor stem cells that stay hidden. These cells are thought to have an unusual ability to begin and sustain the formation of malignant tissues, and it can also proliferate malignancies in transplantation experiments and mimic the phenotypic characteristics of malignant cells in secondary tumors. It explains clinical facts such as tumor recurrence complying with initial effective chemotherapy and/or radiation therapy, as well as tumor dormancy and metastasis. The concept of CSCs has encouraged the development of innovative treatment methods for many cancer types. These innovative treatments aim not just to reduce tumor size but also to eradicate CSCs, the cell subpopulation responsible for long-term tumor progression.

### **2.2.1 CSCs and drug resistance**

CSCs are a type of cell within malignancies that has stem cell-like features, including self-renewal, differentiation, and the ability to initiate and sustain tumor growth [33, 34]. The presence of CSCs has been associated with the emergence of drug resistance across various cancer types [35]. There are several mechanisms by which CSCs may contribute to drug resistance. One contributing factor involves the upregulation of drug efflux pumps, such as ATP-binding cassette (ABC) transporters, which pump drugs out of cells, reducing their efficacy and sensitizing CSCs to chemotherapy [24, 36, 37]. Secondly, CSC-mediated drug resistance can also be attributed to the activation of a unique cancer microenvironment or niche, in which hypoxia is a significant feature that could promote drug resistance and enhances the tumorigenicity of CSCs by enabling them to remain in a quiescent state within tissues, thus avoiding the effects of chemotherapy [38]. Thirdly, CSCs can also develop drug resistance by entering a quiescent state where they temporarily transfer into G0 phase of the cell cycle and remain dormant. As conventional cancer treatments are primarily designed to target rapidly dividing cells, quiescent CSCs can evade these therapies and later resume proliferation, contributing to disease recurrence and treatment failure. Moreover, when exposed to unfavorable microenvironmental stimuli, altered signaling pathways in CSCs may trigger quiescence, such as the transforming growth factor beta (TGF- $\beta$ ), Hedgehog pathway [39]. Fourthly, CSCs could contribute to drug resistance through their ability to undergo “plasticity” wherein non-transformed differentiated cancer cells can shift to a tumorigenically transformed

undifferentiated or CSC state through the process of epithelial-to-mesenchymal transition (EMT) [40]. This phenomenon is critical for cancer growth and development of metastases. EMT is a complicated sequence of molecular changes that give cancer cells the ability to infiltrate surrounding tissues, move to distant places, and reject therapeutic treatments. As a result, selectively targeting the EMT process appears to be a viable treatment strategy for increasing the sensitivity of CSCs to chemotherapy [41] (Figure 3B).

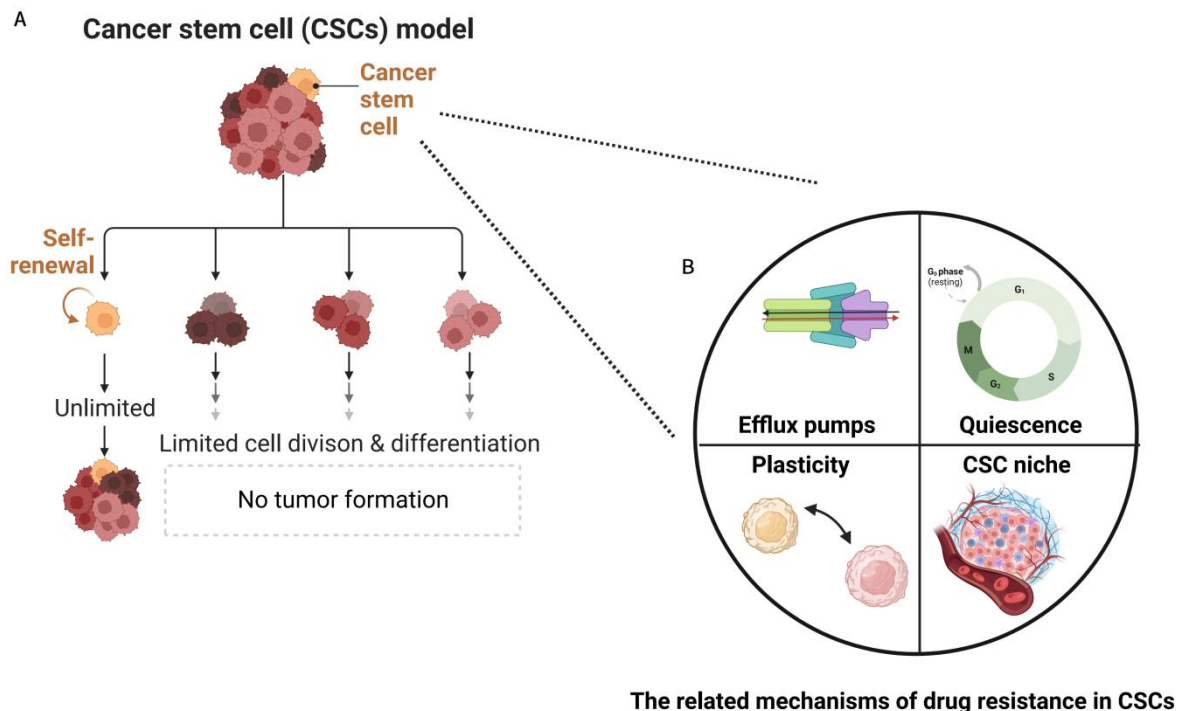


**Figure 3. The mechanism of CSCs in theoretical model and drug resistance.** A. CSCs in heterogeneous tumors promote tumor cell proliferation due to their capacity to self-renew. B. The characteristics of CSCs contributing to drug resistance (Figure created with BioRender.com).

## 2.2.2 CSCs markers

As CSCs exert a profound impact on tumor aggressiveness, the identification of CSC markers—representative of those predominantly expressed in CSCs—forms a pivotal element in forecasting the progression and recurrence of cancer. In our study, we used qPCR and NanoString analysis to test potential CSCs biomarkers and immunotherapeutic targets in RCC. Then, the bioinformatic databases and methods were used to clarify the connection between the potential biomarkers and clinical characteristics of RCC's patients. The three potential candidate biomarkers, namely EZH2, ABCG2, and VCAM1, were thoughtfully chosen to discuss further in this chapter due to their ability of drug resistance, and because they are highly related to RCC prognosis according to our study.

### 2.2.2.1 EZH2

Enhancer of zeste homolog 2 (EZH2) as a typical CSC markers is an enzyme categorized as histone methyltransferase, pivotal in orchestrating the regulation of gene expression by means

of modifying the structural configuration of chromatin [42]. In general, there are three mechanisms by which EZH2 contributes to drug resistance. First, EZH2 has the capability to control the activity of ABC transporter proteins that are accountable for expelling drugs from cancer cells, resulting in a decreased drug concentration inside the cells and ultimately decreasing the efficacy of chemotherapy [43, 44]. Previous studies found that EZH2 could regulate the ABC transporter ABCG2 (ATP binding cassette subfamily G member 2) expression in CSCs and that the inhibition of EZH2 reduced the CSC population and sensitized cancer cells to chemotherapy [45, 46]. Another study showed that EZH2 inhibition reduced the expression of ABCG2 in non-small cell lung cancer cells, which increased the cells' sensitivity to pharmacological treatments [47]. Second, EZH2 contributes to drug resistance through the regulation of DNA repair pathways by key factors, including BRCA1, ATM, and RAD51. Several studies have shown that EZH2 inhibition can sensitize cancer cells to DNA-damaging agents, encompassing, but not confined to, radiation and chemotherapy, by reducing the expression of DNA repair genes [48, 49]. Third, EZH2 has been shown to promote the development and maintenance of CSCs, which are believed to be a major contributor to drug resistance in two ways: a) EZH2 regulates the expression of key signaling pathways that contribute to the ongoing maintenance of CSCs, including Wnt/ $\beta$ -catenin and Hedgehog. Meanwhile, the inhibition of EZH2 reduces the CSC population and suppresses tumor growth in pancreatic and esophageal cancer [50, 51]. b) EZH2 also regulates the expression of several key transcription factors that are involved in the maintenance of CSCs, such as SOX2 and NANOG [52].

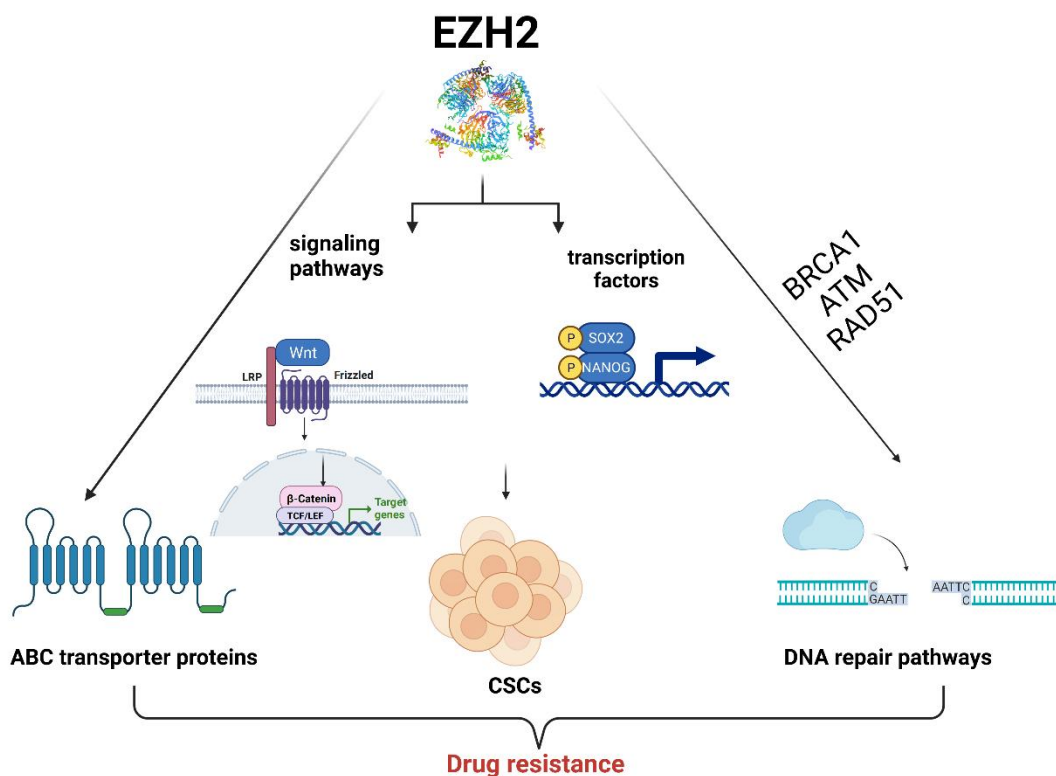


**Figure 4. The mechanisms of EZH2-related drug resistance.** The factors, enhancement of efflux pumps, elevated DNA damage repair and influence on CSCs through signaling pathways and transcription factors, lead to drug resistance (Figure created with BioRender.com).

For RCC, EZH2 has a pivotal role in the advancement and development of RCC and the acquisition of drug resistance [50, 53]. High EZH2 expression has been observed in CSCs

isolated from RCC patients and is associated with increased self-renewal, invasion, and drug resistance [54, 55]. Multiple studies have reported that inhibiting EZH2 expression or activity results in heightened the sensitivity of RCC cells to chemotherapy and targeted therapies. For example, Liu et al. demonstrated that downregulating EZH2 expression in RCC cells can sensitize the cells to sunitinib treatment, a common targeted therapy for RCC [56]. In another study, EZH2 inhibition with the small molecule inhibitor GSK126 sensitized RCC cells to the chemotherapeutic drug cisplatin, resulting in decreased cell proliferation and increased apoptosis [57]. These data clearly suggest that targeting EZH2 might be a potential therapeutic method for overcoming drug resistance in RCC patients. In addition to its role in promoting drug resistance in RCC, EZH2 has also been shown to promote tumor growth and angiogenesis in this malignancy [58]. Previous studies found that EZH2 acts as an oncogenic driver by regulating key genes including but not limited to cell proliferation, cell cycle progression, and angiogenesis in RCC cells [59]. Furthermore, the treatment with GSK126 inhibits the expression of genes involved in angiogenesis in RCC cells, which was associated with a reduction of tumor growth and metastasis in a mouse model of RCC [60, 61]. Moreover, EZH2 expression was found to be a prognostic marker for RCC, with high level EZH2 expression has been linked to several clinical characteristics such as poor prognosis and decreased overall survival in patients with this disease [62-64]. For example, in the research of 134 individuals with RCC, the expression of EZH2 was significantly associated with larger tumors, higher tumor grades, and advanced stages, indicating a more aggressive disease [56]. The underlying mechanism for the upregulation of EZH2 in RCC is unknown, however it is assumed to be linked to deregulation of several signaling pathways, including the phosphatidylinositol 3-kinase(PI3K)/AKT/mTOR and the mitogen activated protein kinase/extracellular-signal-regulated kinase (MAPK/ERK) pathways, which are frequently altered in RCC [65].

In our study, EZH2 was identified as the most promising candidate marker for RCC CSCs due to its significantly elevated expression levels in tumor tissues and sphere cell lines, in contrast to its lower expression in normal tissues and adherent cell lines, respectively. Meanwhile, it has been discovered that EZH2 expression is substantially linked with a variety of clinical features. Furthermore, studies have found a link between EZH2 expression and nine different kinds of tumor-infiltrating immune cells (TICs) in RCC. Follicular helper T cells, regulatory T cells, CD8 T cells, B cells, CD4 T memory resting cells, M2 macrophages, active dendritic cells, and resting mast cells are all examples of TICs. Furthermore, studies have revealed strong correlations between EZH2 expression and numerous immunological signaling pathways. Notably, these pathways include essential components such as natural killer cell-mediated cytotoxicity, primary immunodeficiency, and immunological signaling pathways including TCR, p53, and JAK-STAT. Additionally, EZH2 expression has been linked to metabolic pathways such as pyruvate, propanoate, and butanoate metabolism. These complicated relationships highlight EZH2's varied involvement in RCC and its potential importance in modulating immunological responses, signaling cascades, and metabolic activities. In addition, target genes interacting with EZH2 were predicted to be KIF11, MMP2, and VEGFA, which may play a role and should be examined for potential co-expression in future studies [66].

#### 2.2.2.2 ABCG2

ABCG2, also recognized as the breast cancer resistance protein, is a distinguished constituent of the ABC transporter family [67]. It is a transmembrane protein that plays a crucial role in drug efflux, thereby limiting drug accumulation within cancer cells and leading to drug resistance [68]. The fundamental process of the mechanism typically involves several sequential steps,

including the binding of substrate and Mg<sup>+</sup>/adenosine triphosphate (ATP), dimerization of the nucleotide-binding domain (NBD), conformational changes, characterized by the ABC domains switching between outward/inward conformations (depending on the transport direction), ATP hydrolysis, release of substrate, phosphate and adenosine diphosphate (ADP), and protein regeneration to an initial state to set up for the next cycle. Although the order of these steps varies from protein to protein, various experimental and physical data has shown the occurrence of these steps at some point [69, 70] (Figure 5). In addition, ABCG2 binds to a wide range of structurally diverse drugs, including TKIs and chemotherapeutic agents such as mitoxantrone, topotecan, and doxorubicin. Once these drugs enter cancer cells, ABCG2 pumps them out of the cells, leading to lower intracellular drug concentrations and reduced drug efficacy [71, 72]. In addition, ABCG2-mediated drug resistance is regulated by several signalling pathways, including the PI3K/Akt and nuclear factor kappa-light-chain-enhancer of activated B cells (NF- $\kappa$ B) pathways [73]. Inhibition of these pathways has been shown to downregulate ABCG2 expression and increase the sensitivity of cancer cells to chemotherapeutic agents [74, 75].

For RCC, numerous investigations have documented that the overexpression of ABCG2 in RCC is associated with drug resistance and cancer relapse [76-79]. In recent studies, ABCG2 was discovered to be a marker of renal cancer stem cells, and its involvement in supporting their survival and proliferation *in vitro* was discovered. Furthermore, inhibiting ABCG2 was found to drastically diminish RCC cell resistance to sunitinib, demonstrating its crucial role in drug resistance pathways in RCC [80, 81]. Ko143, a selective and potent inhibitor of ABCG2, has been found to potentiate the antitumor efficacy of chemotherapy in preclinical *in vivo* models of RCC, thus holding promise as a sensitizing agent in RCC therapy [82]. Moreover, numerous clinical investigations have scrutinized the association between ABCG2 expression and drug resistance in RCC patients. For example, several distinct studies revealed a significant increase in ABCG2 expression in RCC patients who demonstrated resistance to sunitinib treatment, and one of the studies reported that patients with elevated ABCG2 expression demonstrated a diminished response to chemotherapy, and a shorter PFS compared to those with low ABCG2 expression [83-85].

In our preliminary study, the mRNA expression level of ABCG2 is considerably greater on RCC-53 cell line CSCs compared to adherent cell lines, whereas it is not on SKRC-17 cell lines [66]. This differently expression level on the RCC CSCs highly motivated us to explore more potential multifunction not only on RCC also in pan-cancer. Therefore, we performed a comprehensive pan-cancer analysis to examine at ABCG2's possible therapeutic functions in 33 distinct cancers. Our investigation revealed variable expression patterns of ABCG2 in tumors, demonstrating diminished expression in individuals diagnosed with kidney chromophobe (KICH) as well as kidney renal papillary cell carcinoma (KIRP). In contrast, a markedly elevated expression was observed in patients afflicted with kidney renal clear cell carcinoma (KIRC). Moreover, RNA stemness score correlated significantly negative with ABCG2 mRNA expression in KIRC and KICH, as well as ESTIMATE scores correlated significantly positive with ABCG2 mRNA expression in KICH and KIRP. The opposite result was observed in the KIRC group. These results implied the multifunction of ABCG2 among various renal cancer types. In addition, within the TCGA database, OS analysis shows that a low expression level of ABCG2 is associated with a poor prognosis for KIRC ( $p < 0.001$ ). Finally, the level of ABCG2 mRNA expression in several cancer cell lines (adherent, sphere and drug-resistant) was tested to investigate the ABCG2-mediated drug resistance. Unexpectedly, we found that in both RCC-53 and SKRC-17, elevated ABCG2 expression was observed in sphere cell lines when compared



to the adherent cell lines' cohort, which was not consistent with our preliminary results with the SKRC-17 cells [86]. We assume that the different expression tendency caused because of the different generation of the SKRC-17 cell lines. The gene expression may differ in sphere cell lines that were generated from various adherent cell lines' generations.

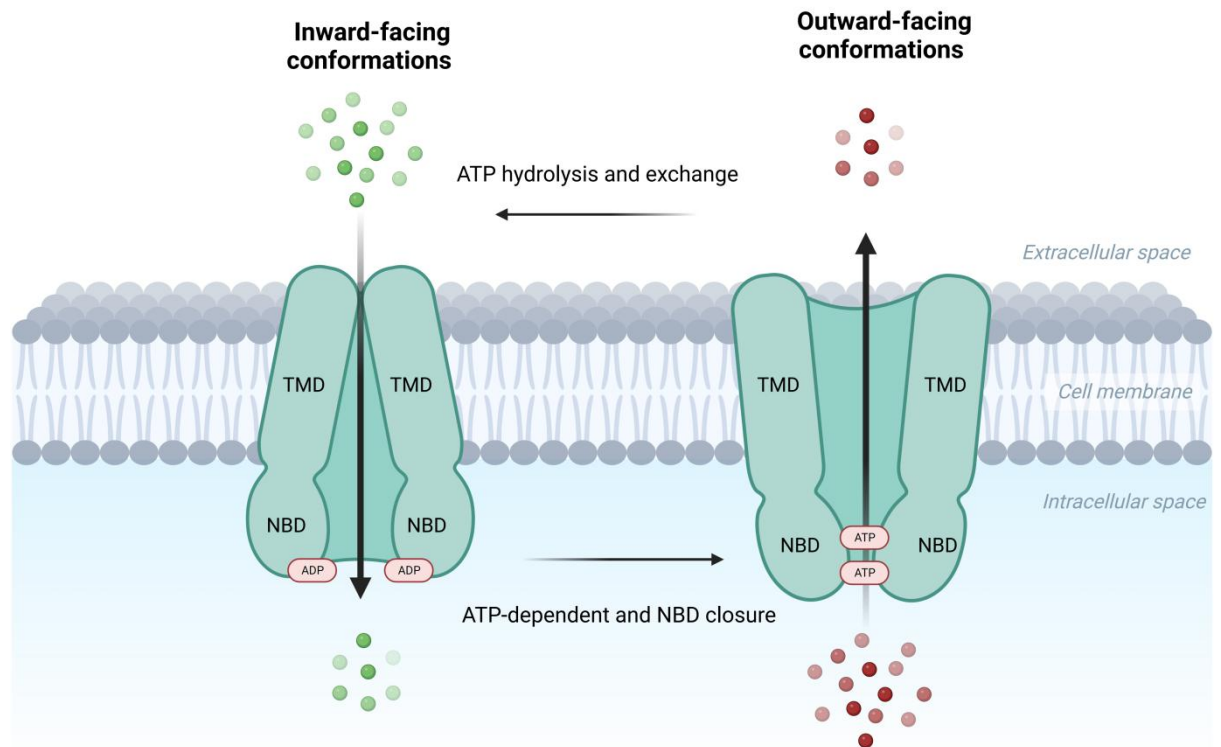


**Figure 5. ABCG2 characteristic mechanism diagram.** The cytoplasmic NBDs' closure/dimerization provides the energy required for the power-stroke that pushes the TMDs from their inward to outward conformations. ATP hydrolysis reverses the conformation to an inward direction. NBD: nucleotide-binding domain; TMD: transmembrane domain; ATP: adenosine triphosphate; ADP: adenosine diphosphate (Figure created with BioRender.com).

### 2.2.2.3 VCAM1

Vascular cell adhesion molecule 1 (VCAM-1) has been identified as a transmembrane glycoprotein found on activated endothelial cells, leukocytes, as well as some stromal cells. It participates in diverse physiological and pathological phenomena, including immune cell trafficking, angiogenesis, as well as vascular adhesion and transendothelial migration of leukocytes associated with inflammation [87]. It is known that the pro-inflammatory cytokine TNF $\alpha$  stimulates the expression of VCAM-1 that linked to the development of a number of immunological diseases, including though not confined to, rheumatoid arthritis, asthma, transplant rejection, and cancer [88] (Figure 6). For cancer, Yong-Bin et al. have observed that gastric cancer tissue exhibiting positive VCAM-1 expression displays a greater abundance of microvessels when compared to tissue that is VCAM-1 negative [89]. In another study, Byrne and colleagues found a significant association between the serum concentrations of VCAM-1 and the microvessel density in breast cancer, suggesting that serum VCAM-1 may function as an alternative marker for assessing angiogenesis in the context of breast cancer [90]. In



addition, VCAM-1 expression has been linked to the induction of EMT, a procedure related to the development of stem-like features and increased metastatic potential in cancer cells [91].

For RCC, recent research has revealed a curious finding: there is a significant increase in the expression of VCAM-1 within RCC tumors when compared to levels seen in healthy kidney tissues. This VCAM-1 overexpression has emerged as a critical component that contributes to the persistent progression of RCC, the facilitation of metastatic distribution, and the challenging development of resistance to treatment therapies [88, 92, 93]. For overcoming drug resistance in RCC, inhibiting VCAM-1 expression with a small molecule inhibitor showed promising results in reducing tumor growth and metastasis, and in enhancing the efficacy of the targeted therapy drug sunitinib in preclinical models of RCC [11, 94, 95]. The mechanism underlying the role of VCAM-1 in RCC pathogenesis and drug resistance is not fully understood. Nonetheless, there is increasing evidence that several signaling pathways are involved in the control of VCAM-1 expression in RCC, including the NF- $\kappa$ B as well as hypoxia-inducible factor-1  $\alpha$  (HIF-1  $\alpha$ ) pathways [96-98].

In our study, VCAM1 was discovered to be a novel CSC marker that is strongly associated with the combination therapy strategy of ipilimumab and shikonin. In addition, VCAM1 expression was significantly greater in ccRCC tumor tissue than in normal tissue at both the mRNA and protein levels. Furthermore, increased VCAM1 mRNA expression was associated with a favorable prognosis in patients with ccRCC, as evidenced by statistically significant improvements in overall survival (OS,  $p = 0.041$ ) and disease-free survival (DFS,  $p = 0.035$ ). Then, we investigated the correlation between VCAM1 expression and the microenvironment in ccRCC patients. The following results indicated that VCAM1 high tumors had a higher prevalence of CD8+ T cells, follicular helper T cells, monocytes, M1 macrophages, eosinophils, and resting dendritic cells compared to VCAM1 low tumors. In addition, a significant relationship was found between VCAM1 expression and the infiltrating immune cells, as well as the immunophenoscore (IPS), which anticipates the efficacy of therapies involving anti-CTLA-4 and anti-PD-1 antibodies. The upregulation of VCAM1 exhibited a positive correlation with the MHC, EC (effector cell), and IPS scores, while demonstrating a negative correlation with the SC (suppressor cell) and CP (checkpoint) scores. Finally, the VCAM-1 related immune genes and signaling pathways were explored. The findings revealed that VCAM1 expression correlated positively with various immune checkpoint genes. For example, we found substantial enrichment of numerous genes in the group with high VCAM1 expression, including CTLA-4, IL10, CXCL9, CXCL10, and HAVCR2. Furthermore, functional network analysis indicated an enrichment of pathways linked to T cell receptor signaling, B cell receptor signaling, natural killer cell-mediated cytotoxicity, rig-I-like receptor signaling, autoimmune thyroid disease, and toll-like receptor signaling. In contrast in the low VCAM1 expression group, we found enrichment in several pathways, including the calcium signaling pathway, neuroactive ligand-receptor interaction, heart muscle contraction, dilated cardiomyopathy, and hypertrophic cardiomyopathy (HCM). These data highlight the intricate connection between VCAM1 expression and immune-related pathways in one group, whereas cardiovascular and neurological pathways are implicated in the other group.

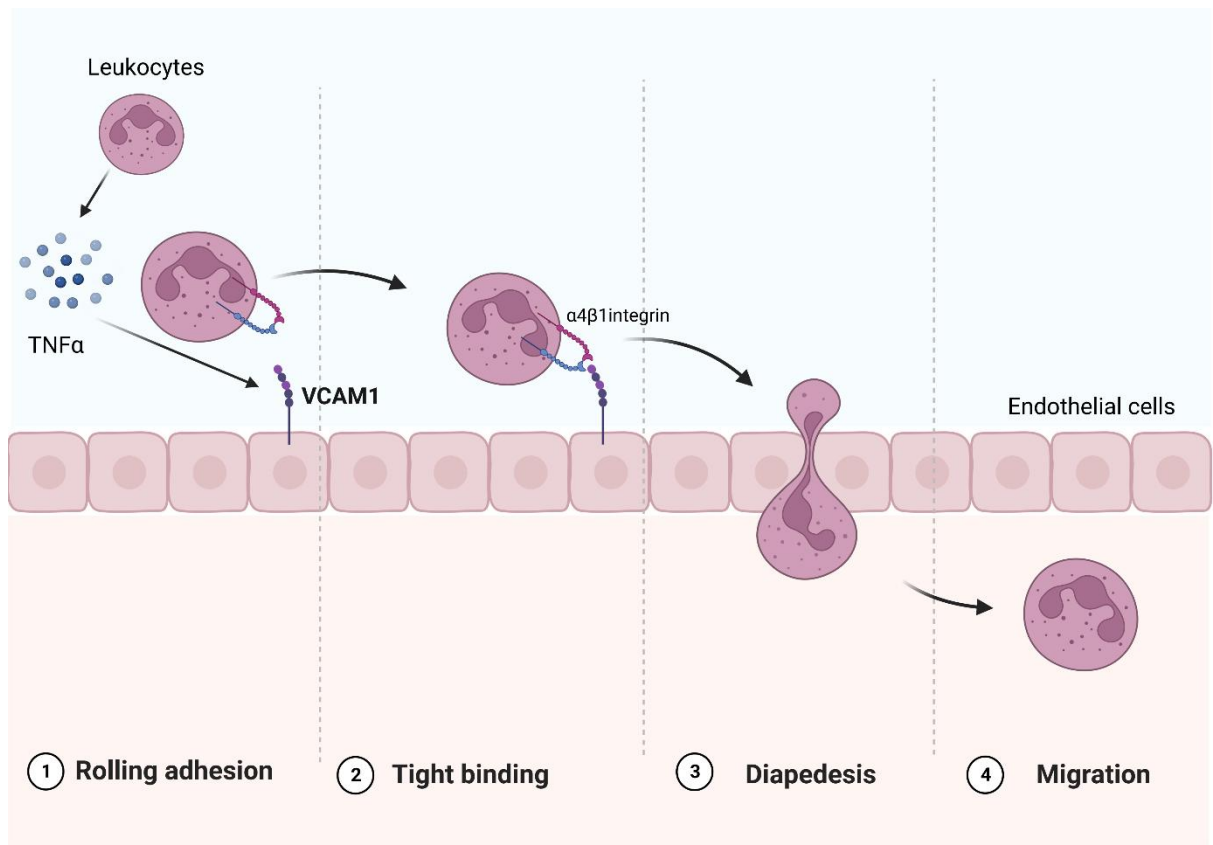


**Figure 6. Mechanism of VCAM-1-mediated leukocyte adhesion and migration across endothelial cells.** TNF $\alpha$ , which is largely released by leukocytes, has a stimulatory impact by increasing VCAM-1 expression on the surface of endothelial cells. This increased VCAM-1 presence on activated endothelial cells acts as a critical site of contact, directly connecting with the integrin  $\alpha 4 \beta 1$  receptors located on the leukocyte surface. TNF $\alpha$ : tumor necrosis factor alpha (Figure created with BioRender.com).

### 2.3 Phytochemicals (PTCs)

PTCs are naturally occurring compounds found in plants that have been shown to have anti-cancer properties [99]. These compounds have been the subject of many research projects in the recent years, as they have the potential to provide a safer and more natural approach to cancer prevention and treatment [100]. PTCs can be classified into different groups based on their chemical structures and on the plants they are found in. Some of the most well-known groups of PTCs include flavonoids, carotenoids, phenolic acids, and terpenoids. Each group of phytochemicals has unique properties and mechanisms of action that make them effective in preventing and treating various types of cancer [101]. Recently, the use of PTCs is expected to be a promising therapeutic option for cancer eradication by eliminating CSCs [102]. This is a significant step forward in cancer treatment because manufactured anticancer medications are generally highly harmful to vital organs and compromising the integrity of the patient's immune system.

For our project, we are firstly screening out 11 PTCs (apigenin, shikonin, wogonin, berbamine, curcumin, resveratrol, piperine, honokiol, corilagin, silibinin and baicalein) to determine the most promising PTC as partner for the ICIs. Apigenin, shikonin and wogonin showed their higher binding probability with therapeutic target proteins and more intersection genes with immune-related genes of the RCC and were selected as PTCs candidates. Then, the selection of

shikonin as the most promising combinatorial agent with ipilimumab for ccRCC patients among 11 potential therapeutic candidates is attributed to its significant inhibitory impact on CSC. In addition, after deeply researching recent PTCs studies, we found that EGCG could have a high potential for the inhibition of RCC CSCs. Therefore, we tested EGCG on the CSCs together with shikonin, apigenin and wogonin to further clarify the combined potential of PTC together with the first line therapy in RCC.

### **2.3.1 EGCG**

In green tea, the active compound epigallocatechin-3-gallate (EGCG) demonstrates diverse biological functions, including anti-oxidant, radical scavenging, anti-microbial, anti-inflammatory, anti-carcinogenic, and anti-apoptotic properties [103]. In cancer, EGCG and other tea catechins are capable of neutralizing reactive oxygen species (ROS) and modulating cell signaling [104, 105]. For antioxidant activity, the properties of green tea phenol contain phase II antioxidant enzymes, including superoxide dismutase, glutathione-S-transferase, glutathione peroxidase, and glutathione reductase, which are linked to the removal of ROS. The nuclear factor erythroid 2-related factor 2 (Nrf2) has been demonstrated to play a distinctive role in regulating the expression of phase II enzymes, a phenomenon closely associated with both oncogenesis and the development of resistance to chemotherapeutic agents in cancers [106]. In addition, EGCG plays a starring role in the inhibition of inflammatory mediators contributing to metastasis and carcinogenesis, including nitric oxide (NO), proinflammatory cytokines like the interleukins IL-12, IL-1 $\beta$ , IL-6, and TNF- $\alpha$ . A prior study found that administration of with EGCG at 10  $\mu$ M and 50  $\mu$ M levels suppressed NO, IL-6, IL-1, and TNF- $\alpha$  in lipopolysaccharide-induced RAW 264.7 cells [107].

Due to its potential multi-function in cancer, EGCG has contributed to various ongoing clinical trials, either alone or in combination, demonstrating its ability to boost the therapeutic effect of traditional medications [108]. For RCC, *in vitro* investigations have demonstrated that EGCG exhibits a dose-dependent inhibition of RCC cell proliferation and induces apoptosis by suppressing the PI3K/Akt signaling pathway. This pathway, implicated in RCC tumorigenesis, is known to play a crucial role [103]. Other studies showed that EGCG significantly decreased RCC cell migration and invasion by decreasing the production of matrix metalloproteinase-2 (MMP-2), an enzyme involved in extracellular matrix degradation that plays an essential part in tumor invasion and metastasis [109, 110]. In addition to its direct effects on RCC cells, EGCG has also been found to enhance the anti-tumor immune response. In a mouse model of RCC, it was found that EGCG could enhance the infiltration of CD8<sup>+</sup> T cells into the TME, and that it promoted the expression of pro-inflammatory cytokines, which are important for the activation of the immune response [111, 112].

In our research, we evaluated the effects of four different PTCs on adherent and sphere cell lines of RCC-53 and SKRC-17 in terms of migration, invasion, and apoptosis. The outcomes of our study demonstrated that EGCG exhibited robust efficacy in inhibiting the migration and invasion, while concurrently enhancing apoptosis in both adherent and CSC cell lines. We also found that EGCG had the highest inhibitory effect on EZH2 expression, which is proven as a CSC biomarker in RCC based in our study. Moreover, we executed the concurrent administration of EGCG and sunitinib, a frontline therapeutic approach for RCC. The results showed that when compared to the control group, this combination treatment significantly reduced the frequency of CD4<sup>+</sup>, CD25<sup>+</sup>, CD127<sup>low</sup>, FOXP3<sup>+</sup>, Treg cells in the peripheral blood

cells of ccRCC patients, providing new insights into potential therapies for ccRCC by targeting CSCs [66].

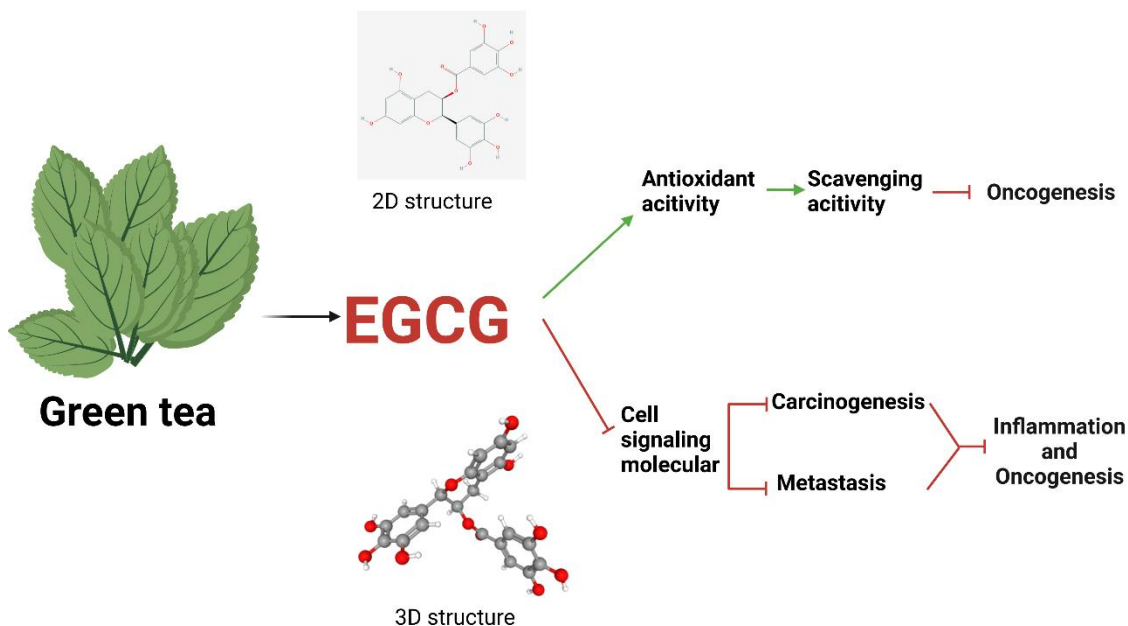


**Figure 7. Main mechanisms of the inhibitory effect of EGCG in cancer.** EGCG is extracted from green tea. The 2D and 3D structure of EGCG is shown, and also the role of EGCG in the inhibition of inflammation and oncogenesis. Arrow ✓ represents induction and symbol ⊥ represents suppression of effects (Figure created with BioRender.com).

### 2.3.2 Shikonin

Shikonin is a naturally occurring chemical extracted from the roots of the plant *Lithospermum erythrorhizon* [113, 114]. It possesses anti-oxidant, anti-inflammatory, and anti-thrombotic properties, and has been studied for its potential use in the management of specific kinds of cancer [115, 116].

Based on previous studies, our group found that shikonin could attack prostate cancer cell lines and their CSCs by inhibiting proliferation, migration and invasion and increasing the rate of apoptosis, also by downregulating ABCG2 and ALDH3A1, shikonin was able to resensitize cabazitaxel-resistant prostate cancer cells to cabazitaxel [31]. Another study in our lab found that shikonin could effectively inhibit the formation of tumour spheres, enhancing the proliferation and apoptosis-inducing effects of temozolomide on glioma cells and their CSCs [117]. For RCC, the newest research in 2022 investigated the effect of shikonin on therapy-sensitive and therapy-resistant RCC cells. The results showed that shikonin substantially decreased parental and sunitinib-resistant RCC cell growth, proliferation, and clone formation via G2/M phase arrest-mediated down-regulation of cell cycle activating proteins. In addition, the induction of apoptosis and necroptosis by shikonin was mediated through the activation of necrosome complex proteins as well as inhibited the activity of the AKT/mTOR signaling pathway, which is known to play a role in RCC tumorigenesis [118]. Additionally, another study found that shikonin treatment in the renal cancer cell lines Caki-1 and ACHN could enhance autophagy. Knockdown of chain 3B (LC3B)-II that bind to the autophagic membranes could significantly restored cell viability when shikonin was present, indicating that autophagy was

involved in shikonin-induced cell death. Meanwhile, shikonin treatment in Caki-1 and ACHN cells led to elevated levels of ROS and mitochondrial dysfunction. In turn, pre-treatment with N-acetyl cysteine, a ROS scavenger, effectively mitigated shikonin-induced cell death and ROS generation [119]. These results indicate that shikonin could serve as a supplementary therapeutic option for individuals diagnosed with advanced and treatment resistant RCC. In our study, the results have demonstrated that shikonin can enhance apoptosis, and inhibit migration, and invasion in both adherent cell lines and CSCs of RCC-53 and SKRC-17. Moreover, shikonin showed strong ability to inhibit most of the CSC markers in SKRC-17. To further improve the efficacy of shikonin treatment, we investigated a combination treatment strategy using three potential ICIs. We found that in combination with shikonin, ipilimumab was particularly effective in suppressing the ccRCC patient's FoxP3+ Treg cells and enhancing CD3+CD4+ T cells. Additionally, compared to the shikonin-only group, the combination of ipilimumab and shikonin dramatically reduced the ccRCC patients' FoxP3+ Treg cells in RCC-53 and increased the CD3+CD4+ T cells in both RCC-53 and SKRC-17.

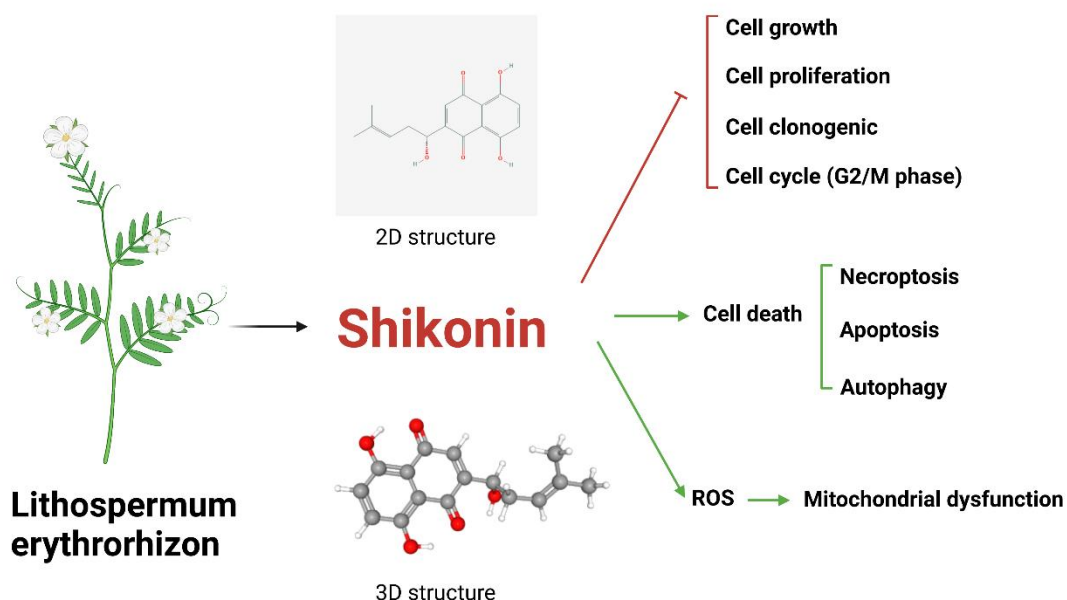


**Figure 8. Main mechanisms of Shikonin in RCC.** Shikonin is extracted from the root of *Lithospermum erythrorhizon*. The 2D and 3D structure of shikonin is shown, and also the role of shikonin in the inhibition of cell growth, the enhancement of cell death as well as in ROS generation. Arrow ✓ represents induction and symbol ⊥ represents suppression of effects (Figure created with BioRender.com).

### 2.3.3 Apigenin

Apigenin is a flavonoid phytochemical that can be found in a variety of fruits and vegetables, including parsley, celery, and chamomile. It has been shown to have anti-cancer properties, including the activation of apoptosis or autophagy, cell cycle modulation, prevention of tumor cell migration and invasion as well as stimulation of patients' immunological responses. Several studies have investigated that apigenin has the potential to be used as a cancer therapy agent [120, 121]. The various anti-cancer properties of apigenin are controlled by different signaling pathways [122]. For example, apigenin triggered apoptosis via either the intrinsic pathway involving mitochondria or the extrinsic pathway mediated by death receptors [123, 124].

Moreover, Coombs et al. demonstrated that in both human and mouse mammary carcinoma cells, apigenin can specifically target STAT1 (signal transducer and activator of transcription 1), leading to the suppression of IFN- $\gamma$ -mediated PD-L1 expression, while simultaneously enhancing the proliferation of PD1-expressing Jurkat T cells, the co-culture with MDA-MB-468 cells also promotes the synthesis of IL-2 [125]. Additionally, in human malignant melanoma cells, the AKT/mTOR pathway was found to be significantly inhibited by 40  $\mu$ M apigenin, leading to reduced cell migration and invasion in both melanoma cell lines A375 and C8161. In the colorectal cancer cell lines SW480 and DLD1, apigenin modulated the developmentally down-regulated 9 (NEDD9)/Src/AKT cascade in neural precursor cells, thereby inhibiting cell migration, invasion, and metastasis [126, 127]. In human prostate cancer cells, apigenin promoted cell cycle arrest via regulating MAPK, PI3K/Akt, and cyclin D1-associated retinoblastoma dephosphorylation [128].

For RCC, recent investigations have shown that apigenin exhibits a time- and dose-dependent inhibition of the proliferation of three distinct renal cell carcinoma (RCC) cell lines. This effect is attributed to G2/M phase cell cycle arrest, mediated by the modulation of the ATM signaling pathway. Furthermore, the studies revealed apigenin-induced apoptosis was probably p53-dependent and caused DNA damage in RCC cells, particularly at higher dosages. Meanwhile, apigenin treatment dramatically decreased tumor development and volume in vivo utilizing an ACHN cell xenograft mice model. Immunohistochemical staining validated apigenin's anti-proliferative actions in vivo, as shown by reduced Ki-67 indices in tumors produced from apigenin-treated mice [129, 130]. Consistently, a new derivative of apigenin-15e with improved properties were synthesized, which exhibited strong anti-growth activity against various RCC cell lines, as well as inhibited Caki-1 cell proliferation, migration and invasion. Mechanistically, apigenin-15e is able to directly target the MET kinase domain-a driving factor in RCC, meanwhile inhibiting the activity of mutant MET V1238I and Y1248H which had developed resistance to approved MET inhibitors [131]. These results indicate that the compound apigenin and its derivative have the capability to be explored as a therapeutic option for RCC, particularly for drug-resistant MET mutations.

Our research has demonstrated that apigenin significantly decreased the transcript levels of major CSC markers in RCC-53 CSCs as well as EZH2 mRNA expression level in RCC-53 and SKRC-17 CSCs. To investigate the biological regulation of apigenin in the RCC-53 and SKRC-17 cells as well as the associated CSCs, the cells were treated with apigenin at three distinct concentrations (0.5 $\times$  IC50, 1 $\times$  IC50, and 2 $\times$  IC50). The results revealed that apigenin in the 2 $\times$  IC50 group greatly reduced cells invasion in adherent cell lines and associated CSCs. The apoptosis rates were significantly increased in the 2 $\times$  IC50 group both for the adherent and sphere cell lines.

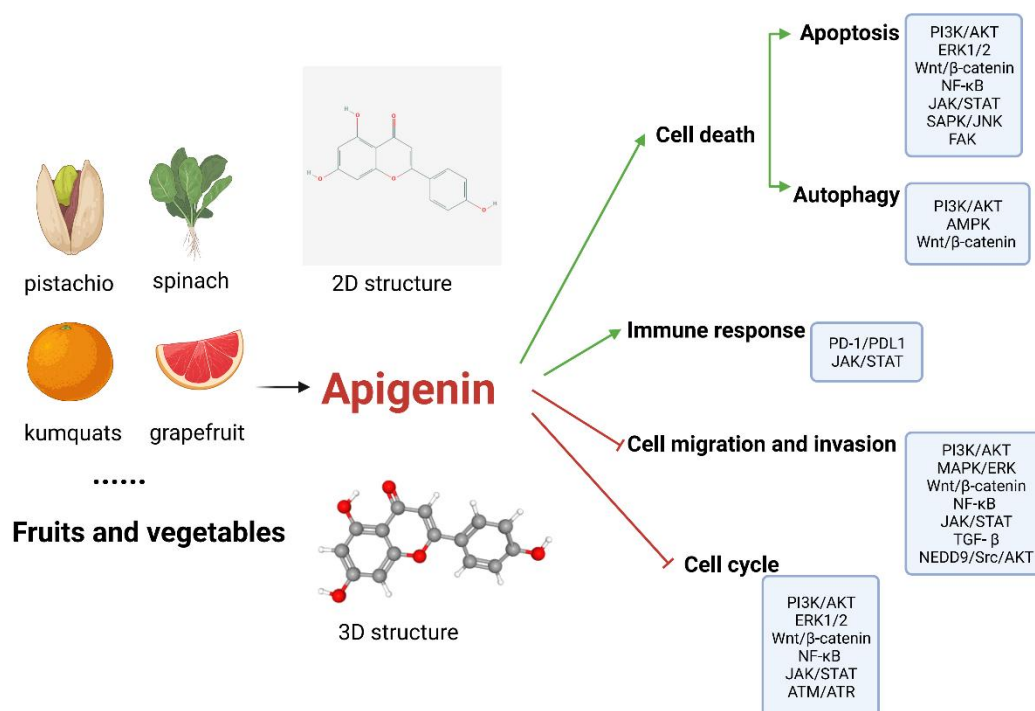


**Figure 9. Main mechanisms of apigenin in cancer.** Apigenin is extracted from fruits and vegetables. The 2D and 3D structure of apigenin is shown, and also the role of apigenin in suppressing cell cycle, migration, and invasion as well as enhancing cell death and immune response. The carcinogenesis-related signaling pathways involved are indicated. Arrow  $\surd$  represents induction and symbol  $\perp$  represents suppression of effects (Figure created with BioRender.com).

### 2.3.4 Wogonin

Wogonin is a flavonoid phytochemical found in the roots of the Chinese plant *Scutellaria baicalensis*, which is being proved to possess several properties, including anti-inflammatory effect, anti-cancer effect, and anti-oxidant activity [132, 133]. Wogonin differentially regulates inflammation in several ways: 1) via inflammation-associated proteins: wogonin was effective in reducing gene expression of cyclooxygenase-2 (COX-2) and TNF- $\alpha$ , while showing weak effects on intercellular adhesion molecule 1 (ICAM-1) and IL-1 $\beta$  in 12-O-tetradecanoylphorbol-13-acetate (TPA)-induced inflammation and in an acute-type model of arachidonic acid (AA)-induced inflammation. 2) via signaling pathways: wogonin has been shown to attenuate the production of endotoxin-Induced prostaglandin E2 and nitric oxide through the src- ERK1/2- NF- $\kappa$ B pathway [134]. In addition, wogonin plays multi-functional roles in antioxidant activity. For example, wogonin has the ability to inhibit the remodeling of action stimulated by H<sub>2</sub>O<sub>2</sub> by reducing phosphorylation of caveolin-1, which is associated with the suppression of the stabilization of vascular endothelial cadherin and catenin [135]. Moreover, wogonin can also inhibit several types of oxidative stress-induced neuronal damage by inhibiting excitotoxicity. Furthermore, the antioxidant and radical scavenging activities could be contributing to the neuroprotective benefits [136]. In cancers, several investigations have explored the potential of wogonin as a therapeutic option by regulating cancer driving pathways and molecules [137-139]. For instance, wogonin treatment of murine sarcoma S180 cells resulted in upregulation of bax and p53 mRNA expression and downregulation of bcl-2 mRNA expression, indicating its pro-apoptotic effect [140]. This phenomenon was noted in both in vitro and in vivo environments,



resulting in the suppression of neoplastic proliferation. Moreover, the leaf extract of *Scutellaria ocmulgee* Small demonstrated potent anti-proliferative activity and contained solely wogonin, indicating that this flavonoid may exhibit exceptional anti-cancer properties and could exhibit synergistic effects with other phytochemicals at even low concentrations [141]. In addition, another study documented that wogonin could inhibit Treg activity induced by transforming growth factor  $\beta$  (TGF- $\beta$ 1) in malignant gliomas, indicating that the potential of wogonin to alleviate tumor-induced immune suppression may be ascribed to its capacity to decrease TGF- $\beta$ 1 production and TGF- $\beta$ 1 response in T cells [142].

For RCC, the administration of wogonin demonstrated inhibitory effects on the proliferation, migration, and invasion of the RCC cell lines 786-O and OS-RC-2, alongside with the induction of significant cytotoxic effects. Moreover, wogonin transcriptionally down-regulated a crucial component in DNA damage response-cell division cycle 6 (CDC6), disrupted DNA replication, increased DNA damage, and death in RCC cells after blocking the cyclin-dependent kinase 4 (CDK4)/RB pathway. Meanwhile, the proficient restoration of sunitinib sensitivity by wogonin through the inhibition of CDK4 suggests that the CDK4-RB pathway could contribute, at least partially, to the development of resistance to sunitinib in RCC. Wogonin could play a potential role of therapeutic implication via regulation the CDK4-RB pathway in the future management of RCC [143].

To understand how wogonin is functionally regulated in RCC-53 and SKRC-17 cells, and associated CSCs, we treated the cells with various concentrations of wogonin (0.5 $\times$  IC50, 1 $\times$  IC50, and 2 $\times$  IC50). In light of our research findings, it was revealed that the number of invaded CSCs was significantly reduced in the group that received wogonin at a concentration of 2 $\times$  IC50. Additionally, the rates of apoptosis were significantly increased in both the adherent and sphere cell lines in the group that received apigenin at a concentration of 2 $\times$  IC50.

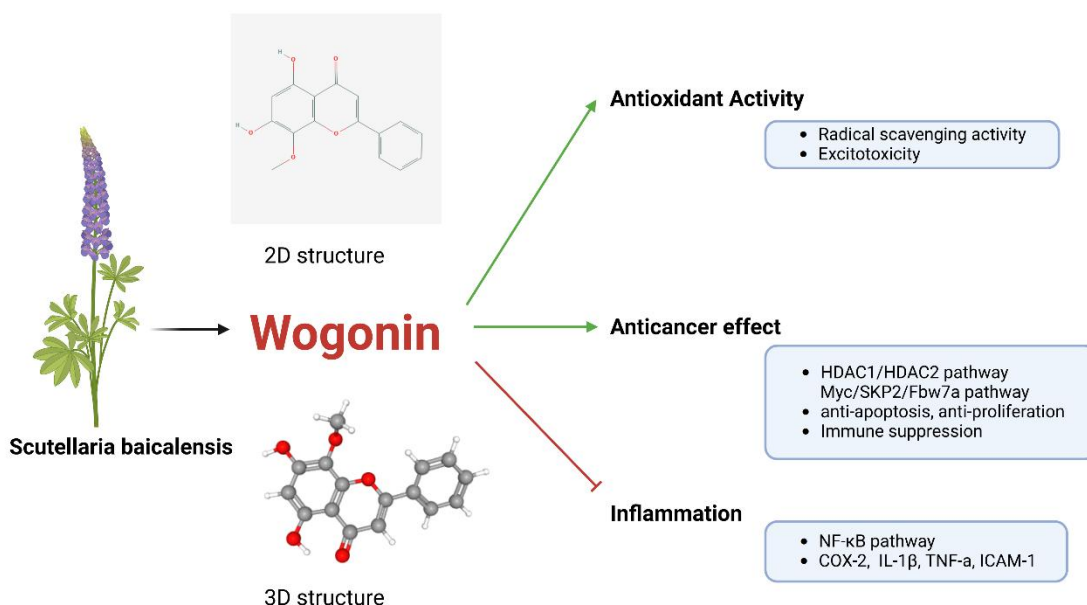


**Figure 10. Main mechanisms of wogonin in cancer.** Wogonin is extracted from *Scutellaria baicalensis*, and the structure of wogonin in two and three dimensions is shown. Wogonin plays a role in the inhibition of inflammation as well as in the enhancement of anticancer effect and antioxidant activity. Molecular



---

structure, signaling pathways and bioactivity are presented. Arrow ↗ represents induction, and symbol ⊥ represents suppression of effects (Figure created with BioRender.com).

### 3. Paper I



#### OPEN ACCESS

EDITED BY  
Junmin Zhang,  
Lanzhou University, China

REVIEWED BY  
Khalil Saleh,  
Gustave Roussy Cancer Campus, France  
Marco Maruzzo,  
Veneto Institute of Oncology (IRCCS), Italy

\*CORRESPONDENCE  
Heike Pohla  
✉ heike.pohla@med.uni-muenchen.de

RECEIVED 14 March 2023

ACCEPTED 24 July 2023

PUBLISHED 09 August 2023

#### CITATION

Lyu C, Stadlbauer B, Wang L, Buchner A and Pohla H (2023) Identification of a novel combination treatment strategy in clear cell renal cell carcinoma stem cells with shikonin and ipilimumab. *Front. Immunol.* 14:1186388. doi: 10.3389/fimmu.2023.1186388

#### COPYRIGHT

© 2023 Lyu, Stadlbauer, Wang, Buchner and Pohla. This is an open-access article distributed under the terms of the [Creative Commons Attribution License \(CC BY\)](https://creativecommons.org/licenses/by/4.0/). The use, distribution or reproduction in other forums is permitted, provided the original author(s) and the copyright owner(s) are credited and that the original publication in this journal is cited, in accordance with accepted academic practice. No use, distribution or reproduction is permitted which does not comply with these terms.

## Identification of a novel combination treatment strategy in clear cell renal cell carcinoma stem cells with shikonin and ipilimumab

Chen Lyu<sup>1</sup>, Birgit Stadlbauer<sup>1,2</sup>, Lili Wang<sup>1,3</sup>, Alexander Buchner<sup>1,2</sup> and Heike Pohla<sup>1,2\*</sup>

<sup>1</sup>Tumor Immunology Laboratory, LIFE Center, LMU Klinikum, University Munich, Planegg, Germany, <sup>2</sup>Department of Urology, LMU Klinikum, University Munich, Munich, Germany, <sup>3</sup>Department of Radiology, First Affiliated Hospital, Zhejiang University School of Medicine, Hangzhou, China

**Background:** Management of clear cell renal cell carcinoma (ccRCC) has changed rapidly in recent years with the advent of immune checkpoint inhibitors (ICIs). However, only a limited number of patients can sustainably respond to immune checkpoint inhibitors and many patients develop resistance to therapy, creating an additional need for therapeutic strategies to improve the efficacy of systemic therapies.

**Methods:** Binding probability and target genes prediction using online databases, invasion, migration, and apoptosis assays as well as the inhibition of cancer stem cells (CSCs) markers in ccRCC cell lines were used to select the most promising phytochemicals (PTCs). Mixed lymphocyte tumor cell culture (MLTC) system and flow cytometry were performed to confirm the potential combination strategy. The potential immunotherapeutic targets and novel CSC markers were identified via the NanoString analysis. The mRNA and protein expression, immune signatures as well as survival characteristics of the marker in ccRCC were analyzed via bioinformatics analysis.

**Results:** Shikonin was selected as the most promising beneficial combination partner among 11 PTCs for ipilimumab for the treatment of ccRCC patients due to its strong inhibitory effect on CSCs, the significant reduction of FoxP3<sup>+</sup> Treg cells in peripheral blood mononuclear cells (PBMCs) of patients and activation of the endogenous effector CD3<sup>+</sup>CD8<sup>+</sup> and CD3<sup>+</sup>CD4<sup>+</sup> T cells in response to the recognition of tumor specific antigens. Based on NanoString analysis VCAM1, CXCL1 and IL8 were explored as potential immunotherapeutic targets and novel CSC markers in ccRCC. The expression of VCAM1 was higher in the tumor tissue both at mRNA and protein levels in ccRCC compared with normal tissue, and was significantly positively correlated with immune signatures and survival characteristics in ccRCC patients.

**Conclusion:** We propose that a combination of shikonin and ipilimumab could be a promising treatment strategy and VCAM1 a novel immunotherapeutic target for the treatment of ccRCC.

#### KEYWORDS

renal cell carcinoma, immune checkpoint inhibitor (ICI), phytochemical, immunotherapy, cancer stem cells (CSCs), tumor microenvironment (TME), tumor infiltrating immune cell (TIC)

## 1 Introduction

Renal cell carcinoma (RCC) is the most common type of renal malignancy, of which clear cell renal cell carcinoma (ccRCC) or kidney renal clear cell carcinoma (KIRC) accounts for about 70–85% of cases ranging from an indolent evolution to a rapid and widespread progression. More than 30% of ccRCC patients are metastatic at the time of the diagnosis, and nearly 30% will progress to metastasis during the course of follow-up (1, 2). Recently, the management of metastatic ccRCC has been revolutionized by the advent of immune checkpoint inhibitors (ICIs) replacing or being added to treatments with tyrosine kinase inhibitors (TKIs) alone, and each combination regimen is considered highly effective, with objective response rates ranging from 42% to 71% (3–6). Meanwhile, dual ICI treatment, combining nivolumab and ipilimumab, has also shown a survival benefit and reduced the risk of death by 32%. In 2018, this therapy was approved for previously untreated RCC patients with intermediate and low risk (7). Furthermore, in a recent phase 3 clinical trial (NCT03937219), the combination of cabozantinib, nivolumab, and ipilimumab demonstrated statistically significant improvements in progression-free survival (PFS) among 428 participants. However, it is worth noting that the treatment also resulted in a high rate of grade 3/4 adverse events (AEs), with nearly 80% of participants experiencing these severe AEs (8). Despite significant improvements in systemic therapies for ccRCC, only a few patients have achieved a durable clinical response, with the median PFS ranging from 11.6 to 15.4 months, even with first-line treatment (9) followed by the therapy-resistance. Additional therapeutic strategies to improve the efficacy of systemic therapies are therefore urgently needed, especially in patients with limited disease burden.

Targeting cancer stem cells (CSCs), a small population of cancer cells in the tumor microenvironment (TME), has been suggested as the key to successful treatment against the increased relapse rate of cancers toward current chemo- or radiotherapy (10). Emerging evidence has indicated that renal tumorigenesis and RCC treatment resistance may originate from renal CSCs with tumor-initiating capacity (11, 12). So far, many studies have tried to establish unique biomarkers to identify CSC populations in RCC. Consequently, several markers were found to be specifically expressed in CSCs and cancer stem-like cells derived from RCC such as CD105, ALDH1, OCT4, CD133, and CXCR4 which have the ability to play multiple

functional roles in regulating stem cell function (13). For example, CXCR4<sup>+</sup> cells derived from several RCC cell lines exhibit resistance to therapy (TKIs) and enhanced capability to form spheres *in vitro* and tumors *in vivo* compared to CXCR4<sup>-</sup> cells (14). Furthermore, several CSC markers such as EZH2, OCT4 and NANOG could be considered as novel independent prognostic predictors in patients with renal cancer (15, 16). Therefore, the identification of a specific CSC marker for RCC that either initiate or maintain tumorigenesis is of most importance for understanding tumor biology and in the development of novel therapies.

To target CSCs, phytochemicals have been proposed due to their economical nature, less immunological response and relatively low side effects (17, 18). Moreover, merging evidence showed that several phytochemicals such as curcumin, piperine, berbamine, shikonin, genistein as well as the whole extract of some plants are able to kill CSCs (19, 20). For instance, epigallocatechin-3-gallate (EGCG) as an active compound in green tea is involved in several ongoing alone or combination clinical trials with cisplatin and oxaliplatin, because of the potential to suppress cancer stemness and tumorigenicity and its ability to improve the efficacy of conventional drugs in several types of cancers including RCC (21–23). The usage of phytochemicals is likely to be a potential treatment strategy for eradicating cancer through the elimination of CSCs. This is a milestone in the improvement of cancer treatment because the synthetic anticancer drugs that are currently used are often highly toxic to healthy organs and weaken the patient's immune system. Therefore, more clinical trials could be released to improve the outcomes of these patients through the usage of a combination therapy with phytochemicals and immunotherapy or other more efficient systemic therapies.

## 2 Materials and methods

### 2.1 Prediction of binding probability and intersection genes

The two-dimensional (2D) and three-dimensional (3D) structure of phytochemicals was acquired from the PubChem database (<https://pubchem.ncbi.nlm.nih.gov/>). The three-dimensional structures of the target proteins were downloaded from protein data bank (<https://www.rcsb.org/>) with the PDB ID:

7KEZ (VEGF), 3HN4 (HGF), 3MJG (PDGF), 3FUB (GDNF) and 4DRH (mTOR) respectively. The binding probability based on the predicted structures between target proteins and phytochemicals was evaluated by the online platform Kdeep (<https://playmolecule.com/Kdeep/>). Kdeep is a protein-ligand affinity predictor based on Deep Convolutional Neural Networks (DCNNs). The SDF file of the 3D structure was uploaded to the PharmMapper database (<http://www.lilab-ecust.cn/pharmmapper/>) for potential target gene prediction.

ccRCC (KIRC, n=539) immune-related genes were extracted from The Cancer Genome Atlas database (TCGA) database (<https://portal.gdc.cancer.gov/>). The intersection of ccRCC immune genes and phytochemicals' potential target genes were obtained using a Venn diagram.

## 2.2 Cell culture

SKRC-17 (kind gift from J. Vissers, Nijmegen), and RCC-53 (derived from a patient with stage IV disease (pT2N1MxG2-3)) were grown in RPMI1640 supplemented with 10% fetal calf serum (FCS "Gold Plus", Bio & Sell GmbH, Feucht, Germany), 1% minimal essential medium, 1 mM sodium pyruvate, and 2 mM L-glutamine (Invitrogen, Life Technologies GmbH, Darmstadt, Germany) under the condition at 37°C in a humidified incubator with 5% CO<sub>2</sub>. The corresponding CSCs were generated using CSC medium containing DMEM/F12 medium supplemented with 2% B-27 (Invitrogen), 10 ng/ml epidermal growth factor (EGF, Sigma Aldrich Chemie GmbH, Taufkirchen, Germany), and 10 ng/ml basic fibroblast growth factor (bFGF, Sigma Aldrich).

## 2.3 Sphere formation assay

All the CSCs were generated by the sphere-forming assay in CSC specific medium. Initially, SKRC-17 and RCC-53 were harvested using 3-5 ml Accutase cell detach solution (Life Technologies, Thermo Fisher Scientific, Waltham, MA, USA) and incubated for 8-10 minutes at 37°C. Then, 3-10 × 10<sup>5</sup> cells were seeded in 75 cm<sup>2</sup> ultra-low attachment flasks (Corning, New York, NY, USA) and cultured with 10 ml CSC specific medium for 7 days.

## 2.4 Quantitative reverse transcription PCR (RT-qPCR)

Total RNA was extracted from cells using the RNeasy Mini-Kit (Qiagen, Hilden, Germany) based on the manufacturer's instructions. cDNA was synthesized according to the kit instructions (Reverse Transcription System, Promega GmbH, Mannheim, Germany). The real-time PCR procedure was performed using the LightCycler® 96 (Roche) and the DNA Green Master kit (Roche, Penzberg, Germany). The reaction started with 95°C for 10 minutes, followed by 40 cycles of denaturation at 95°C for 10 seconds, annealing at 56-62°C for 10 seconds, and extension at 72°C for 10 seconds. Data were analyzed by the LightCycler® 96 software version 1.1. The relative expression analysis was carried out by the 2<sup>-ΔΔCt</sup> method. The transcription level of *GAPDH* and *ACTB* was used as an internal control, and the primers of *VCAM1* (GeneGlobe ID: PPH00623E-200), *CXCL1* (GeneGlobe ID: PPH00696C-200) and *IL8* (GeneGlobe ID: PPH00568A-200) were obtained from the RT<sup>2</sup> qPCR Primer Assays (Qiagen, Hilden, Germany). The other primers were listed in Table 1.

TABLE 1 Primers used for RT-qPCR.

Transcript	Primer	Sequence (5'-3')	product size (bp)
<i>GAPDH</i>	GAPDH-F	CATGGGTGTGAACCATGA	104
	GAPDH-R	TGTCATGGATGACCTTGG	
<i>ACTB</i>	ACTB-F	CTGCCCTGAGGCACTC	197
	ACTB-R	GTGCCAGGGCAGTGAT	
<i>ABCA13</i>	ABCA13-f	AGGAGTGTGAGGCTCTTTGC	207
	ABCA13-r	TCAGGTGCTGTCCCTTGAAC	
<i>ABCB1</i>	ABCB1-f	GGAGGCCAACATACATGCCT	205
	ABCB1-r	CAGGGCTTCTTGGACAACCT	
<i>ABCG2</i>	ABCG2-f	CATCAACTTCCGGGGGTGA	266
	ABCG2-r	CCTGGTTGGTCGTCAGGAA	
<i>ALDH1A1</i>	ALDH1A1-f	TGTTAGCTGATGCCGACTTG	154
	ALDH1A1-r	TTCTTAGCCCGCTCAACACT	
<i>ALDH1A3</i>	ALDH1A3-f	GAGGAGATTTGGGGCCAGT	186
	ALDH1A3-r	GAGGGCGTTGTAGCAGTTGA	

(Continued)

TABLE 1 Continued

Transcript	Primer	Sequence (5'-3')	product size (bp)
<i>ALDH3A1</i>	ALDH1A3-f	GCAGACCTGCACAAGAATGA	186
	ALDH1A3-r	TGTAGAGCTCGTCTGCTGA	
<i>CD105</i>	ENG-f	TCACCACAGCGGAAAAAGGT	141
	ENG-r	GGACACTCTGACCTGCACAA	
<i>CD133</i>	PROM1-f	TTGCGGTAAAACTGGCTAAG	155
	PROM1-r	TGGGCTTGTCATAACAGGAT	
<i>CXCR4</i>	CXCR4-f	TGGGTGGTTGTGTCCAGTIT	80
	CXCR4-r	ATGCAATAGCAGGACAGGATG	
<i>DAB2IP</i>	DAB2IP-f	TGTCGCCCTCACTCTTCAAC	225
	DAB2IP-r	CGGCTGTATTGGAGAGGGTC	
<i>DNMT1</i>	DNMT1-f	GGCAGACCATCAGGATTCT	220
	DNMT1-r	ACCATGCTCTGCAGGCTTT	
<i>EZH2</i>	hEZH2-f	AGGACGGTCTCTTAACCAT	179
	EZH2-r	CTTGTGTTGCCTGTGCTT	
<i>KLF4</i>	KLF4-f	TCCCATCTTCTCCACGTTT	239
	KLF4-r	GGTCTCTCCGAGGTAGGG	
<i>LIN28A</i>	LIN28A-f	TTGGGCTTCTGTCCATGAC	124
	LIN28A-r	CCACTGCCTCACCTCTCTT	
<i>MTGR1</i>	MTGR1-f	CCTCTACCCCTGAATGGTGC	214
	MTGR1-r	GTGCAAGAAACAAGAGTCCGC	
<i>NANOG</i>	NANOG-f	TGTGTTCTCTCCACCAGC	205
	NANOG-r	CTTCTGCGTCACACATTGC	
<i>POU5F1</i>	POU5F1-f	CCCTGGGGTTCTATTGGG	231
	POU5F1-r	TCTCCAGGTTGCCTCTCACT	
<i>SALL4</i>	SALL4-f	GCTCTGTTAGGTACGGACGG	96
	SALL4-r	CTGGTTCCACACAACAGGGT	
<i>SOX2</i>	SOX-2-f	CATCACCCACAGCAAATGAC	258
	SOX-2-r	GCAAACCTCTGCAAGCTC	

## 2.5 Apoptosis assay

Apoptosis assay was executed by flow cytometry using Annexin V and 7-aminoactinomycin D (both from BD Biosciences). A total of  $4 \times 10^5$  cells were seeded in 25 cm<sup>2</sup> flasks and cultured with or without phytochemicals. After five days cells were harvested and resuspended in Annexin V binding buffer, stained with APC-conjugated Annexin V and 7-aminoactinomycin D (7-AAD) and incubated for 15 minutes in the dark at room temperature. Samples were measured within one hour using the FACSCalibur (Becton Dickinson, San Jose, CA, USA). For each sample, a minimum of  $1 \times 10^4$  cells were recorded. Data acquisition was done using BD CellQuest software (version 4.0.2) and analyzed using FlowJo (version 9.9.5; Tree Star Inc., Ashland, OR, USA).

## 2.6 Drug sensitivity assay

CellTiter Blue Cell Viability Assay (Promega, Madison, USA) was used to determine IC<sub>50</sub> of ICIs.  $1-5 \times 10^3$  cells per well were seeded in 96-well plates and incubated overnight at 37°C and 5% CO<sub>2</sub>. Then, the culture medium was exchanged with or without ICIs on the following day. After 48h, a volume of 20 µl CellTiter Blue Solution was added to each well, and the plates were incubated for two hours at 37°C and 5% CO<sub>2</sub>. Finally, the data were collected using the FLUOstar OPTIMA microplate reader (BMG LABTECH, Ortenberg, Germany) at 560 (20) nm excitation and 590 (10) nm emission. The wells without cells were again used as background controls, while the wells with cells but without treatment were the

control group. The OPTIMA software version 2.0 was utilized to collect and analyze the data, while the IC50 was calculated using the logit regression model.

## 2.7 Mixed lymphocyte tumor cell culture (MLTC)

After 7 days incubation CSCs were harvested, dissociated, treated with or without shikonin, seeded into a 24-well plate with  $5 \times 10^4$  cells per well and incubated overnight with CTL Test medium (Cellular Technology Ltd. Europe, Bonn, Germany). Next day, PBMCs were thawed and washed in CTL wash supplemented medium (45 ml RPMI 1640 medium, 5 ml CTL Wash (Cellular Technology Ltd. Europe)) and 50 U/ml Benzonase (Novagen Merck Biosciences, Darmstadt, Germany). PBMCs and ICIs were added and incubated for five days together with the CSCs with addition of a final concentration of 50 U/ml IL-2 (Proleukin, Novartis, Basel, Switzerland) after 48 hours.

## 2.8 Flow cytometry

Tumor cells were diluted to  $1-2 \times 10^6$  cells and incubated with the LIVE/DEAD<sup>TM</sup> Fixable Blue Dead Cell Stain (Molecular Probes, Life Technologies, ThermoFisher Scientific, Waltham, MA, USA) for 30 min at room temperature, then washed with PBS twice. To stain with the directly labeled monoclonal antibodies, cells with antibodies were incubated for 30 min at 4°C in the dark, then washed with PBS twice. For intracellular staining with the FoxP3 antibody, the FoxP3/Transcription Factor Staining Buffer Set (eBiosciences) was used, and staining was done for 60 min at 4°C in the dark and washed with the Perm buffer twice.

For lymphocyte staining the following directly conjugated mouse monoclonal antibodies were purchased from BD Biosciences: CD3 (clone UCHT1, FITC), CD4 (clone SK3, PE-Cy7), CD8 (clone RPA-T8, APC), CD25 (clone M-A251, PerCP-Cy5.5), CD127 (clone hIL-7R-M21, PE), respectively. For Treg analysis, the monoclonal antibody FoxP3 (clone PCH101, eFluor450; eBiosciences, Frankfurt, Germany) was used.

All measurements were accomplished using the LSRII flow cytometer (BD Biosciences). Data analyses were performed by FlowJo software (version 9.9.0; Tree Star Inc., Ashland, OR, USA).

## 2.9 Migration assay

A scratch wound healing assay was performed with 24-well  $\mu$ -plates containing small 2-well silicone inserts per well, which included a cell-free gap of 500  $\mu$ m as space for the cells to migrate (ibidi GmbH, Martinsried, Germany). 70  $\mu$ l of a cell suspension of  $4 \times 10^5$  cells/ml culture medium were added to each well of the small insert and incubated at 37°C and 5% CO<sub>2</sub> for at least 24 hours until a confluent cell monolayer was achieved. Then the inserts were removed and the cell layer was washed with PBS to remove cell debris and non-attached cells. After addition of new culture medium with or without the phytochemicals at different concentrations the

plate was incubated for another 15 hours and pictures were taken at several time points (0, 3, 6, 9, 12, and 15 h). The percentage of covered area of the gap was assessed and analyzed by the Automated Cellular Analysis System (ACAS, MetaVi Labs, Bottrop, Germany) based on the FastTrack AI image analysis algorithms.

## 2.10 Invasion assay

Invasion assay was performed using the Boyden Chamber system with transwell inserts (8.0  $\mu$ m pores; Falcon, Corning, New York, NY, USA) in 24-well plates coated with growth factor reduced Matrigel Basement Matrix (Corning; 30  $\mu$ g/100  $\mu$ l/insert). 30,000 cells were seeded in 250  $\mu$ l serum-free medium with or without phytochemicals onto the Matrigel-coated insert, and the lower chamber was filled with 750  $\mu$ l DMEM with 10% FCS. The cells were incubated at 37°C and 5% CO<sub>2</sub> for 48 hours. Then, the upper surface of the transwell membrane was gently wiped with a moistened cotton swab to remove Matrigel with not migrated cells. Invaded cells were fixed with 4% paraformaldehyde for 5 minutes, stained with 1% crystal violet for 1 minute, washed twice with water, and dried on a paper towel at room temperature. Finally, pictures were taken with a digital camera (three fields per insert), and cells were counted using the Fiji Image J software.

## 2.11 NanoString analysis

Gene expression analysis was performed using the human nCounter<sup>®</sup> PanCancer-Immune-Profilng-Panel-(Human) (NanoString Technologies, Seattle, WA, USA) according to the manufacturer's protocol with 100 ng of total RNA from corresponding cells. Downstream analysis in terms of heatmaps and volcano plot were performed using nSolver 4.0.

## 2.12 Target gene prediction

The three-dimensional (3D) structure of shikonin was acquired from the PubChem database (<https://pubchem.ncbi.nlm.nih.gov/>). The SDF file of the 3D structure was uploaded to the PharmMapper database (<http://www.lilab-ecust.cn/pharmmapper/>) for potential target gene prediction. Top 100 of CTLA-4-related genes based on the ccRCC samples of the TCGA database were obtained from GEPIA (<http://gepia.cancer-pku.cn/index.html>). Protein-protein interaction (PPI) network was constructed by STRING database with a confidence score > 0.4, followed by reconstruction with Cytoscape version 3.6.1. Nodes with confidence of interactive relationship larger than 0.95 were used for building the network.

## 2.13 Gene expression in tumor and normal tissue

Transcriptome RNA-seq data of 611 ccRCC cases (KIRC, normal samples: 72 cases; tumor samples: 539 cases) were



downloaded from the TCGA database. Significantly differently expressed genes in ccRCC samples were displayed in a volcano plot from R software's package limma (<https://www.R-project.org>).

The UALCAN portal (<http://ualcan.path.uab.edu/analysis-prot.html>) was used to conduct mRNA and protein expression analysis of the CPTAC (Clinical Proteomic Tumor Analysis Consortium) dataset [49]. Herein, we explored the expression level of total protein of VCAM1 between primary tumor and normal tissues, respectively, by entering "VCAM1".

We used the "Expression Analysis-Box Plots" module of the GEPIA2 (Gene Expression Profiling Interactive Analysis, version 2) web server (<http://gepia2.cancer-pku.cn/#analysis>) to obtain box plots of the expression differences between these tumor tissues and the corresponding normal tissues of the GTEx (Genotype-Tissue Expression) database [48], upon the settings  $p$ -value cutoff = 0.01, log2FC (fold change) cutoff = 1, and "Match TCGA normal and GTEx data".

Immunohistochemistry pictures of VCAM1 were downloaded from the human protein atlas ([www.proteinatlas.org](http://www.proteinatlas.org)) to confirm the protein expression.

## 2.14 Prognosis analysis

Survival analysis of ccRCC patients was obtained from the website-GEPIA (<http://gepia.cancer-pku.cn/index.html>). Kaplan-Meier method was used to calculate the cumulative event (death) rate, according to the duration from the date of operation to the date of death as the outcome variable. Survival curves stratified by risk factors were operated by log-rank test, the  $p$ -values < 0.05 were considered to show the statistical significance. The median group cutoff was median survival times of the groups. Multivariable COX regression was shown in the forest plot, which was conducted by the R statistical software language with package survival and survminer.

## 2.15 Tumor immunological signatures

CIBERSORT computational method was applied for estimating the profile of tumor-infiltrating cell (TIC) subtypes in ccRCC tumor samples, followed by quality filtering resulting in 539 tumor samples with  $p < 0.05$  for display in a plot, which was conducted by R software.

TIMER (<https://cistrome.shinyapps.io/timer/>) was used to determine the correlation with the infiltration of the immune cells (neutrophils, macrophages, dendritic cells, B cells, and CD4/CD8 T cells) in the TME upon the module of somatic copy number alteration (SCNA) module in ccRCC.

The data from UCSC database (<https://xenabrowser.net/>) was used to perform the ESTIMATE score and immunophenoscore (IPS) analysis. R package named ESTIMATE was operated to conduct the stromal, immune, and ESTIMATE scores in ccRCC; package-IOBR was utilized to value the MHC (Antigen processing), CP (checkpoint), EC (effector cells), SC (suppressor cells), average Z-score (AZ) and immunophenoscore (IPS) in ccRCC.

## 2.16 VCAM1-related genes

The correlation between 60 genes for immune checkpoint genes as well as 44 genes for RNA modifications modulate genes and VCAM1 were studied based on the UCSC database (<https://xenabrowser.net/>). The correlations were calculated by the Pearson correlation coefficient.

GeneMANIA online database tool (<http://www.genemania.org>) was applied for VCAM1-related gene analysis and its protein-protein interaction (PPI) analysis, which includes physical interaction, co-expression, co-localization, gene enrichment analysis, genetic interaction and website prediction.

## 2.17 Gene Set Enrichment Analysis (GSEA)

KEGG gene sets (c2.cp.kegg.v7.0.symbols.gmt) were downloaded from the Molecular Signatures Database (<https://www.gsea-msigdb.org/gsea/msigdb/genesets.jsp>) as target sets with which GSEA was performed by the software gsea-4.1. For analysis, gene set permutations were done 1000 times to obtain a normalized enrichment score, which was used for sorting pathway enrichment. NOM  $p < 0.05$  and false discovery rate (FDR)  $q < 0.06$  were considered as significant.

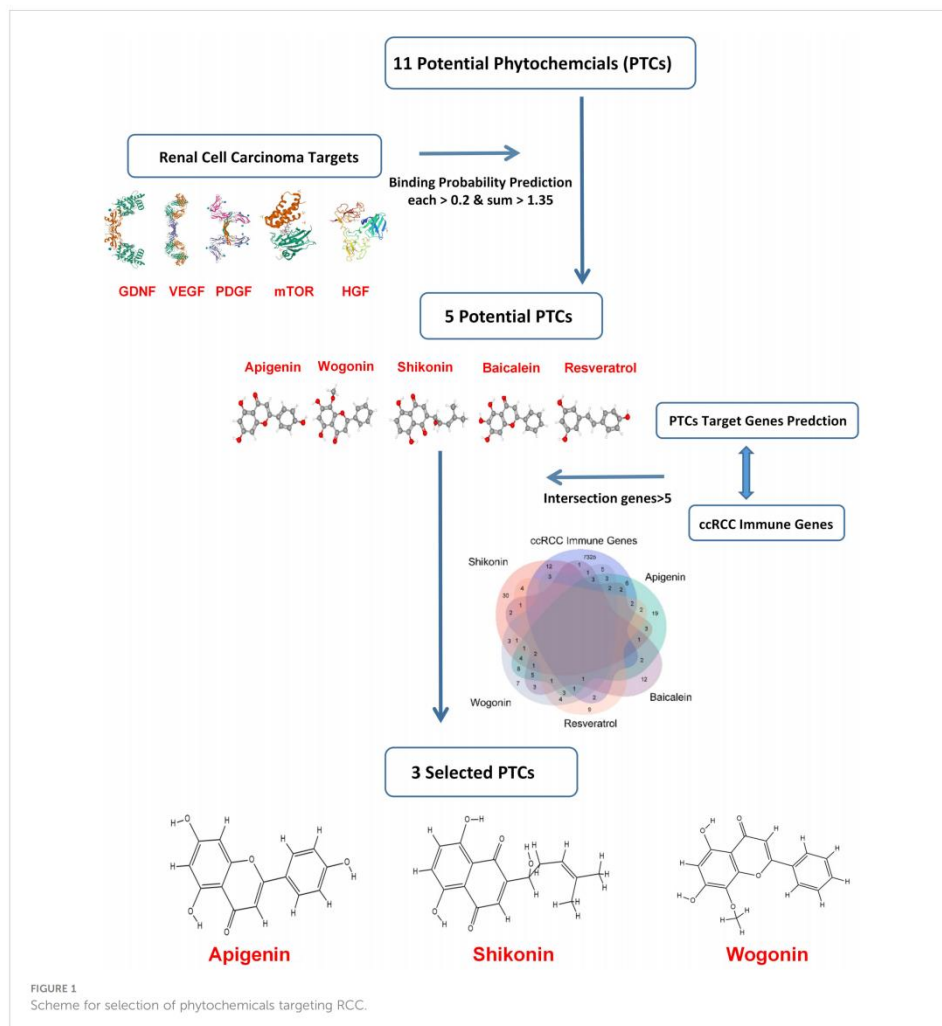
# 3 Results

## 3.1 Prediction of potential RCC-targeting phytochemicals

Based on previous research, the RCC therapeutic target proteins taken for the study were VEGF (vascular endothelial growth factor), HGF (hepatocyte growth factor), PDGF (platelet-derived growth factor), GDNF (glial cell derived neurotrophic factor), and mTOR (mammalian target of rapamycin) (24–27). Then the binding probability between 11 potential RCC-targeted phytochemicals and five RCC therapeutic target proteins was predicted, and only the binding probability value for each protein target above 0.2 and the sum value for five target proteins above 1.35 could be moved to the next selection. Finally, taking the intersection of five phytochemicals' potential target genes and ccRCC immune-related genes, three phytochemicals: shikonin, apigenin, and wogonin had more than five of the intersection genes and were decided for further testing in this study (Figure 1).

## 3.2 Shikonin, apigenin and wogonin enhance the apoptosis rate and inhibit migration and invasion of adherent cell lines and CSCs

SKRC-17 and RCC-53 and the corresponding CSCs were treated with increasing doses of the PTCs according to the IC50



values tested in our former study ( $0.5 \times IC_{50}$ ,  $IC_{50}$ , and  $2 \times IC_{50}$ ) for 5 days, and the results demonstrate a dose-dependent effect of the PTCs on the apoptosis (Figure 2A; Supplementary Figure S1) (15). The data showed that SKRC-17 CSCs and RCC-53 CSCs were much less sensitive to the phytochemicals than the corresponding adherent cells in apigenin and wogonin groups. It supported the point that cancer stem cells were a special cell population like drug-resistant cells. Furthermore, since migration and invasion ability are two important biological characteristics, we evaluated the effect of phytochemicals on the migration and invasion of SKRC-17, RCC-53 and their corresponding sphere cells. For the invasion assay, the cells were treated again with different concentrations of the PTCs

( $0.5 \times IC_{50}$ ,  $1 \times IC_{50}$ , and  $2 \times IC_{50}$ ) for 48 h. The number of invaded cells was significantly decreased in the adherent cell lines and even in the corresponding CSCs for the apigenin and shikonin group (Figure 2B; Supplementary Figure S2). For the migration assay the cells were treated with a dose of  $0.5 \times IC_{50}$ . Pictures were taken at different time points (0 h, 3 h, 6 h, 9 h, 12 h and 15 h). The percentage of covered area of the gap was assessed and analyzed by the Automated Cellular Analysis System based on the FastTrack AI image analysis algorithms (Figure 2C; Supplementary Figure S3). Shikonin had the highest potential and was able to inhibit both the migration and invasion remarkably in the cell's lines and corresponding CSCs.



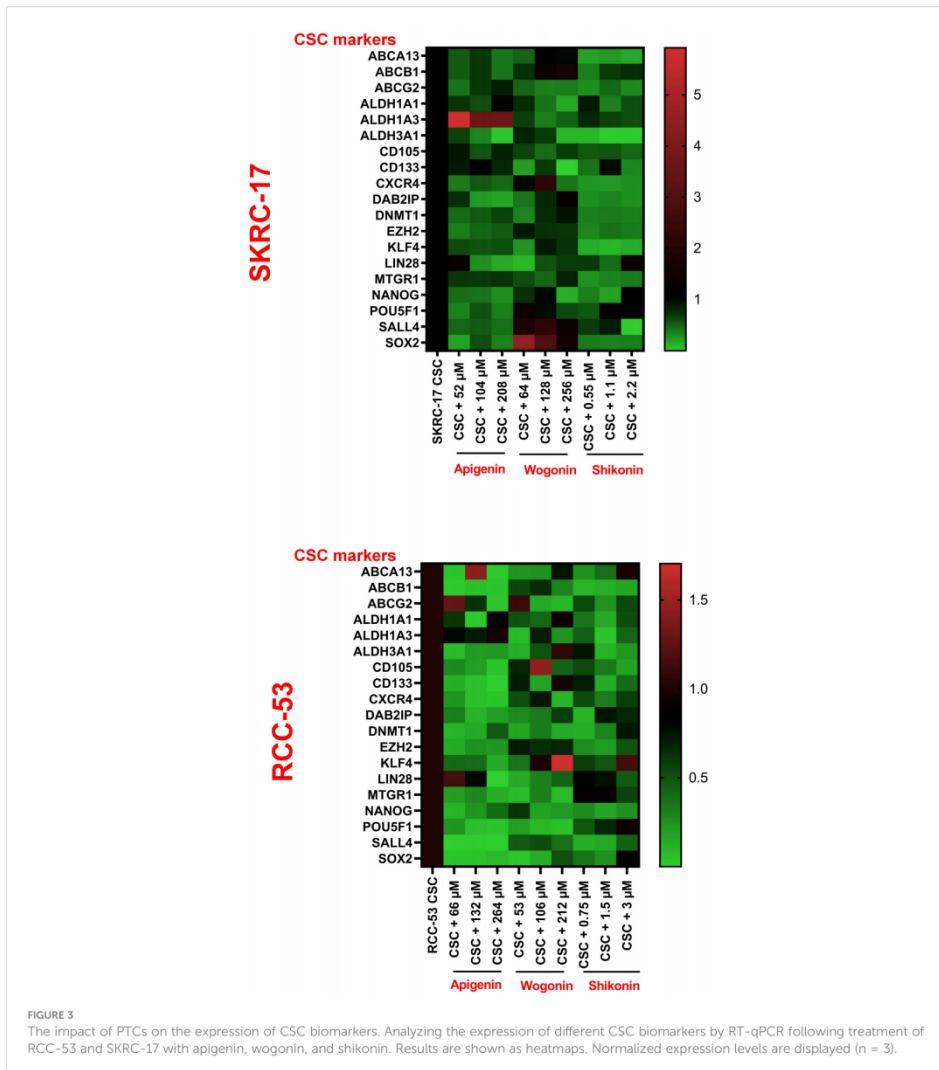


### 3.3 Phytochemicals regulate the expression of CSC biomarkers

To further determine the therapeutic strategies against CSC, 19 potential RCC CSC markers were selected. The CSCs of RCC-53 and SKRC-17 were treated with apigenin, wogonin, and shikonin in a concentration of  $0.5 \times IC_{50}$ ,  $1 \times IC_{50}$ , and  $2 \times IC_{50}$ . The mRNA expression was tested by RT-qPCR. Based on the results, apigenin showed downregulation of most of the markers in RCC-53 CSCs. Shikonin showed downregulation of most of the markers in SKRC-17 CSCs (Figure 3).

### 3.4 The impact of the combination ICI and shikonin on T cell subpopulations co-cultured with treated RCC adherent cells or CSCs

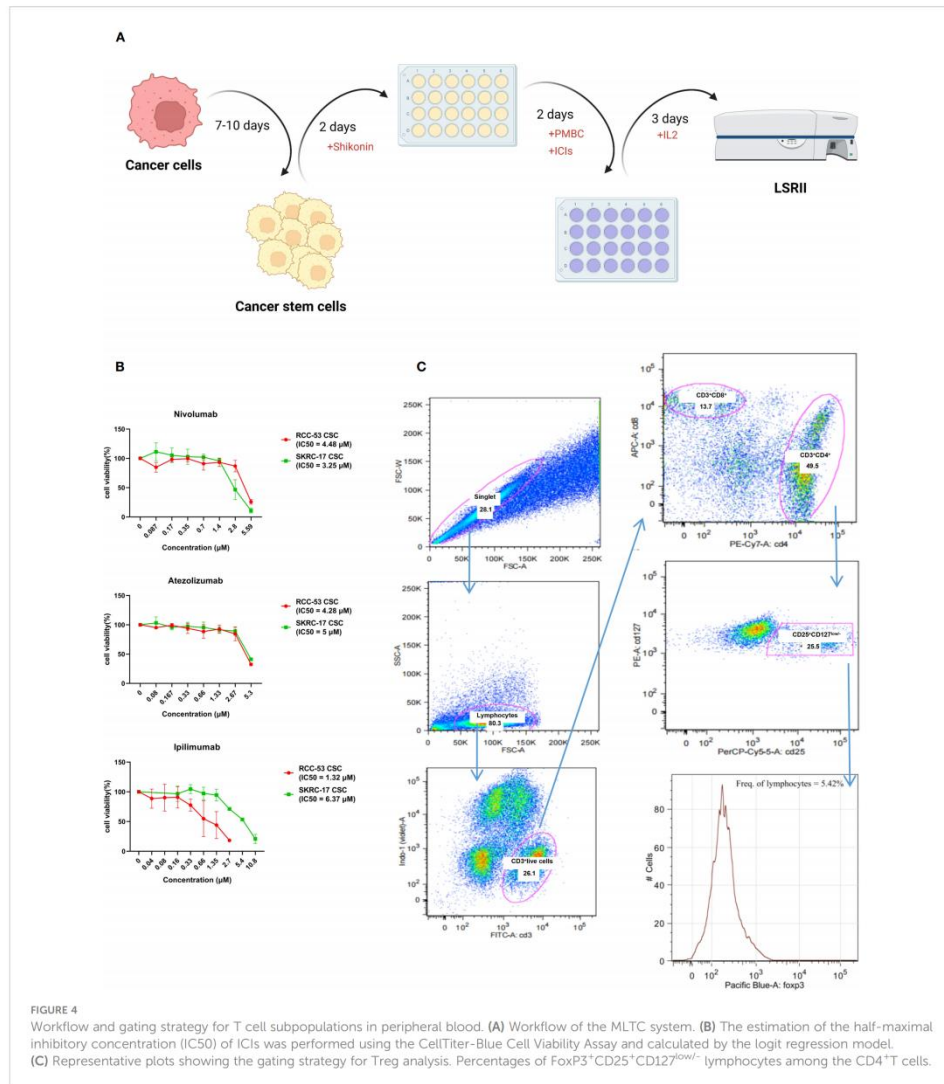
Three ICIs (nivolumab, atezolizumab and ipilimumab) were selected to analyze the phenotype of PBMC in healthy donors co-cultured with RCC adherent cells or CSCs after treatment with or without shikonin. To guide the selection of treatment concentrations for ICIs, the cell viability was performed to determine the respective  $IC_{50}$  values of ICIs as shown in

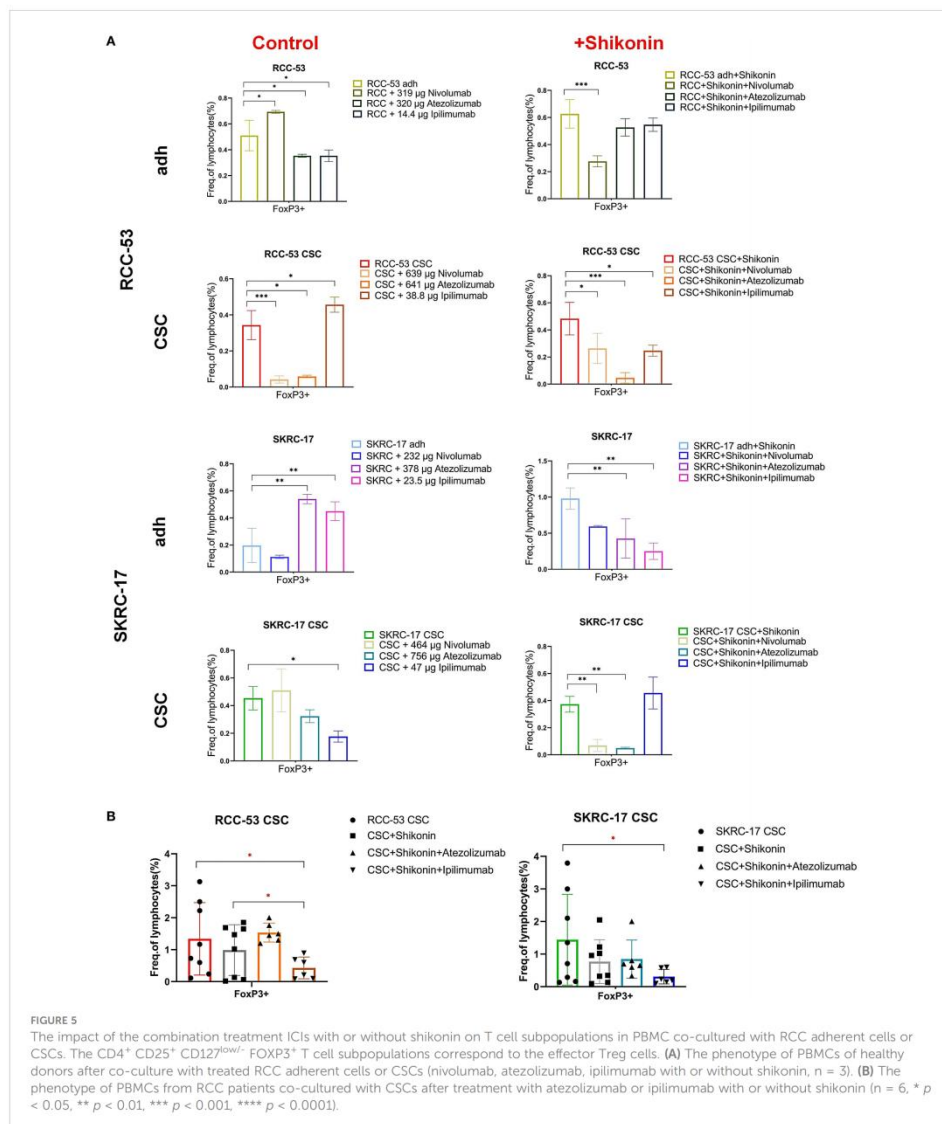


**Figure 4B.** The co-culture system is shown in **Figure 4A** and the gating strategy for the T cell subpopulations is shown in **Figure 4C**. The CD4<sup>+</sup>, CD25<sup>+</sup>, CD127<sup>low</sup>, FOXP3<sup>+</sup> T cell subpopulation corresponds to the effector Treg cells. Based on the results, the percentage of the FoxP3<sup>+</sup> Treg subpopulation was significantly decreased in the ICI group as compared to the group without treatment. Ipilimumab in SKRC-17 CSCs and RCC-53, atezolizumab in RCC-53 and RCC-53 CSCs as well as nivolumab in RCC-53 CSCs. After combination with shikonin, the percentage

of the FoxP3<sup>+</sup> Treg subpopulation was significantly decreased compared to the group without treatment in following groups: ipilimumab in SKRC-17 adherent cells and RCC-53 CSC, atezolizumab in SKRC-17 adherent cells, SKRC-17 CSCs, and RCC-53 CSCs, nivolumab in RCC-53 adherent cells, RCC-53 CSCs as well as in SKRC-17 CSCs (**Figure 5A**).

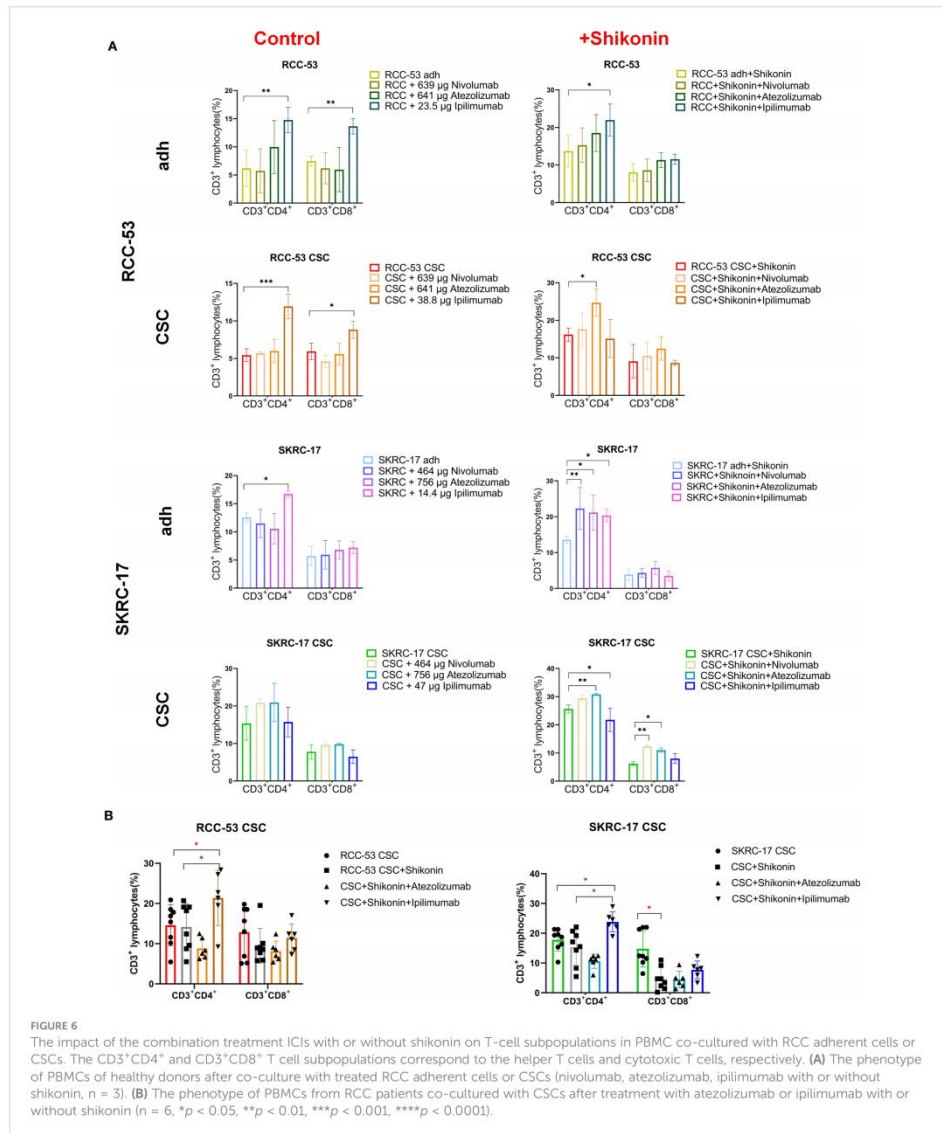
Moreover, ipilimumab significantly enhanced the CD3<sup>+</sup>CD4<sup>+</sup> T cells in adherent cell lines of SKRC-17 and RCC-53 as well as in RCC-53 CSCs. Also the CD3<sup>+</sup>CD8<sup>+</sup> T cells in RCC-53 adherent





cells and RCC-53 CSCs were enhanced. In combination with shikonin, ipilimumab significantly enhanced CD3<sup>+</sup>CD4<sup>+</sup> T cells in adherent cell lines of SKRC-17 and RCC-53, atezolizumab significantly elevated the CD3<sup>+</sup>CD4<sup>+</sup> T cells population in SKRC-17 adherent cells and its CSCs as well as in RCC-53 CSCs. The CD3<sup>+</sup>CD8<sup>+</sup> T cell population was enhanced by atezolizumab in SKRC-17 CSCs, and by nivolumab in SKRC-17 CSCs (Figure 6A).

Although the results in other groups may not exhibit consistent trends, the focus on the CSCs group provides valuable insights for determining the next steps in the study and guiding further experiments. So, atezolizumab and ipilimumab were selected in combination with shikonin for further testing in MLTCs with PBMC from RCC patients and CSCs from SKRC-17 and RCC-53. Ipilimumab again suppressed the FoxP3<sup>+</sup> Treg



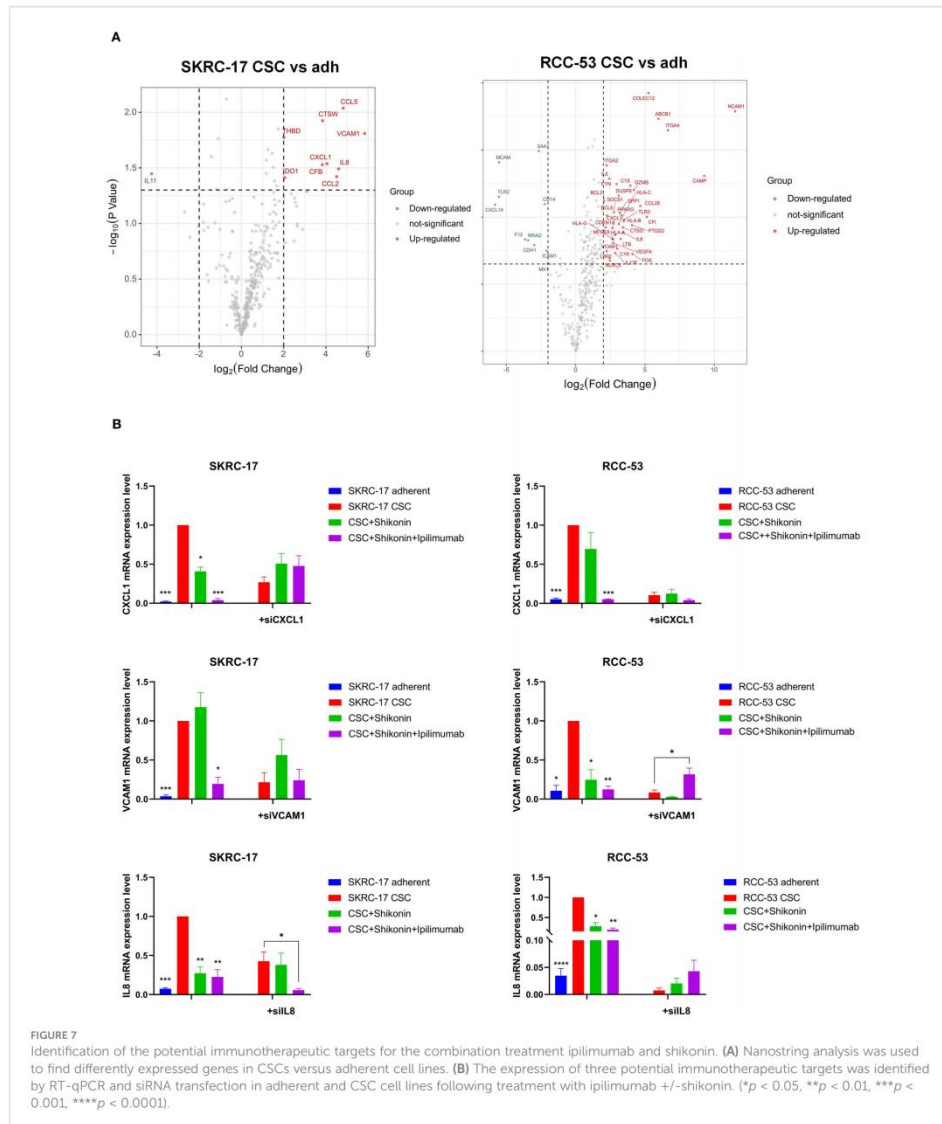
subpopulation and enhanced the CD3<sup>+</sup>CD4<sup>+</sup> T cells. Furthermore, compared with the single shikonin treatment group, ipilimumab combined with shikonin significantly decreased the FoxP3<sup>+</sup> Treg subpopulation in RCC-53 and enhanced the CD3<sup>+</sup>CD4<sup>+</sup> T cells population in SKRC-17 and RCC-53 (Figures 5B, 6B). Based on this result, the selection of ipilimumab guided the subsequent steps of our study.

### 3.5 Identification of potential immunotherapeutic targets

To further understand the relative immunotherapeutic targets and novel potential CSC markers in RCC, a NanoString analysis was done using the adherent cell lines and their corresponding CSCs without treatment, with treatment with shikonin alone as well as with shikonin

combined with ipilimumab. Three common new CSC markers (IL-8, CXCL1 and VCAM1) were identified as promising immunotherapeutic targets due to the fact, that they were significantly higher expressed in each treatment group (Figure 7A). RT-qPCR analysis confirmed the higher expression of these three markers in RCC-53 CSCs and SKRC-17 CSCs compared to the adherent cell lines (Figure 7B). Furthermore, the combined treatment with shikonin and ipilimumab significantly inhibits

the mRNA expression of *IL-8*, *CXCL1*, and *VCAM1*, verified by siRNA technology (Figure 7B). Moreover, the potential signaling pathways regulated by the different treatments groups were also analyzed using the NanoString analysis system: immune-related signaling pathway, cell cycle, macrophage functions and senescence pathways in RCC-53 CSC cell lines; NK cell functions, B-cell functions, interleukin pathways in SKRC-17 CSC cell lines (Supplementary Figure S4).





### 3.6 Network of potential target genes between combination treatment and *IL-8*, *CXCL1* and *VCAM1*

To further uncover the potential pharmacological mechanisms of various treatments, *IL-8*, *CXCL1* and *VCAM1* as well as predicted target genes of ipilimumab and shikonin were analyzed in networks. A total of 38 genes were predicted to be direct targets of shikonin and 55 genes were predicted to be targets of ipilimumab, of which 19 genes were found that directly target shikonin and have a connection with ipilimumab's target genes. Interactions between the potential target genes and *IL-8*, *CXCL1* and *VCAM1* are shown in Figure 8. *IL-8*, *CXCL1*, and *VCAM1* are connected with each other, *IL-8* is connected with ipilimumab and shikonin potential target genes, and *CXCL1* and *VCAM1* are connected with shikonin potential target genes.

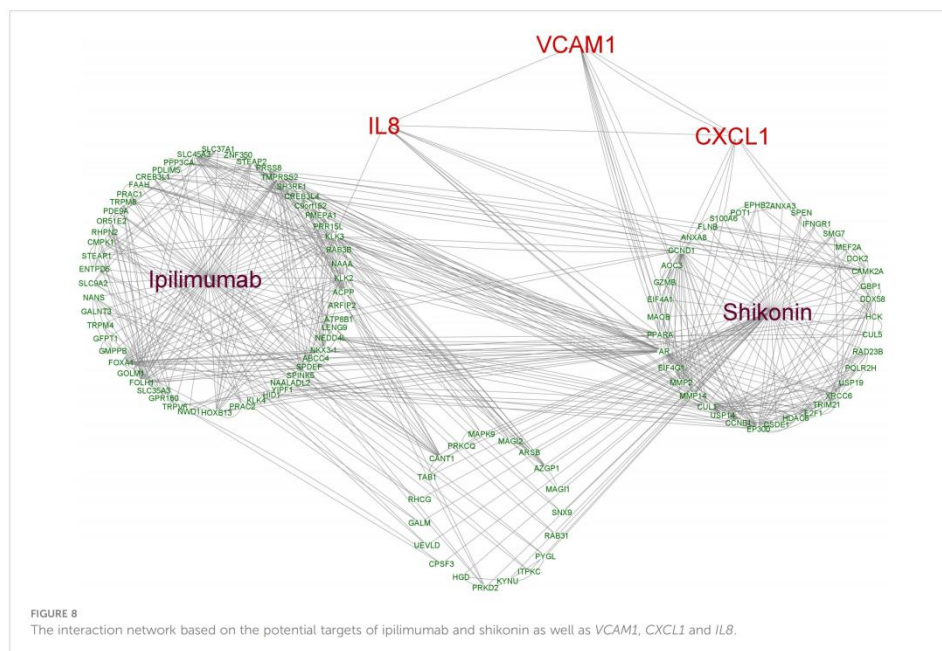
### 3.7 VCAM1 expression in ccRCC patients

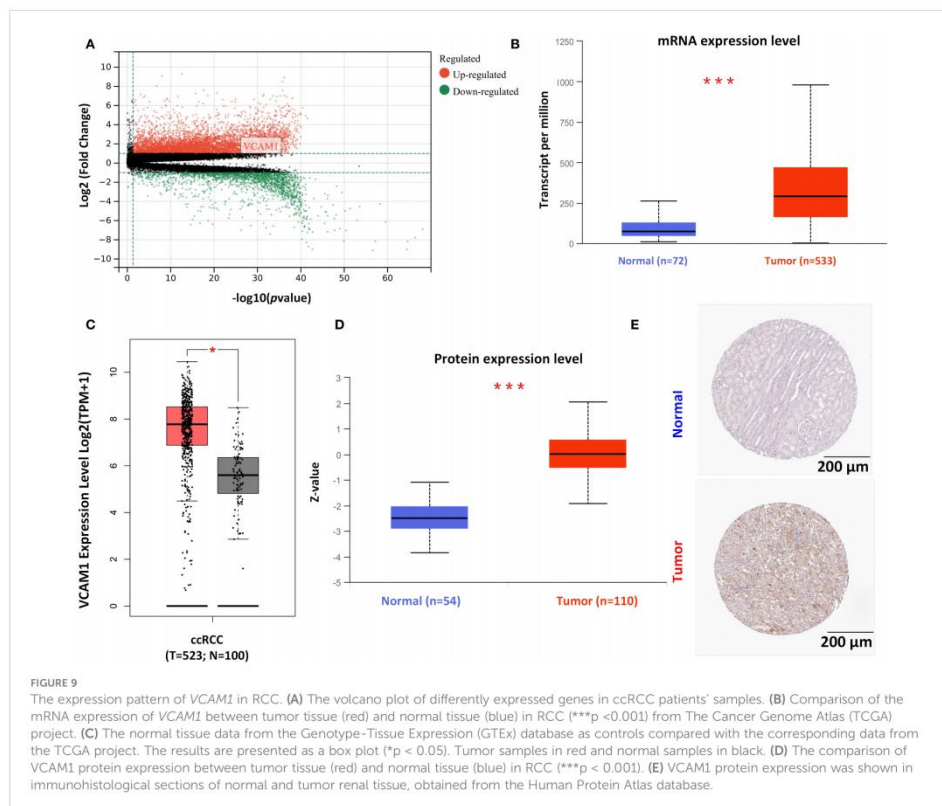
After identifying *VCAM1* as a promising immunotherapeutic target in RCC through NanoString analysis, further detailed analyses were performed to investigate its potential in the treatment of RCC. All significantly differently expressed genes in ccRCC are shown in Figure 9A, of which *VCAM1* is highly expressed in the ccRCC data set. Significant expression differences of *VCAM1* on the mRNA (Figure 9B) and protein level (Figure 9D)

between tumor and normal tissues were found in ccRCC patients. Because not enough normal tissue samples were available in the TCGA database, normal tissues from the GTEx data set were used as control in Figure 9C. Moreover, the *VCAM1* protein expression between normal samples and kidney cancer samples was further validated using The Human Protein Atlas. An example is shown in Figure 9E.

### 3.8 Correlation of *VCAM1* expression with the survival and clinical characteristics of ccRCC patients

The clinical characteristics of ccRCC patients including stage, grade and TNM classification, gender and age were grouped into *VCAM1* high and low expression according to the median expression level. Multivariable Cox regression analysis showed that several clinical characteristics including age, grade, stage and N classification could be an independent prognostic factor to assess outcomes for ccRCC patients (Figure 10A). Based on the log-rank test in GEPIA, high mRNA expression of *VCAM1* ( $p = 0.041$ ) was significantly associated with a better prognosis in ccRCC patients, as shown for overall survival (Figure 10B). In addition, after normalization by the *CTLA-4* (cytotoxic T-lymphocyte-associated Protein 4) gene expression (= ipilimumab target protein), lower expression of *VCAM1* mRNA was significantly associated with better prognosis in ccRCC patients ( $p = 0.012$ ). For disease free





survival, high expression of *VCAM1* mRNA) was significantly associated with better prognosis of ccRCC patients ( $p = 0.035$ ). After normalization by the CTLA-4 gene expression, low *VCAM1* mRNA expression was significantly associated with better prognosis in ccRCC patients ( $p = 0.008$ ) (Figure 10B).

### 3.9 Correlation of *VCAM1* expression with immune signatures in ccRCC patients

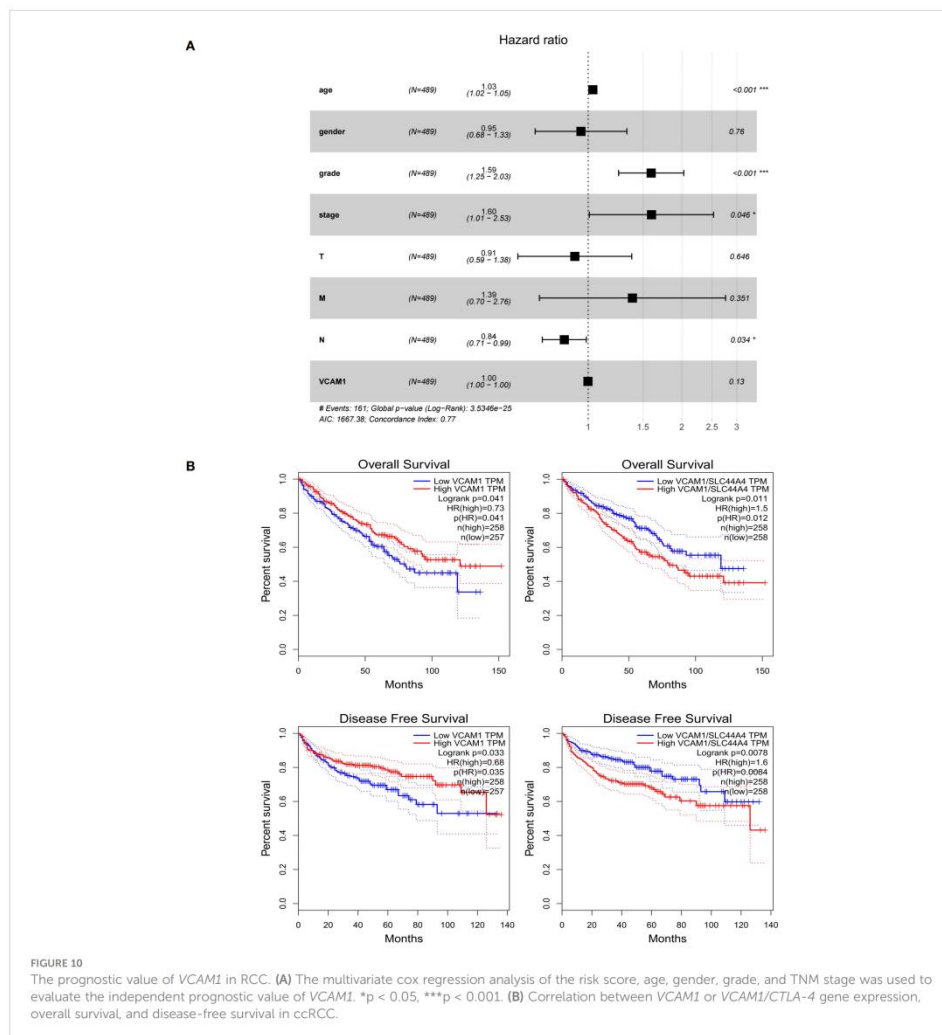
To explore a potential correlation between *VCAM1* expression and the ccRCC tumor microenvironment (TME), the proportion of tumor-infiltrating immune cell (TIC) subsets was determined, and eight types of TICs had different frequencies in *VCAM1* high versus low tumors. Follicular helper T cells, monocytes, CD8 T cells, M1 macrophages, eosinophils, and resting dendritic cells were more prevalent in *VCAM1* high tumors than in *VCAM1* low tumors, while M0 macrophages and resting NK cells were more abundant in *VCAM1* low tumors (Figure 11). Particularly, the copy number variants (CNV) of *VCAM1* CNV showed significant correlations with the infiltrating of B cells, CD8<sup>+</sup> T cells, CD4<sup>+</sup> T cells,

macrophages, neutrophils, and dendritic cells (Figure 12A). Moreover, based on the TCGA plus GTEx database, significant correlations were found between *VCAM1* expression and the StromalScore, ESTIMATEScore, and ImmuneScore (Figure 12B). In 2017, Charoentong et al. developed an algorithm named immunophenoscore (IPS), which can predict the efficiency of anti-CTLA-4 and anti-PD-1 antibody therapies including MHC (Antigen processing), CP (checkpoint), EC (effector cells), and SC (suppressor cells) (28). We evaluated the differences in MHC, EC, SC, CP, ICS and average Z-score (AZ) with *VCAM1* expression. *VCAM1* expression was significantly positively correlated with the MHC, EC, and immunophenoscore (IPS), and negatively correlated with the SC and CP scores (Figure 12C).

### 3.10 Correlation of *VCAM1* expression with associated genes and pathways

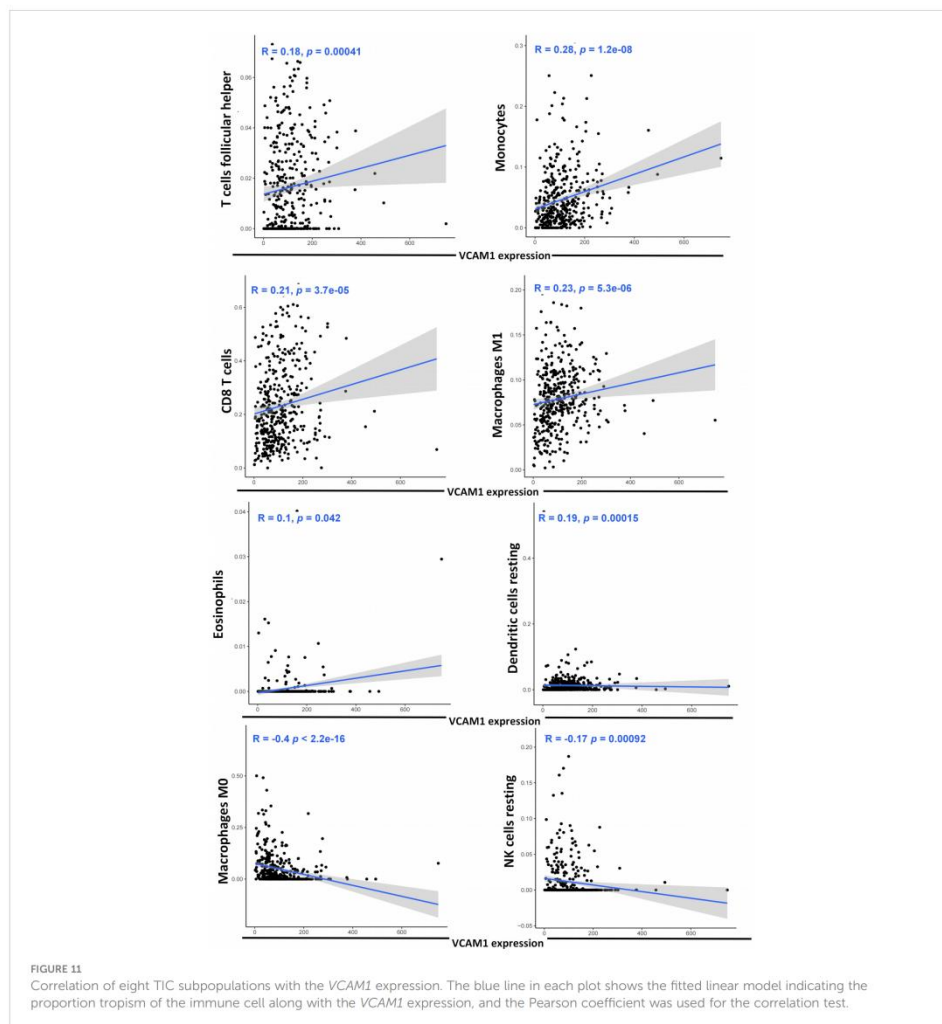
The relationship between *VCAM1* gene expression and a total of 60 immune checkpoint genes (inhibitory (24) and stimulatory (29)) and 44 RNA modifications modulate genes (N1-





methyladenosine (m1A) (10), 5-methylcytosine (m5C) (13) and N 6-methyladenosine (m6A) (21) in ccRCC patients was analyzed (Figures 13A, B). We found that *VCAM1* expression showed a positive correlation with several immune checkpoint genes, for example *CTLA4*, *HAVCR2*, *IL10*, *CXCL9* and *CXCL10*. Thirty-four RNA modifications modulate genes were significantly correlated with *VCAM1* expression. Furthermore, the top 20 *VCAM1*-related genes from the GeneMANIA online tool were analyzed by the protein-protein interaction (PPI) network in Figure 14A. Finally, we used GSEA that included related genes in

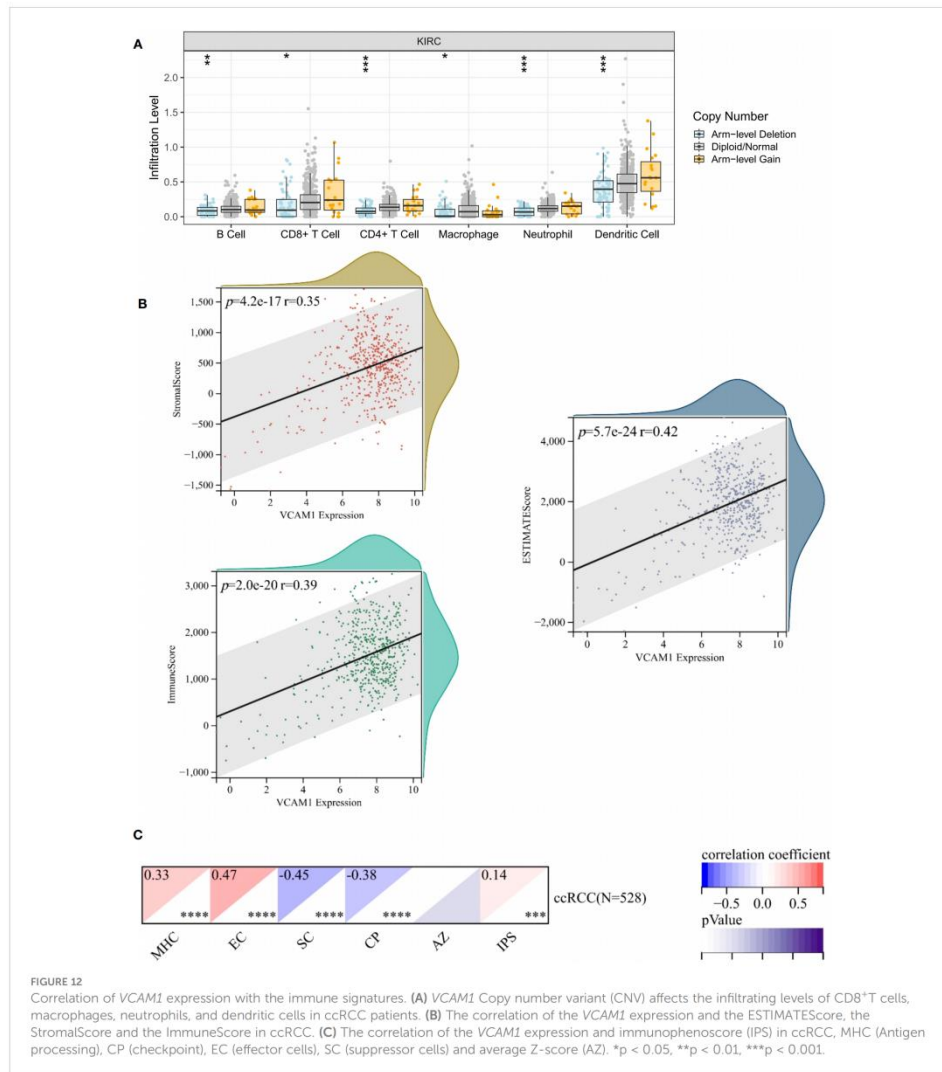
human to find general enrichment trends and to identify KEGG enrichment of different expression levels of *VCAM1* in ccRCC patients (Figure 14B). Autoimmune thyroid disease, B cell receptor signaling pathway, natural killer cell mediated cytotoxicity, rig I like receptor signaling pathway, T cell receptor signaling pathway, toll-like receptor signaling pathway were enriched in the high *VCAM1* expression group. Calcium signaling pathway, cardiac muscle contraction, dilated cardiomyopathy, hypertrophic cardiomyopathy (HCM), and neuroactive ligand-receptor interaction were enriched in the low expression group.



## 4 Discussion

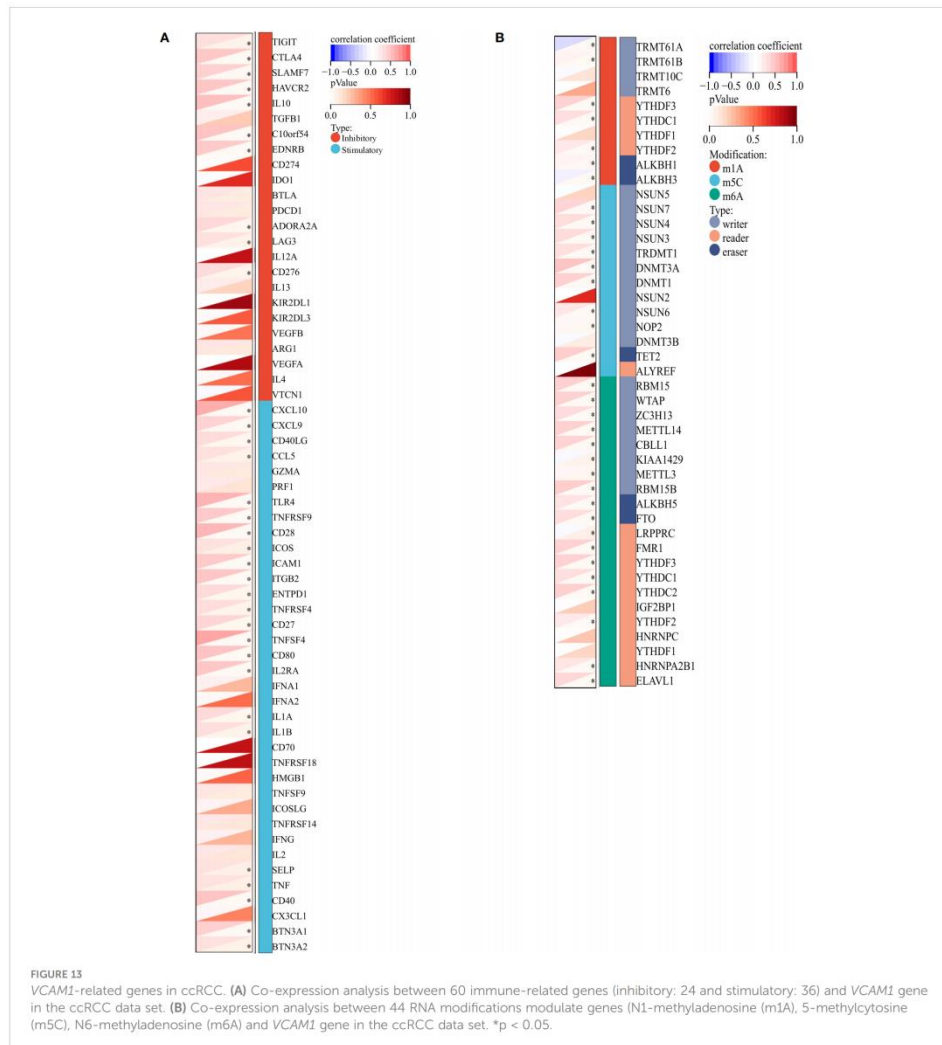
Over 30% of ccRCC patients already have distant metastases at the time of initial diagnosis and most of them are not sensitive to chemotherapy and radiation therapy. Currently, angiogenesis inhibition with TKIs combined with the immune checkpoint inhibitor has revolutionized the treatment landscape of ccRCC patients with metastases. However, higher objective response rate and survival rates were seen in immune checkpoint positive patients and those in the intermediate-poor risk subgroups of the International mRCC Database Consortium (IMDC). Thus,

additional therapies or promising additives to the current therapeutic strategies for those non-responders are urgently needed (1, 2). The presence of CSCs was discussed to be one of the causes for resistance to standard treatment strategy due to its strong abilities of self-renewal and differentiation (10, 13). Moreover, to target CSCs, some phytochemicals had a high potential to uncover the molecular mechanisms of metastatic initiation and dynamics of RCC CSCs. Thus, the combination therapy strategy between phytochemicals and ICIs was came up to improve the therapy management of RCC in this study. The key findings can be summarized as follows: (1) Shikonin,



wogonin, and apigenin were promising phytochemicals for targeting the RCC CSCs among 11 phytochemicals tested, which showed a substantially higher binding probability prediction score and more intersection genes with ccRCC immune-related genes, respectively. (2) Shikonin was the most promising PTC, which can significantly inhibit the ability of migration and invasion as well as increasing apoptosis of CSCs. (3) Among the three ICIs tested, the combination treatment of shikonin with ipilimumab confirmed a significantly decrease of

the frequency of CD4<sup>+</sup> CD25<sup>+</sup> CD127<sup>low/-</sup> FOXP3<sup>+</sup> Treg in PBMC of ccRCC patients as well as an enhancement of the CD3<sup>+</sup>CD4<sup>+</sup> T cells, compared to the group without treatment. (4) *VCAM1*, *CXCL1* and *IL8* were identified as novel CSC markers that are strongly related to the combination therapy strategy. (5) The expression of *VCAM1* was statistically higher both at the mRNA and protein level, and was significantly correlated with the clinical characteristics and several immune-related signatures in ccRCC patients.



Based on our previous research, the influence of shikonin depends on the RCC cell line being investigated. For example, shikonin was proven to significantly trigger necrosis and apoptosis as well as enhances autophagy via the elevation of ROS (reactive oxygen species) level and p38 activity in different RCC cell lines like Caki-1 and ACHN cells in proportion to its concentration (29). Consistently, recent research in 2022 showed that shikonin has a strong ability to induce apoptosis and necroptosis of parental and sunitinib-resistant RCC cell lines (30). These findings suggested that shikonin may be an additional option for the treatment of patients

with advanced and therapy resistant RCC. More recently, a new study conducted in 2023 showed that shikonin significantly reduces PD-L1 expression specifically on macrophages, without affecting PD-1 expression on T cells, both *in vivo* and *in vitro*. Furthermore, the study revealed that shikonin's mechanism of action involves the attenuation of PD-L1 expression on macrophages by downregulating phosphorylation and nuclear import of PKM2 (pyruvate kinase M2), which was found to bind to the PD-L1 promoter, thereby influencing its expression (31). Unfortunately, so far not so many combination treatment studies between shikonin

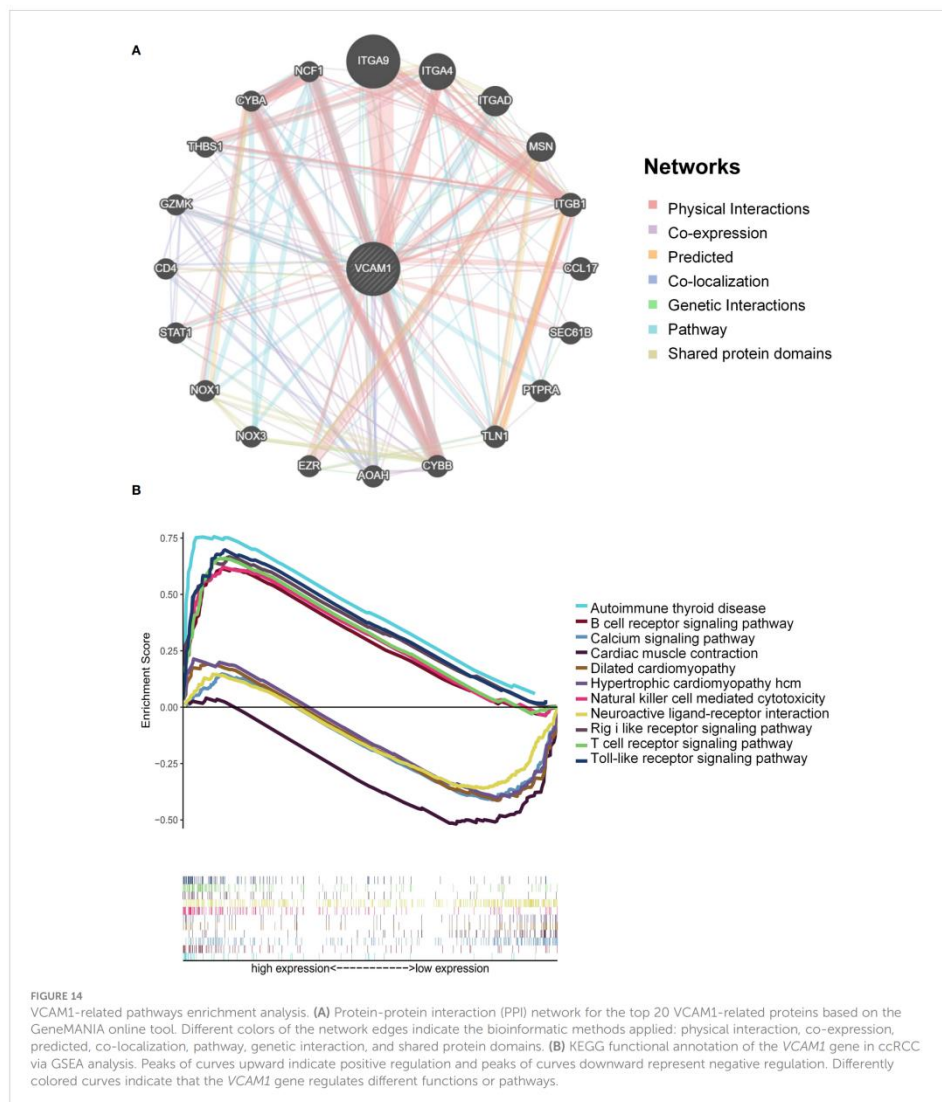


**FIGURE 14** VCAM1-related pathways enrichment analysis. **(A)** Protein-protein interaction (PPI) network for the top 20 VCAM1-related proteins based on the GeneMANIA online tool. Different colors of the network edges indicate the bioinformatic methods applied: physical interaction, co-expression, predicted, co-localization, pathway, genetic interaction, and shared protein domains. **(B)** KEGG functional annotation of the VCAM1 gene in ccRCC via GSEA analysis. Peaks of curves upward indicate positive regulation and peaks of curves downward represent negative regulation. Differently colored curves indicate that the VCAM1 gene regulates different functions or pathways.

and immune therapy were explored. In 2019, Huang et al. found that the synergistic combination of shikonin and the suppressor of PD-L1 (JQ1) as well as the treatment potency of the PD-L1 checkpoint blockage mannosylated lactoferrin nanoparticulate system could reprogram the tumor immune microenvironment and metabolism via tumor-associated macrophages and glucose metabolism (32). This result revealed that the poly-pharmacological

activities of shikonin were ideal for a combined immunotherapeutic application. Particularly, the suppressive effect of glucose metabolism by shikonin leveraged a positive regulation of the cancer-immunity circle. More and more combination strategies with phytochemicals and immune checkpoint inhibitors were investigated and demonstrated an effective strategy for cancer immunotherapy to date (33). For example, the combination of



curcumin and anti-CTLA-4 therapy enhanced the anti-tumor effects via inhibition of PD-L1 and COP9 signalosome 5 compared to the single treatment group (34). Icaritin plus anti-PD-1/CTLA-4 treatment reduced the growth of melanoma cell line in C57BL/6 mice by 65% compared to anti-PD-1/CTLA-4 treatment alone (34.2%) (35). Collectively, phytochemicals showing anti-tumor effects in combination with immune checkpoint inhibitors are a promising therapeutic option for clinical trials in the future.

Immune recognition of therapeutic targets is essential for the immune response against tumors, also avoiding severe adverse effects. VCAM1, IL8 and CXCL1 were identified in ipilimumab and shikonin treatment as potential immunotherapeutic targets and as novel RCC CSC markers in this study. Similarly, the concentration of these factors were altered via ipilimumab plus bevacizumab treatment in patients with metastatic melanoma (36), which confirms the function as immunotherapeutic targets in ICI combination therapy. VCAM1 as one of adhesion molecules contributes to critical physiologic functional roles in cancer metastasis and therapy resistance (37), and is the only one showing a significantly higher expression level in RCC tissues than in normal tissues both at protein and mRNA level. Currently, the specific functional role of VCAM1 in RCC is less explored, with data pointing towards its overexpression involving in RCC tumor immune evasion (38). In 2022, a novel specific cell surface expression pattern in RCC represented by the NCI-60 tumor cell panel was identified and confirmed that VCAM1 is a promising novel immunotherapeutic target for the treatment of renal cancer particularly (39). Moreover, our results are consistent with the previous report that VCAM1 plays a protective role in RCC as a prognostic biomarker (40). However, this tendency of prognostic result is reversed following normalization by the CTLA-4 genes expression (Figure 10B), implying that the combination therapy strategy may have multiple factors that could influence the prognostic progress.

In this study, we hypothesize that shikonin may be a beneficial combination partner for ipilimumab for the treatment of ccRCC patients due to its strong inhibitory effect on cancer stem cells, the significant reduction of FoxP3<sup>+</sup> Treg cells in PBMC of patients and the activation of the endogenous effector CD3<sup>+</sup>CD8<sup>+</sup> and CD3<sup>+</sup>CD4<sup>+</sup> T cells in response to the recognition of tumor specific antigens. Despite the numerous limitations encountered in this study, such as the unavailability of PBMC samples for testing certain therapeutic settings and the assessment of off-target effects in cell cytotoxicity about PTCs, it is important to note that this study represents one of the pioneering efforts in the field. In future studies, efforts will be made to overcome these limitations by expanding sample availability and incorporating a wider range of therapeutic settings, allowing for a more comprehensive understanding of the topic. In summary, we propose that a combination of shikonin and ipilimumab could be a promising treatment strategy.

## Data availability statement

The raw data supporting the conclusions of this article will be made available by the authors without undue reservation.

## Ethics statement

The studies involving human participants were reviewed and approved by Ethics Committee of the Ludwig Maximilians University Munich. The patients/participants provided their written informed consent to participate in this study.

## Author contributions

CL and HP contributed to conception and design of the study. CL and LW organized the database and performed the statistical analysis. CL wrote the first draft of the manuscript. BS, AB, and HP offered technical or material support, critical reading, and text revisions. All authors contributed to the article and approved the submitted version.

## Funding

The author CL is funded by the China Scholarship Council (ID: 201908080121).

## Conflict of interest

The authors declare that the research was conducted in the absence of any commercial or financial relationships that could be construed as a potential conflict of interest.

## Publisher's note

All claims expressed in this article are solely those of the authors and do not necessarily represent those of their affiliated organizations, or those of the publisher, the editors and the reviewers. Any product that may be evaluated in this article, or claim that may be made by its manufacturer, is not guaranteed or endorsed by the publisher.

## Supplementary material

The Supplementary Material for this article can be found online at: <https://www.frontiersin.org/articles/10.3389/fimmu.2023.1186388/full#supplementary-material>

## References

- Capitaino U, Bensalah K, Bex A, Boorjian SA, Bray F, Coleman J, et al. Epidemiology of renal cell carcinoma. *Eur Urol* (2019) 75(1):74–84. doi: 10.1016/j.euro.2018.08.036
- Siegel RL, Miller KD, Fuchs HE, Jemal A. Cancer statistics, 2021. *CA Cancer J Clin* (2021) 71(1):7–33. doi: 10.3322/caac.21654
- Motzer R, Alekseev B, Rha S-Y, Porta C, Eto M, Powles T, et al. Lenvatinib plus Pembrolizumab or Everolimus for advanced renal cell carcinoma. *New Engl J Med* (2021) 384(14):1289–300. doi: 10.1056/NEJMoa2035716
- Rini BI, Plimack ER, Stus V, Gafanov R, Hawkins R, Nosov D, et al. Pembrolizumab plus Axitinib versus Sunitinib for advanced renal-cell carcinoma. *New Engl J Med* (2019) 380(12):1116–27. doi: 10.1056/NEJMoa1816714
- Choueiri TK, Powles T, Burotto M, Escudier B, Boursin MT, Zurawski B, et al. Nivolumab plus Cabozantinib versus Sunitinib for advanced renal-cell carcinoma. *New Engl J Med* (2021) 384(9):829–41. doi: 10.1056/NEJMoa2026982
- Motzer RJ, Penkov K, Haanen J, Rini B, Albiges L, Campbell MT, et al. Avelumab plus Axitinib versus Sunitinib for advanced renal-cell carcinoma. *New Engl J Med* (2023) 388(12):1103–15. doi: 10.1056/NEJMoa2216047
- Motzer RJ, Tannir NM, McDermott DF, Frontera OA, Melichar B, Choueiri TK, et al. Nivolumab plus Ipilimumab versus Sunitinib in advanced renal cell carcinoma. *New Engl J Med* (2018) 378(14):1277–90. doi: 10.1056/NEJMoa1712126
- Choueiri TK, Powles T, Albiges L, Burotto M, Szczylik C, Zurawski B, et al. Cabozantinib plus Nivolumab and Ipilimumab in renal-cell carcinoma. *New Engl J Med* (2023) 388(19):1767–78. doi: 10.1056/NEJMoa2212851
- Le Guevelou J, Sargos P, Siva S, Ploussard G, Ost P, Gillesen S, et al. The emerging role of extracranial stereotactic ablative radiotherapy for metastatic renal cell carcinoma: A systematic review. *Eur Urol Focus* (2023) 9(1):114–24. doi: 10.1016/j.euf.2022.08.016
- Clevers H. The cancer stem cell: premises, promises and challenges. *Nat Med* (2011) 17(3):313–9. doi: 10.1038/nm.2304
- Khan MI, Czarniecka AM, Helbrecht I, Bartnik E, Lian F, Szczylik C, et al. Current approaches in identification and isolation of human renal cell carcinoma cancer stem cells. *Stem Cell Res* (2015) 6(1):1–11. doi: 10.1186/s13287-015-0177-z
- Yuan Z-X, Mo J, Zhao G, Shu G, Fu H-L, Zhao W. Targeting strategies for renal cell carcinoma: from renal cancer cells to renal cancer stem cells. *Front Pharmacol* (2016) 7:423. doi: 10.3389/fphar.2016.00423
- Corro C, Moch H. Biomarker discovery for renal cancer stem cells. *J Pathol: Clin Res* (2018) 4(1):3–18. doi: 10.1002/cjp.2191
- Gassenmaier M, Chen D, Buchner A, Henkel L, Schiemann M, Mack B, et al. Cxcr4 Chemokine Receptor 4 is essential for maintenance of renal cell carcinoma-initiating cells and predicts metastasis. *Stem Cells* (2013) 31(8):1467–76. doi: 10.1002/stem.1407
- Lyu C, Wang L, Stadlbauer B, Noessner E, Buchner A, Pohl H. Identification of EZH2 as cancer stem cell marker in clear cell renal cell carcinoma and the anti-tumor effect of epigallocatechin-3-Gallate (EGCG). *Cancers* (2022) 14(17):4200. doi: 10.3390/cancers14174200
- Rasti A, Mehrazma M, Madjd Z, Abolhasani M, Saeednejad Zanjani L, Asgari M. Co-expression of cancer stem cell markers Oct4 and Nanog predicts poor prognosis in renal cell carcinomas. *Sci Rep* (2018) 8(1):1–11. doi: 10.1038/s41598-018-30168-4
- Heng WS, Krut FA, Cheah S-C. Understanding lung carcinogenesis from a morphostatic perspective: prevention and therapeutic potential of phytochemicals for targeting cancer stem cells. *Int J Mol Sci* (2021) 22(11):5697. doi: 10.3390/ijms22115697
- Manogaran P, Umapathy D, Karthikeyan M, Venkatachalam K, Singaravelu A. Dietary phytochemicals as a potential source for targeting cancer stem cells. *Cancer Invest* (2021) 39(4):349–68. doi: 10.1080/07357907.2021.1894569
- Naujokat C, McKee DL. The "Big Five" Phytochemicals targeting cancer stem cells: Curcumin, EGCG, Sulforaphane, Resveratrol and Genistein. *Curr Med Chem* (2021) 28(22):4321–42. doi: 10.2174/0929867327666200228110738
- Das PK, Zahan T, Rakib A, Khanam JA, Pillai S, Islam F. Natural compounds targeting cancer stem cells: A promising resource for chemotherapy. *Anti-Cancer Agents Med Chem* (2019) 19(15):1796–808. doi: 10.2174/1871520619666190704111714
- Khan N, Mukhtar HJN. Tea polyphenols in promotion of human health. *Nutrients* (2018) 11(1):39. doi: 10.3390/nu11010039
- Chen Y-J, Wang Z-W, Lu T-L, Gomez CB, Fang H-W, Wei Y, et al. The synergistic anticancer effect of dual drug-(Cisplatin/Epigallocatechin Gallate) loaded gelatin nanoparticles for lung cancer treatment. *J Nanomater* (2020) 15:9181549. doi: 10.1155/2020/9181549
- Ferri F. In renal cell carcinoma, the role of natural supplement compounds as anticancer agents. *Int J Collab Res Internal Med Public Health* (2022) 14(02):001–2. doi: 10.35248/1840-4529.22.14.341
- Graham J, Wells JC, Dudani S, Gan CL, Donskov F, J-L L, et al. Outcomes of patients with advanced non-clear cell renal cell carcinoma treated with first-line immune checkpoint inhibitor therapy. *Eur J Cancer* (2022) 171:124–32. doi: 10.1016/j.ejca.2022.05.002
- Li J, Tan G, Cai Y, Liu R, Xiong X, Gu B, et al. A novel Apigenin derivative suppresses renal cell carcinoma via directly inhibiting wild-type and mutant met. *Biochem Pharmacol* (2021) 190:114620. doi: 10.1016/j.bcp.2021.114620
- Zaki K, Aslam S, Eisen T, Regorafenib (Bay 73–4506): stromal and oncogenic multikinase inhibitor with potential activity in renal cell carcinoma. *Curr Oncol Rep* (2013) 15(2):91–7. doi: 10.1007/s11912-013-0292-x
- Posadas EM, Limvorasak S, Figlin RA. Targeted therapies for renal cell carcinoma. *Nat Rev Nephrol* (2017) 13(8):496–511. doi: 10.1038/nrneph.2017.82
- Charoentong P, Finotello F, Angelova M, Mayer C, Efremova M, Rieder D, et al. Pan-cancer immunogenomic analyses reveal genotype-immunophenotype relationships and predictors of response to checkpoint blockade. *Cell Rep* (2017) 18(1):248–62. doi: 10.1016/j.celrep.2016.12.019
- Tsai M-F, Chen S-M, Ong A-Z, Chung Y-H, Chen P-N, Hsieh Y-H, et al. Shikonin induced program cell death through generation of reactive oxygen species in renal cancer cells. *Antioxidants* (2021) 10(11):1831. doi: 10.3390/antiox10111831
- Markovitsch SD, Vakhrusheva O, Schupp P, Akele Y, Kitano J, Slade KS, et al. Shikonin inhibits cell growth of sunitinib-resistant renal cell carcinoma by activating the necrosome complex and inhibiting the Akt/Mtor signaling pathway. *Cancers* (2022) 14(5):1114. doi: 10.3390/cancers14051114
- Yuan L, Wang Y, Chen Y, Chen X, Li S, Liu X. Shikonin inhibits immune checkpoint Pd-L1 expression on macrophage in sepsis by modulating Pkm2. *Int Immunopharmacol* (2023) 121:110401. doi: 10.1016/j.intimp.2023.110401
- Wang H, Tang Y, Fang Y, Zhang M, Wang H, He Z, et al. Reprogramming Tumor Immune Microenvironment (Time) and metabolism via biomimetic targeting codelivery of Shikonin/Jq1. *Nano Lett* (2019) 19(5):2935–44. doi: 10.1021/acs.nanolett.9b00021
- Lee DY, Im E, Yoon D, Lee Y-S, Kim G-S, Kim D, et al. Pivotal Role of Pd-1/Pd-L1 Immune Checkpoints in Immune Escape and Cancer Progression: Their Interplay with Platelets and Foxp3+ Tregs Related Molecules, Clinical Implications and Combinational Potential with Phytochemicals. In: *Seminars in Cancer Biology*. Elsevier, Amsterdam: The Netherlands (2022) 86(3):1033–57. doi: 10.1016/j.semcancer.2020.12.001
- Lim S-O, Li C-W, Xia W, Cha J-H, Chan L-C, Wu Y, et al. Deubiquitination and stabilization of Pd-L1 by Csn5. *Cancer Cell* (2016) 30(6):925–39. doi: 10.1016/j.ccr.2016.10.010
- Hao H, Zhang Q, Zhu H, Wen Y, Qiu D, Xiong J, et al. Icaritin promotes tumor T-cell infiltration and induces antitumor immunity in mice. *Eur J Immunol* (2019) 49(12):2235–44. doi: 10.1002/eji.201948225
- Wu X, Giobbie-Hurder A, Liao X, Lawrence D, McDermott D, Zhou J, et al. Vegf neutralization plus Ccl4 blockade alters soluble and cellular factors associated with enhancing lymphocyte infiltration and humoral recognition in melanomaipilimumab plus anti-Vegf augments tumor immune recognition. *Cancer Immunol Res* (2016) 4(10):858–68. doi: 10.1158/2326-6066.CIR-16-0084
- VanHeyst KA, Choi SH, Kingsley DT, Huang AY. Ectopic tumor Vcam-1 expression in cancer metastasis and therapy resistance. *Cells* (2022) 11(23):3922. doi: 10.3390/cells11233922
- Wu TC. The role of vascular cell adhesion molecule-1 in tumor immune evasion. *Cancer Res* (2007) 67(13):6003–6. doi: 10.1158/0008-5472.CAN-07-1543
- Heumos S, Dehn S, Bräutigam K, Codrea MC, Schürch CM, Lauer UM, et al. Multomics surface receptor profiling of the Nci-60 tumor cell panel uncovers novel therapeutics for cancer immunotherapy. *Cancer Cell Int* (2022) 22(1):1–14. doi: 10.1186/s12935-022-02710-y
- Shioi K-I, Komiya A, Hattori K, Huang Y, Sano F, Murakami T, et al. Vascular cell adhesion molecule 1 predicts cancer-free survival in clear cell renal carcinoma patients. *Clin Cancer Res* (2006) 12(24):7339–46. doi: 10.1158/1078-0432.CCR-06-1737



*Supplementary Material*

**Identification of novel combination treatment strategy in clear cell renal cell carcinoma stem cells with shikonin and ipilimumab**

**Chen Lyu<sup>1</sup>, Birgit Stadlbauer<sup>1,2</sup>, Lili Wang<sup>1,3</sup>, Alexander Buchner<sup>1,2</sup>, Heike Pohla<sup>1,2\*</sup>**

<sup>1</sup>Tumor Immunology Laboratory, LIFE Center, LMU Klinikum, University Munich, Germany

<sup>2</sup>Department of Urology, LMU Klinikum, University Munich, Germany

<sup>3</sup>Department of Radiology, First Affiliated Hospital, Zhejiang University School of Medicine, Hangzhou, China

**\* Correspondence:**

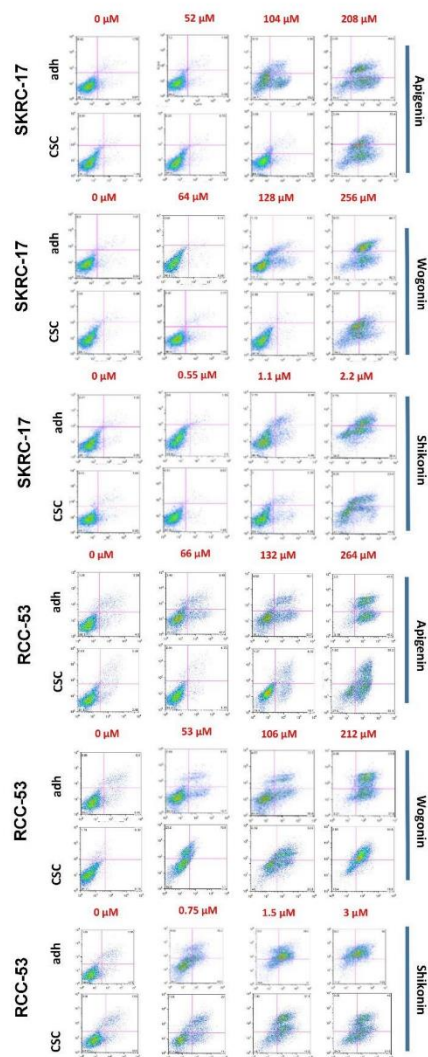
Heike Pohla

heike.pohla@med.uni-muenchen.de

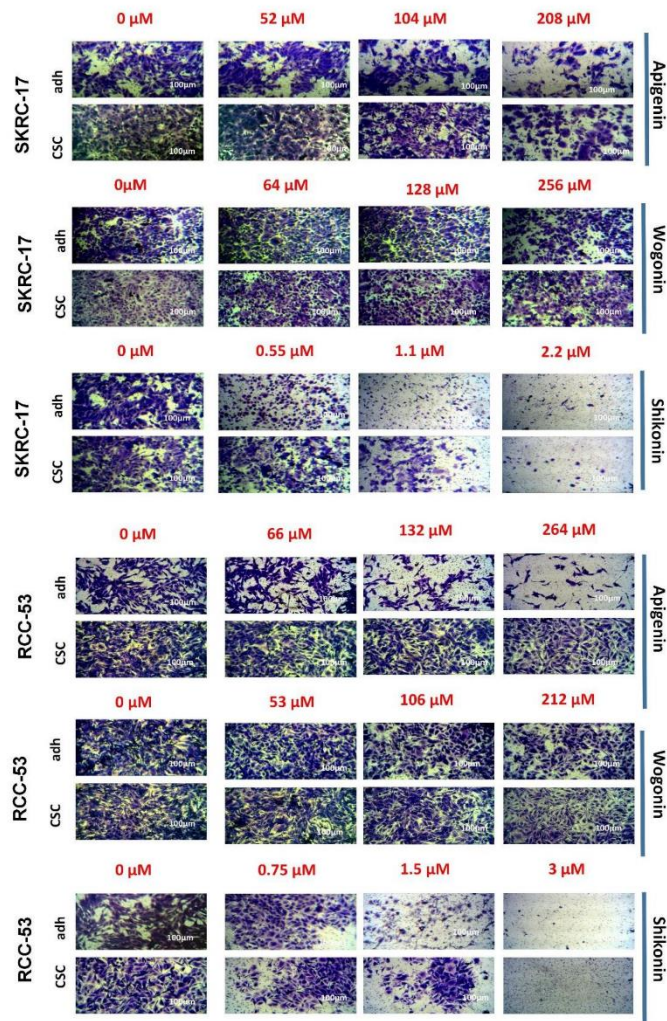


## Supplementary Material

## Supplementary Figures

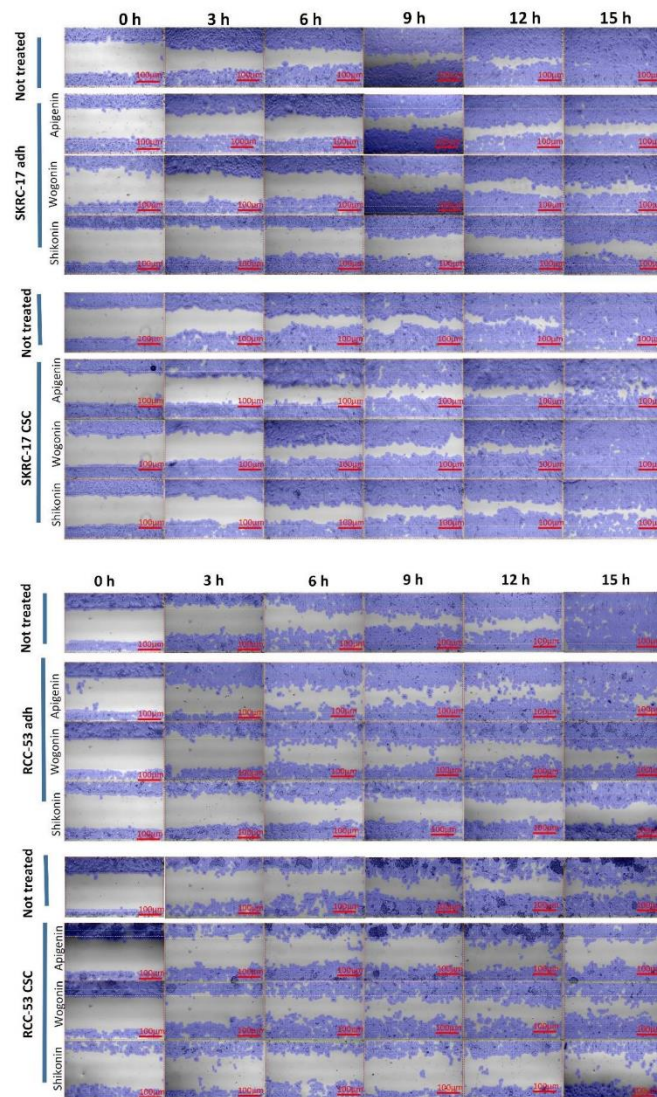


**Supplementary Figure S1. Apoptosis assay.** SKRC-17 adherent cell, SKRC-17 CSCs, RCC-53 adherent cells and RCC-53 CSCs were treated with apigenin, wogonin, and shikonin.

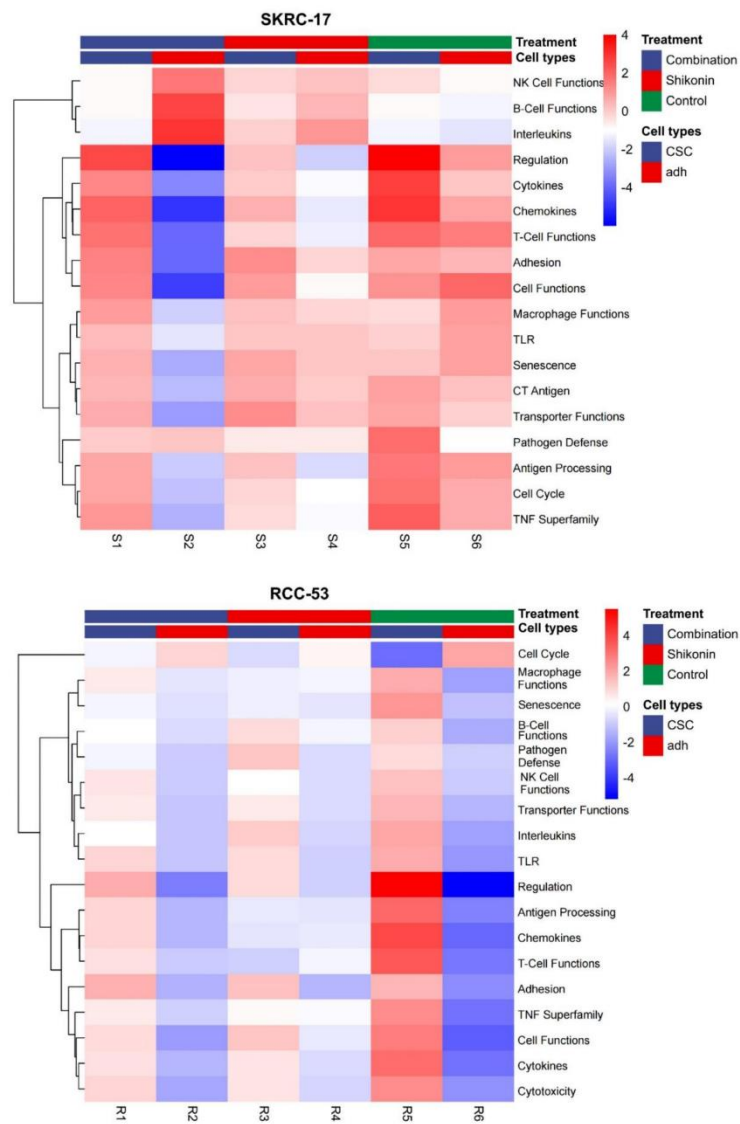


**Supplementary Figure S2. Invasion assay.** Photos were taken at the magnification of 40x and the cells were counted (three fields per insert; Fiji ImageJ software).

## Supplementary Material



**Supplementary Figure S3. Migration assay.** Photos were taken under the microscope at different time points at the magnification of 40× (Bresser GmbH DE-46414 Rhede Germany).



**Supplementary Figure S4. Heatmap of the differentially expressed pathways.** Between CSCs and adherent cells, groups were treated with or without shikonin or with the combination shikonin plus ipilimumab (NanoString analysis).



## 4. Paper II





cancers



Article

# Identification of EZH2 as Cancer Stem Cell Marker in Clear Cell Renal Cell Carcinoma and the Anti-Tumor Effect of Epigallocatechin-3-Gallate (EGCG)

Chen Lyu <sup>1</sup>, Lili Wang <sup>1,2</sup>, Birgit Stadlbauer <sup>1,3</sup>, Elfriede Noessner <sup>4</sup> , Alexander Buchner <sup>1,3</sup>  and Heike Pohla <sup>1,3,\*</sup>

<sup>1</sup> Tumor Immunology Laboratory, LIFE Center, LMU Klinikum, University Munich, D-82152 Planegg, Germany

<sup>2</sup> Department of Radiology, First Affiliated Hospital, Zhejiang University School of Medicine, Hangzhou 310030, China

<sup>3</sup> Department of Urology, LMU Klinikum, University Munich, D-81377 Munich, Germany

<sup>4</sup> Immunoanalytics Research Group Tissue Control of Immunocytes, Helmholtz Zentrum München, D-81377 Munich, Germany

\* Correspondence: heike.pohla@med.uni-muenchen.de

**Simple Summary:** Cancer stem cells (CSCs) refer to a group of undifferentiated heterogeneous tumor cells, defined as capable of self-renewal, differentiation, and may be linked to therapeutic resistance and tumor relapse. The development of novel therapeutic strategies to target CSCs and the identification of typical CSC markers are essential to improve therapy efficacy and prevent tumor relapse. Our study identifies CSC markers in renal cell carcinoma (RCC) and explores a potential treatment strategy and the underlying pharmacological mechanisms.

**Abstract:** The aim of the study was to develop a new therapeutic strategy to target cancer stem cells (CSCs) in clear cell renal cell carcinoma (ccRCC) and to identify typical CSC markers to improve therapy effectiveness. It was found that the corrected-mRNA expression-based stemness index was upregulated in kidney renal clear cell carcinoma (KIRC) tissues compared to non-tumor tissue and increased with higher tumor stage and grade. EZH2 was identified as a CSC marker and prognosis factor for KIRC patients. The expression of EZH2 was associated with several activated tumor-infiltrating immune cells. High expression of EZH2 was enriched in immune-related pathways, low expression was related to several metabolic pathways. Epigallocatechin-3-gallate (EGCG) was identified as the most potent suppressor of EZH2, was able to inhibit viability, migration, and invasion, and to increase the apoptosis rate of ccRCC CSCs. KIF11, VEGF, and MMP2 were identified as predictive EGCG target genes, suggesting a potential mechanism of how EZH2 might regulate invasiveness and migration. The percentages of FoxP3+ Treg cells in the peripheral blood mononuclear cells of ccRCC patients decreased significantly when cultured with spheres pretreated with EGCG plus sunitinib compared to spheres without treatment. Our findings provide new insights into the treatment options of ccRCC based on targeting CSCs.

**Keywords:** cancer stem cells; kidney renal clear cell carcinoma; prognosis; tumor microenvironment; phytochemicals



**Citation:** Lyu, C.; Wang, L.; Stadlbauer, B.; Noessner, E.; Buchner, A.; Pohla, H. Identification of EZH2 as Cancer Stem Cell Marker in Clear Cell Renal Cell Carcinoma and the Anti-Tumor Effect of Epigallocatechin-3-Gallate (EGCG). *Cancers* **2022**, *14*, 4200. <https://doi.org/10.3390/cancers14174200>

Received: 18 July 2022

Accepted: 19 August 2022

Published: 30 August 2022

**Publisher's Note:** MDPI stays neutral with regard to jurisdictional claims in published maps and institutional affiliations.



**Copyright:** © 2022 by the authors. Licensee MDPI, Basel, Switzerland. This article is an open access article distributed under the terms and conditions of the Creative Commons Attribution (CC BY) license (<https://creativecommons.org/licenses/by/4.0/>).

### 1. Introduction

Renal cell carcinoma (RCC) has become one of the most common genitourinary tumors, of which clear cell renal cell carcinoma (ccRCC) is involved in approximately 70–85% of cases. Over 30% of ccRCC patients face metastasis at the time of initial diagnosis and most of them are not sensitive to chemotherapy and radiation therapy [1–3]. At present, cancer stem cells (CSCs) are acknowledged to play an essential role in the metastasis, recurrence, and therapeutic resistance of the tumor through the abilities of self-renewal

and differentiation [4–6]. It is known that CSCs represent phenotypically and functionally heterogeneous cell populations [7]. The identification of CSC markers as a surrogate for tumor development can indicate tumor metastasis spread and progression.

Enhancer of Zeste Homolog 2 (EZH2), as one of the classical CSC markers, is the key transcriptional regulator involved in histone H3 lysine 27 trimethylation [8]. Previous studies have reported that inhibiting expression can eradicate ovarian CSCs in vitro, blocks disease recurrence, and decreases chemotherapy resistance in acute myeloid leukemia [9–11] as well as results in a reduction in the CSC properties and invasion in a number of cancers [12–15]. In ccRCC, high EZH2 expression was significantly linked to several prognosis values such as shortened overall ( $p < 0.0027$ ) and recurrence free survival ( $p < 0.0001$ ) [16]. More and more CSC markers have been identified, and they play a role in clinical diagnosis and prognosis [17–19]. A deeper understanding of the mechanism by which CSC markers mediate and accelerate ccRCC metastasis may help in the development of more efficient treatment strategies. Based on the molecular profiles of normal cells with varying degrees of stemness-associated mRNA expression, a computational algorithm has been developed that calculates a stemness index (mRNAsi) [20], which can be used to describe the similarity between tumor cells and cancer stem cells after controlling the intra-tumor heterogeneity. A higher mRNAsi index was found to be associated with active biological processes in CSCs and greater tumor dedifferentiation, as described by histopathological grades [20–22]. So far, a mRNAsi index has not been established for ccRCC.

The tumor microenvironment (TME), as a collaborative interaction between tumor cells and their supporting cells, plays a crucial role in the initiation and progression in ccRCC [23,24]. Tumor-infiltrating immune cells (TICs) in the TME can serve as indicators for the therapeutic effects of immune therapies such as checkpoint inhibition. Moreover, TICs have been found to interact with CSCs to maintain their stemness [25]. Previous studies have found a positive correlation between the CSC markers ALDH and CD3<sup>+</sup>/CD8<sup>+</sup> cytotoxic T cells and helper T cells in non-small cell lung cancer (NSCLC) [26]. However, no correlation was observed between CD8<sup>+</sup> TILs (tumor infiltrating lymphocytes) and the CSC marker CD133 in 172 resected NSCLC samples [27]. For the ccRCC patients, several types of TILs were significantly correlated with unfavorable tumor characteristics and a higher rate of recurrence [28,29], but there is less evidence connecting CSC biomarkers with ccRCC TME.

Phytochemicals (PTCs) have obtained attention because of their good safety profile and the ability to target heterogeneous populations of cancer cells as well as CSCs [30,31]. PTCs were found to regulate CSC markers, thereby influencing the biological characteristics of CSCs and several key signaling pathways. For example, epigallocatechin-3-gallate (EGCG), which is an active compound in green tea, shows potential in suppressing cancer stemness and tumorigenicity in several types of cancers [32–36]. Other PTCs showed similar inhibitory effects: wogonin abolished the CSC traits of cutaneous squamous cell carcinoma through downregulating the expression of CSC markers as well as reducing the percentage of CD133<sup>+</sup> cells; apigenin was found to inhibit the stemness features of triple-negative breast cancer cells by decreasing YAP/TAZ activity [37]. Meanwhile, combining PTCs with other treatment options was observed to further enhance anti-CSC activities [35,38]. Our group found that shikonin, derived from the roots of lithospermum erythrorhizon, combined with cabazitaxel enhanced the anti-tumor effect in prostate CSCs and reversed cabazitaxel resistance by inhibiting the CSC markers ABCG2 and ALDH3A1 [39]. Thus, it is promising to identify typical ccRCC CSC markers and find novel treatment strategies to reverse therapy resistance in cancer patients.

In this study, the effect of EGCG on the expression of the CSC marker EZH2 and the corresponding biological functions were studied using ccRCC lines. Furthermore, the TIC composition was analyzed using the TCGA dataset and deconvolution algorithms and set in relation to the EZH2 expression. Results showed that the expression of EZH2 can be inhibited by EGCG and potentially regulates and affects the prognosis of ccRCC patients as well as TIC composition. Furthermore, the combination of EGCG and sunitinib caused a

significant reduction in the FoxP3<sup>+</sup> Treg cells in the PBMC of patients, indicating potential new treatment options for ccRCC.

## 2. Materials and Methods

### 2.1. Cell Culture

SKRC-17 (kind gift from J. Vissers, Nijmegen), RCC-53 (derived from a patient with stage IV disease (pT2N1MxG2-3) [19]), and RCC-26 (derived from a patient with stage I disease (pT1N0M0G2)) [19,40] cell lines were cultured in RPMI 1640 medium supplemented with 10% fetal calf serum (FCS “Gold Plus”, Bio & Sell GmbH, Feucht, Germany), 2 mM L-glutamine, 1 mM sodium pyruvate, and 1% minimal essential medium (Invitrogen, Life Technologies GmbH, Darmstadt, Germany) at 37 °C in a humidified incubator with 5% CO<sub>2</sub>. CSCs were cultured in DMEM/F12 culture medium, containing 2% B-27 (Invitrogen), 10 ng/mL human recombinant basic fibroblast growth factor (bFGF, Sigma Aldrich Chemie GmbH, Taufkirchen, Germany), and 10 ng/mL epidermal growth factor (EGF, Sigma Aldrich), named as the CSC medium.

### 2.2. Sphere Formation Assay

The SKRC-17, RCC-26, and RCC-53 cells were harvested by StemPro<sup>®</sup> Accutase<sup>®</sup> (Life Technologies, Thermo Fisher Scientific, Waltham, MA, USA). Then, cells were filtered through a cell strainer with 40 µm nylon mesh (BD Biosciences, Heidelberg, Germany), and seeded in 75 cm<sup>2</sup> ultra-low attachment flasks (Corning, New York, NY, USA) with the 10 mL CSC medium. After seven days, photos were taken and the spheres were harvested into a 15 mL tube, centrifuged at 500 × g for 4 min at room temperature, and dissociated by Accutase for 10 min at 37 °C. After centrifugation, cells were collected and used for the subsequent assays.

### 2.3. Quantitative Reverse Transcription PCR (RT-qPCR)

The total RNA was extracted from cells using a RNeasy Mini-Kit (Qiagen, Hilden, Germany) based on the manufacturer’s instructions. cDNA was synthesized according to the instructions in the kit (Reverse Transcription System, Promega GmbH, Walldorf, Germany). mRNA amplification was performed using the FastStart Essential DNA Green Master kit (Roche, Penzberg, Germany) and LightCycler<sup>®</sup> 96 (Roche, Basel, Switzerland). The reaction started with 95 °C for 10 min, followed by 40 cycles of denaturation at 95 °C for 10 s, annealing at 60 °C for 10 s, and extension at 72 °C for 10 s. Then, a melting process at 95 °C for 10 s, 65 °C for 60 s, and 97 °C for 1 s was performed. Data were analyzed by the LightCycler<sup>®</sup> 96 software (1.1 version). The relative expression analysis was carried out by the 2<sup>-ΔΔCt</sup> method. The transcription level of *GAPDH* and *ACTB* was used as an internal control and all primers are listed in Table 1.

### 2.4. KIRC Data Download

Transcriptome RNA-Seq data of 611 KIRC cases (normal samples, 72 cases; tumor samples, 539 cases) and the corresponding clinical data and stemness indices were downloaded from the TCGA database (<https://portal.gdc.cancer.gov/>, (accessed on 4 March 2021)).

### 2.5. Survival and Clinical Characteristics Analysis

The R language loaded with package survival and survminer was applied for the survival analysis. A total of 539 tumor samples out of 510 cases had a detailed survival time record, with a time span from 0 to 10 years, which were used for the survival analysis. The Kaplan–Meier method was used to plot the survival curve, and log rank as the statistical significance test;  $p < 0.05$  was considered as significant. The analysis of clinical characteristics was performed by R language, the Wilcoxon rank sum or Kruskal–Wallis rank sum test as the significance test, depending on the number of clinical stages for comparison.

**Table 1.** The primers used for RT-qPCR.

Transcript	Primer	Sequence (5'-3')	Product Size (bp)
GAPDH	GAPDH-F	CATGGGTGTGAACCATGA	104
	GAPDH-R	TGTCATGGATGACCTTGG	
ACTB	ACTB-F	CTGCCCTGAGGCACTC	197
	ACTB-R	GTGCCAGGGCAGTGAT	
ABCA13	ABCA13-f	AGGAGTGTGAGGCTCTTTGC	207
	ABCA13-r	TCAGGTGCTGTCCCTTGAAC	
ABCB1	ABCB1-f	GGAGGCCAACATACATGCCT	205
	ABCB1-r	CAGGGCTTCTTGGACAACCT	
ABCG2	ABCG2-f	CATCAACTTTCGGGGGTGA	266
	ABCG2-r	CACTGGTTGGTCGTCAGGAA	
ALDH1A1	ALDH1A1-f	TGTTAGCTGATGCCGACTTG	154
	ALDH1A1-r	TTCTTAGCCCGCTCAACACT	
ALDH1A3	ALDH1A3-f	GAGGAGATTTTCGGGCCAGT	186
	ALDH1A3-r	GAGGGCGTTGTAGCAGTTGA	
ALDH3A1	ALDH1A3-f	GCAGACCTGCACAAGAATGA	186
	ALDH1A3-r	TGTAGAGCTCGTCTGCTGA	
CD105	ENG-f	TCACCACAGCGAAAAAGGT	141
	ENG-r	GGACACTCTGACCTGCACAA	
CD133	PROM1-f	TTGCGGTAAAACCTGGCTAAG	155
	PROM1-r	TGGGCTTGTCATAACAGGAT	
CXCR4	CXCR4-f	TGGGTGGTTGTGTCCAGTTT	80
	CXCR4-r	ATGCAATAGCAGGACAGGATG	
DAB2IP	DAB2IP-f	TGTCGCCCTCACTCTTCAAC	225
	DAB2IP-r	CGGCTGTATTGGAGAGGGTC	
DNMT1	DNMT1-f	GGCAGACCATCAGGCATTCT	220
	DNMT1-r	ACCATGTCCTTGCAGGCTTT	
EZH2	hEZH2-F	AGGACGGCTCCTCTAACCAT	179
	EZH2-R	CTTGGTGTGCACTGTGCTT	
KLF4	KLF4-f	TCCCATCTTCTCCACGTTT	239
	KLF4-r	GGTCTCTCTCCGAGGTAGGG	
LIN28A	LIN28A-f	TTCGGCTTCTGTCCATGAC	124
	LIN28A-r	CCACTGCCTCACCCCTCTT	
MTGR1	MTGR1-f	CCTCCTACCCTGAATGGTGC	214
	MTGR1-r	GTGCAAGAACAAGAGTCCGC	
NANOG	NANOG-f	TGTGTTCTCTCCACCCAGC	205
	NANOG-r	CTTCTGCGTCACACCATTGC	
POU5F1	POU5F1-f	CCCTGGGGTCTATTTGGG	231
	POU5F1-r	TCTCCAGGTTCCTCTCACT	
SALL4	SALL4-f	GCTCTGTAGGTACGGACGG	96
	SALL4-r	CTGGTTCACACAACAGGGT	
SOX2	SOX-2-f	CATCACCCACAGCAAATGAC	258
	SOX-2-r	GCAAACCTCCTGCAAAGCTC	



### 2.6. Gene Expression in Tumor and Normal Tissue

The mRNA expression level difference and correlation analysis shown in the box plot, heatmap, and the corheatmap were performed by R language software (version 3.6.3, download from <https://www.cran.r-project.org> (accessed on 17 April 2021)) through the package ggpubr and pheatmap. Immunohistochemistry pictures of potential CSC markers were downloaded from the Human Protein Atlas ([www.proteinatlas.org](http://www.proteinatlas.org), (accessed on 17 April 2021)) to confirm the protein expression.

### 2.7. Mixed Lymphocyte Tumor Cell Culture (MLTC)

Healthy human donors and patients gave their written informed consent before the experiments were conducted and approved by the Ethics Committee of the Ludwig Maximilians University Munich. Human serum samples were produced from the blood of healthy male donors, which were also approved by the Ethics Committee (Project No. 003/02, Project No. 214/04). Tumor cells were harvested and diluted to  $5 \times 10^4$  per well with the CTL test medium (Cellular Technology Ltd. Europe, Bonn, Germany) in a 24-well plate. The plate was placed in a sterile tin box in a 37 °C incubator overnight. The next day, the PBMCs were thawed and washed in CTL wash supplemented medium (45 mL RPMI 1640 medium, 5 mL CTL Wash (Cellular Technology Ltd. Europe)) and 50 U/mL benzonase (Novagen Merck Biosciences, Darmstadt, Germany). The PBMC and drugs were added to the tumor cells into a final volume of 1.5 mL per well and incubated for 48 h. Finally, IL-2 in a final concentration of 50 U/mL (Proleukin, Novartis, Basel, Switzerland) was added and the cells were incubated for an additional three days. The workflow for MLTC was conducted by Bio-render (<https://biorender.com/>, (accessed on 16 May 2022)).

### 2.8. Flow Cytometry

Spheres and adherent tumor cell lines were harvested and stained with the following mouse monoclonal antibodies: EZH2 (clone 11/EZH2 Alexa Fluor<sup>®</sup> 647, BD Biosciences, Heidelberg, Germany), ALDH1A3 (clone OTI4E8, ORIGENE, Rockville, MD, USA), SALL4 (clone 6E3, Abcam, Cambridge, UK), and ABCG2 (clone 5D3/CD338, APC, BD Biosciences), respectively. As a secondary antibody for the detection of ALDH1A3 and SALL4, a goat F(ab')<sub>2</sub> anti-mouse IgG + IgM (H + L)-FITC antibody (Dianova GmbH, Hamburg, Germany) was used. For intracellular staining, the Cytotfix/Cytoperm<sup>™</sup> Fixation/Permeabilization Kit from BD Biosciences was used according to the manufacturer's protocol.

For lymphocyte staining, the following directly conjugated mouse monoclonal antibodies were purchased from BD Biosciences: CD3 (clone UCHT1, FITC), CD4 (clone SK3, PE-Cy7), CD8 (clone RPA-T8, APC), CD25 (clone M-A251, PerCP-Cy5.5), and CD127 (clone hIL-7R-M21, PE), respectively. For Treg analysis, the monoclonal antibody FoxP3 (clone PCH101, eFluor450; eBiosciences, Frankfurt, Germany) was used. Operating steps were as follows:  $1-2 \times 10^6$  cells were counted and incubated with the LIVE/DEAD<sup>™</sup> Fixable Blue Dead Cell Stain (Molecular Probes, Life Technologies, ThermoFisher Scientific, Waltham, MA, USA) for 30 min at room temperature (RT) to stain the dead cells, washed with PBS twice, then stained with the directly labeled monoclonal antibodies for 30 min at 4 °C in the dark, and washed with PBS twice. For intracellular staining with the FoxP3 antibody, the FoxP3/Transcription Factor Staining Buffer Set (eBiosciences) was used and staining was conducted for 60 min at 4 °C in the dark and washed with the Perm buffer twice.

All measurements were accomplished using the LSRII flow cytometer (BD Biosciences). Data analyses were performed by FlowJo software (version 9.9.0; Tree Star Inc., Ashland, OR, USA).

### 2.9. COX Regression Analysis

R language loaded with package survival and survminer were used for univariate and multivariable COX regression. Nine OS-related genes were selected with  $p$  value < 0.05 by univariate COX regression analysis and eight typical factors of prognosis were analyzed using multivariable COX regression shown in the forest plot.

#### 2.10. TICs Profile

The CIBERSORT computational method was applied to estimate the abundance profile of 22 TIC subtypes in the KIRC tumor samples, followed by quality filtering resulting in 539 tumor samples with  $p < 0.05$  for display in a bar plot and heatmap.

#### 2.11. Gene Set Enrichment Analysis

KEGG gene sets (c2.cp.kegg.v7.0.symbols.gmt) were downloaded from the Molecular Signatures Database (<https://www.gsea-msigdb.org/gsea/msigdb/genesets.jsp>, (accessed on 28 January 2021)) as target sets with which GSEA was performed using the software gsea-4.1 downloaded from the Broad Institute. For analysis, gene set permutations were performed 1000 times to obtain a normalized enrichment score, which was used for sorting pathway enrichment, and a NOM  $p < 0.05$  and false discovery rate (FDR) of  $q < 0.06$  were considered as significant.

#### 2.12. Cell Viability Assay

Cell viability was performed using the CellTiter-Blue Cell Viability Assay (Promega, Mannheim, Germany) according to the manufacturer's protocol. Cells were seeded into a 96-well microtiter plate (1500 cells/well) and treated with different concentrations of the PTCs EGCG, wogonin, apigenin, and shikonin (all from Selleckchem, Houston, TX, USA). After 24 h and 48 h, the measurement of fluorescence was conducted at a 560(20) excitation/590(10) emission using the FLUOstar OPTIMA microplate reader (BMG LABTECH, Ortenberg, Germany) and the OPTIMA software version 2.0. The half-maximal inhibitory concentration ( $IC_{50}$ ) was assessed by the logit regression model using SPSS version 25.0 (IBM, Armonk, NY, USA).

#### 2.13. Apoptosis Assay

The apoptotic assay was assessed by flow cytometry using Annexin V and 7-aminoactinomycin D (both from BD Biosciences). Cells were seeded in a 25 cm<sup>2</sup> flask at a density of  $4 \times 10^5$  cells and treated with or without EGCG for five days. Then, the cells were harvested and resuspended in 100  $\mu$ L Annexin V Binding Buffer with 5  $\mu$ L APC-Annexin V and 5  $\mu$ L 7-aminoactinomycin D. After co-incubation for 15 min in the dark at room temperature, 100  $\mu$ L Annexin V Binding Buffer was added and the cells were measured using a FACSCalibur (Becton Dickinson, San Jose, CA, USA). Data acquisition was conducted using BD CellQuest software (version 4.0.2) and analyzed using FlowJo software (version 9.9.5; Tree Star Inc., Ashland, OR, USA).

#### 2.14. Migration Assay

For cell migration, 24-well culture plates with two small silicone inserts per well were used to establish a cell-free gap of 500  $\mu$ m (ibidi GmbH, Martinsried, Germany). Cells were seeded into each culture insert at a concentration of  $4 \times 10^5$  cells/mL in a volume of 70  $\mu$ L and incubated at 37 °C until a confluent cell monolayer was achieved. Then, the inserts were removed with sterile tweezers and a medium with or without EGCG was added. Pictures were taken under a microscope at different time points (0, 3, 6, 9, 12, 15, and 18 h). The proportion of gap covered by cells at each time was analyzed with the web-based Automated Cellular Analysis System (ACAS, MetaVi Labs, Bottrop, Germany) using FastTrack AI image analysis algorithms.

#### 2.15. Invasion Assay

The cell invasion assay was conducted using the Boyden Chamber system. The Transwell inserts (8.0  $\mu$ m pores; Falcon, Corning, New York, NY, USA) in 24-well plates were coated with growth factor reduced Matrigel Basement Matrix (Corning; 30  $\mu$ g/100  $\mu$ L/insert) and incubated at 37 °C for at least 4 h until Matrigel solidification. Then, 30,000 cells were seeded in 250  $\mu$ L serum-free DMEM medium with and without EGCG onto the Matrigel and the lower chamber was filled with 750  $\mu$ L DMEM with 10% FCS. After 48 h, the upper surface of

the Transwell membrane was gently wiped with a moistened cotton swab to remove Matrigel with the not migrated cells. A total of 4% paraformaldehyde was used to fix the lower surface of the membrane for 5 min and then stained with 1% crystal violet for 1 min. After drying, pictures were taken and cells were counted (three fields per insert, Fiji ImageJ software, download from: <https://imagej.net/software/fiji/> (accessed on 18 November 2020)) [41].

#### 2.16. Prediction of EGCG Target Genes and Construction of Network

The two-dimensional (2D) and three-dimensional (3D) structure of EGCG was acquired from the PubChem database (<https://pubchem.ncbi.nlm.nih.gov/>, (accessed on 18 November 2020)). The SDF file of the 3D structure was uploaded to the PharmMapper database (<http://www.lilab-ecust.cn/pharmmapper/>, (accessed on 28 November 2020)) for potential target gene prediction. The protein–protein interaction (PPI) network was constructed by the STRING database with a confidence score >0.4, followed by the reconstruction with Cytoscape of version 3.6.1 (download from: <https://cytoscape.org/>) [42]. Nodes with a confidence of interactive relationship larger than 0.95 were used to build the network.

### 3. Results

The analysis workflow of our study is shown in Figure 1. A total of 611 KIRC patients from the TCGA database were used to dissect the gene expression profiles, clinicopathological characteristics, and immune-associated molecular classification. Then, the CSC biomarker EZH2 was identified and validated using the KIRC patient data and ccRCC cell lines. The correlation analysis between EZH2 expression and the clinical characteristics, the composition of TICs in KIRC patients, and the signaling pathway analysis were performed. The anti-tumor effect of EGCG against the ccRCC cell lines was evaluated and the potential target genes of EGCG were predicted. The combination therapy of sunitinib with EGCG was tested using coculture experiments and flow cytometry to provide new insights into a new therapeutic option for ccRCC patients.

#### 3.1. Corrected-mRNAsi for KIRC

The mRNAsi of ccRCC was downloaded from the TCGA database (KIRC mRNAsi). The mRNAsi expresses the degree of dedifferentiation and similarity between tumor cells and stem cells, which can be considered as a surrogate of CSCs. The mRNAsi as a stemness comprehensive score is derived from the molecular profiles of normal cells with different degrees of stemness based on the OCLR algorithm [20]. Using the mRNAsi, no difference was seen between the normal and tumor tissue, and among the tumor tissues, only high grade tumors had higher mRNAsi (Figure 2A). Previous studies have suggested that tumor “impurities” such as stromal and immune cell types can influence the mRNAsi factor [43,44]. A corrected-mRNAsi was calculated using the ESTIMATE score from previous transcriptomic studies [45]. After correcting by tumor purity, the tumor tissues had a significantly higher stemness index compared to the normal tissue (Figure 2B). The corrected-mRNAsi did significantly increase with the tumor differentiation grade, but also did not correlate to the tumor stage.

#### 3.2. Expression Analysis of 19 Potential CSC Marker Genes

Nineteen potential CSC markers for ccRCC based on previous studies were selected [46–48]. The mRNA expression values of the tumor and normal tissues of sixteen genes were successfully extracted from the TCGA datasets and are presented as a box plot and heat map (Figure 2C,D). Some of the genes such as *ABCA13*, *CXCR4*, *ABCG2*, *EZH2*, *SALL4*, and *ALDH1A3* were significantly differentially expressed between the ccRCC tissues and normal tissues and showed a higher expression level in sphere cells than in the adherent cells (see later in Figure 3B). The pairs *EZH2* and *DNMT1* ( $r = 0.57$ ,  $p < 0.0001$ ), *NANOG* and *ABCA13* ( $r = 0.67$ ,  $p < 0.0001$ ) had the highest correlation among all the pairwise correlations of the sixteen genes, suggesting that they may share some common features or functions (Figure 2E). Univariate COX regression analysis for the survival of ccRCC patients was performed among the markers, determining that

seven of them (*ABCG2*, *ALDH1A3*, *ABCB1*, *CD105*, *DAB2IP*, *EZH2*, *SALL4*) had the potential to be a prognosis factor for ccRCC patients (Figure 2F).

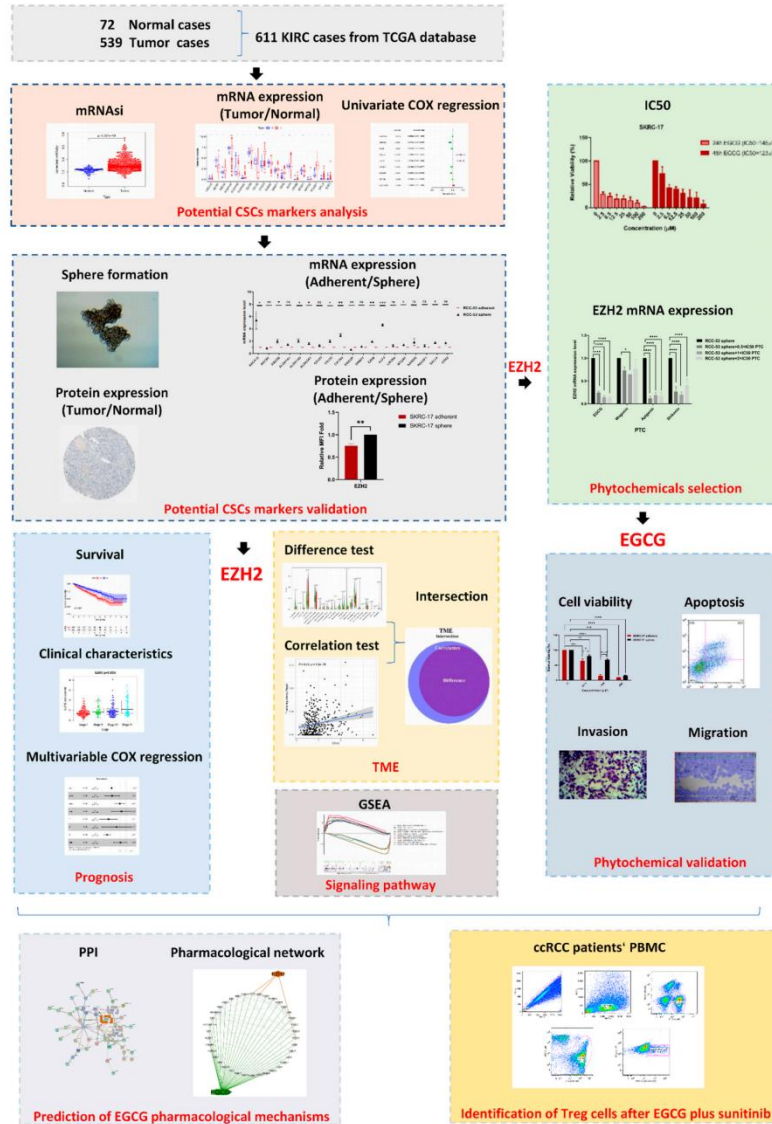


Figure 1. The analysis workflow of this study.

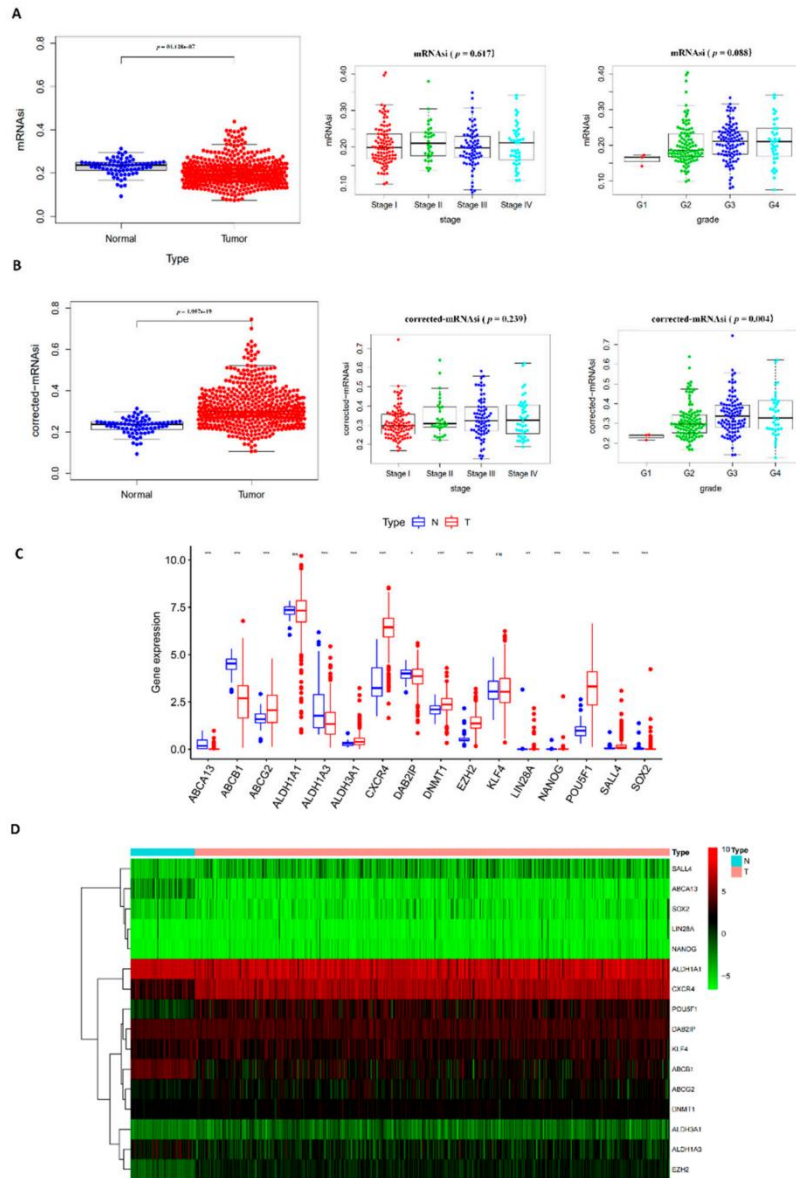
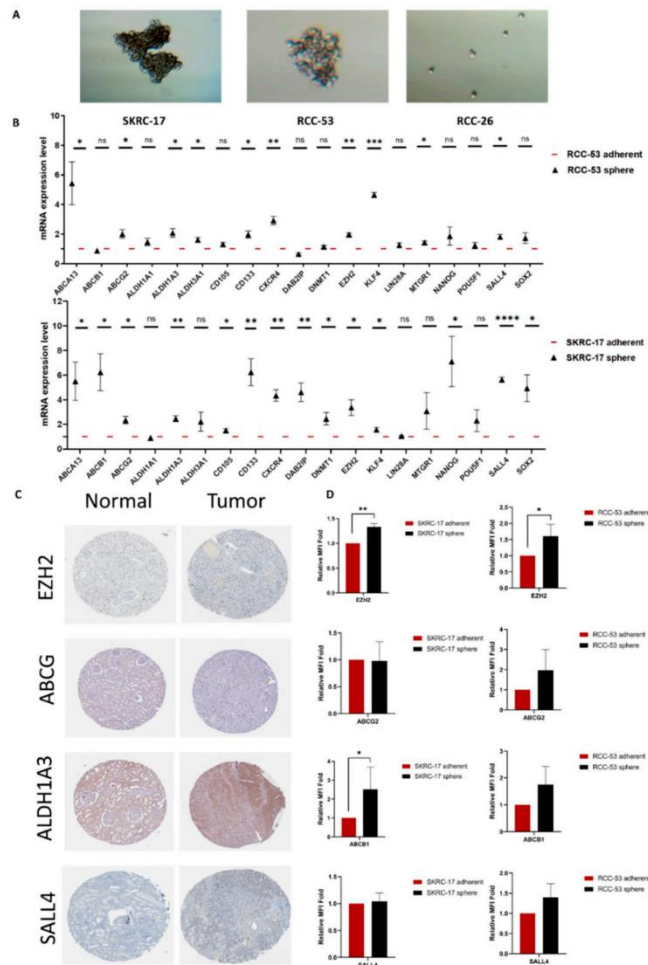


Figure 2. Cont.







**Figure 3.** The sphere formation ability of the RCC cell lines and the expression of potential CSC markers on the mRNA and protein levels. (A) Sphere formation: SKRC-17 and RCC-53 formed spheres around day 7, RCC-26 did not. Photos were taken by a microscope digital camera at the magnification of 100× (Bresser GmbH DE-46414 Rhede Germany). (B) mRNA expression of 19 potential CSC markers in SKRC-17, RCC-53, and their corresponding CSCs analyzed by RT-qPCR analysis ( $p < 0.05$  indicates statistical significance), the expression level observed in spheres was normalized to the corresponding adherent line. \*  $p < 0.05$ , \*\*  $p < 0.01$ , \*\*\*  $p < 0.001$ , \*\*\*\*  $p < 0.0001$ . (C) Representative images of IHC staining for the EZH2, ABCG2, ALDH1A3, and SALL4 expression in the KIRC and normal tissue, photos derived from the Human Protein Atlas database. (D) Measurement of the protein expression in the adherent and sphere cell lines by flow cytometry ( $n = 3$ , adherent cell value was set as 1).

### 3.3. Validation of Potential CSC Markers on mRNA and Protein Level

First, we tested the ability of the SKRC-17, RCC-53, and RCC-26 cell lines to generate CSCs using a sphere formation assay over 2–3 passages. Using ultra-low attachment flasks with serum-free medium, CSCs formed non-adherent free-floating spheres, while the differentiated adherent renal cancer cells shrank and died [19,49]. Only SKRC-17 and RCC-53 were capable of generating spheres, as shown in Figure 3A, after 7 days. Next, the mRNA expression levels were analyzed in the SKRC-17 and RCC-53 adherent and sphere cell lines by RT-qPCR (Figure 3B). Four typical CSC markers (EZH2, ABCG2, ALDH1A3, and SALL4) were selected to verify the protein expression. Immunohistochemical images were collected from the Human Protein Atlas (Figure 3C). Flow cytometry was performed to determine the protein expression of the four markers between the adherent and sphere cell lines (Figure 3D). Among them, EZH2 was selected as the most potential ccRCC CSC marker, which was significantly higher expressed in the sphere cell lines than in the adherent cell lines on the mRNA level as well as on the protein level, with the ability to be an OS-related prognostic factor.

### 3.4. Correlation of EZH2 Expression with the Survival and Clinical Characteristics of KIRC Patients

The clinical characteristics of the KIRC patients including survival, stage, grade, and TNM classification were grouped into EZH2 high and low expression according to the median expression level. There was a statistically significant negative correlation between the expression of EZH2 and the prognosis of KIRC patients. The low expression group showed a longer survival than the high expression group (Figure 4A). The expression of EZH2 increased significantly, along with the progression of stage, grade, and TNM stages (Figure 4B). Multivariable Cox regression analysis showed that EZH2 could be an independent prognostic factor to assess the outcomes for KIRC patients (Figure 4C).

### 3.5. Correlation of EZH2 with the Composition of TICs

To explore a potential correlation between CSC features and the KIRC TME, the proportion of tumor-infiltrating immune subsets was determined via CIBERSORT algorithm and correlated to the expression of EZH2. Of the 22 types of immune cell profiles in KIRC samples (Figure 5), nine types of TICs had different frequencies in high versus low expression of EZH2 (Figure 6A–C): follicular helper T cells, regulatory T cells (Tregs), and CD8 T cells were more prevalent in EZH2 high tumors than in the EZH2 low tumors, while B cells, CD4 T memory resting, and M2 macrophages activated dendritic cells as well as resting mast cells were more abundant in EZH2 low tumors.

### 3.6. Functional Enrichment Analysis of EZH2

To further explore the potential association between the immune activity and EZH2, GSEA analysis was implemented for the high expression group compared to the low expression group. As shown in Figure 6D, in the high expression group, immune-related activities such as natural killer cell-mediated cytotoxicity, primary immunodeficiency, and immune signaling pathways such as T cell receptor, p53, and JAK-STAT were mainly enriched. In the low expression group, the genes were enriched, which correlated with the metabolic pathways including pyruvate, propanoate, and butanoate metabolisms.

### 3.7. Influence of Four Different Phytochemicals on EZH2 mRNA Expression

Four phytochemicals (EGCG, shikonin, apigenin, and wogonin) were selected based on the results of previous studies. The SKRC-17 and RCC-53 cell lines were treated with different concentrations of apigenin, EGCG, wogonin, and shikonin, as indicated in the figures, for 24 h and 48 h (Figure 7A). All PTCs inhibited the cell viability in a dose-dependent manner. The half-maximal inhibitory concentration (IC<sub>50</sub>) was calculated. Then, we treated the SKRC-17 and RCC-53 spheres with different concentrations (0.5 × IC<sub>50</sub>, 1 × IC<sub>50</sub>, and 2 × IC<sub>50</sub>) based on the results from the 48 h treatment to identify the influence on the mRNA expression level of EZH2 by RT-qPCR (Figure 7B). Transcript levels



of *EZH2* in SKRC-17 and RCC-53 CSCs were significantly decreased by shikonin, EGCG, and apigenin, but not significantly by wogonin. EGCG showed the best inhibitory effect of all of the tested PTCs.

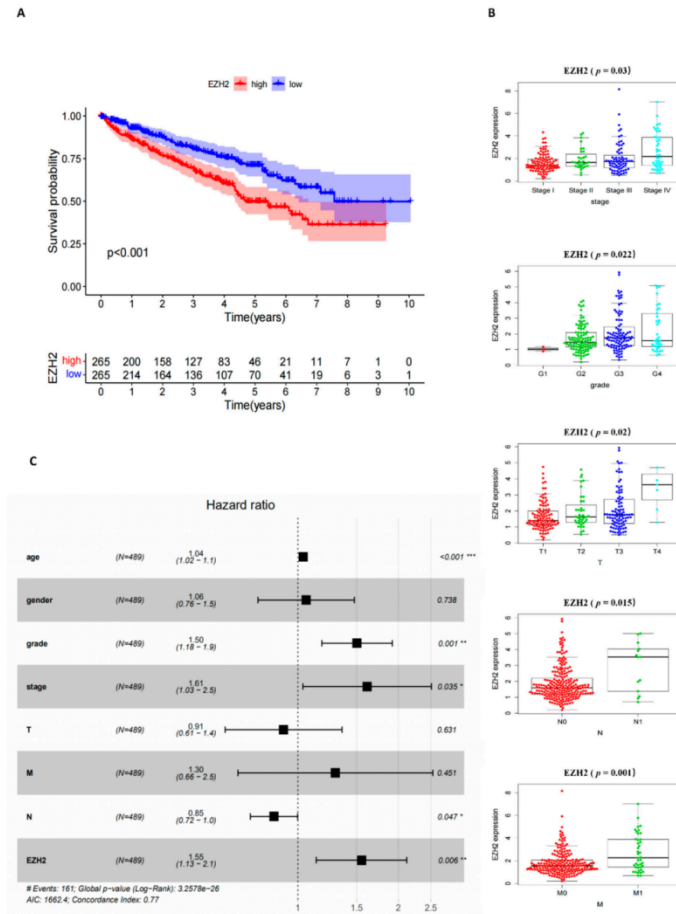


**Figure 4.** The correlation of *EZH2* expression with clinicopathological characteristics: (A) Kaplan–Meier survival analysis for the KIRC patients grouped into high or low score in *EZH2* expression determined by the comparison with the median,  $p < 0.001$  by log-rank test. (B) Distribution of *EZH2* expression concerning the stage, grade, and T classification, the  $p$ -values  $p = 0.003$ ,  $0.022$ , and  $0.002$ , respectively, were calculated by the Kruskal–Wallis rank sum test, distribution of scores in M and N classification, the  $p$ -values  $p = 0.001$  and  $0.0015$ , respectively, were calculated by the Wilcoxon rank sum test. (C) The multivariate Cox regression analysis of the risk score, age, gender, grade, and TNM stage was used to evaluate the independent prognostic value of *EZH2*. \*  $p < 0.05$ , \*\*  $p < 0.01$ , \*\*\*  $p < 0.001$ .

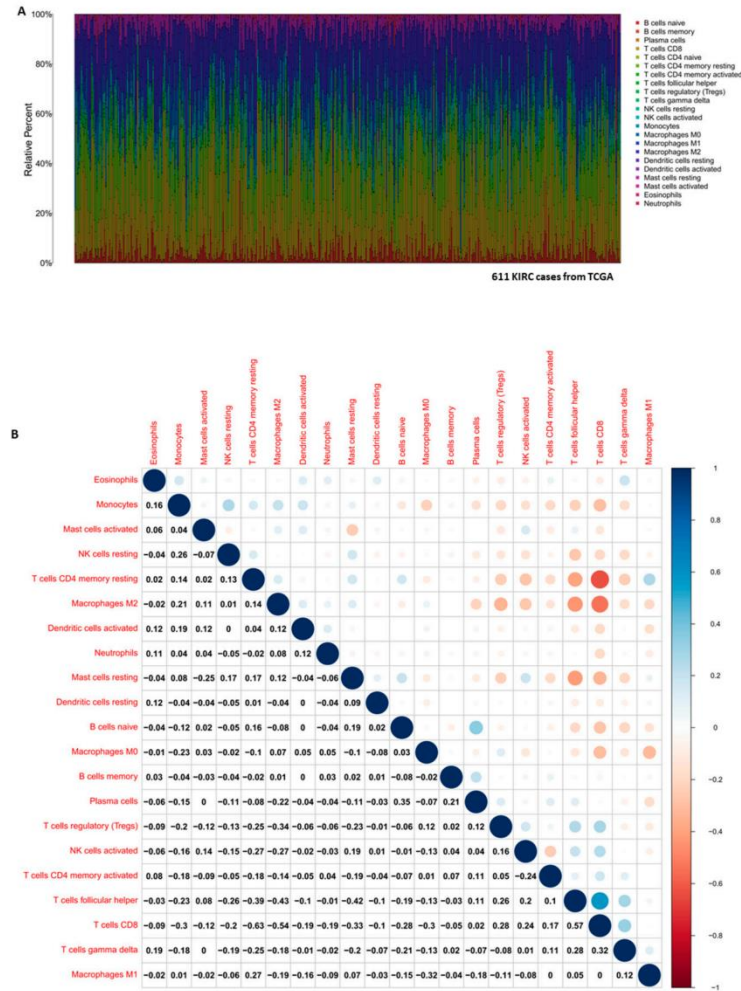


**Figure 5.** The TIC profile in the KIRC tumor samples and correlation analysis. (A) The barplot shows the proportion of 22 types of TICs in the KIRC tumor samples, columns are the 611 KIRC case samples and the different colors are types of TICs. (B) The heatmap shows the correlation between 22 TIC populations and the numbers in each tiny box indicate the  $p$  value of the correlation between two cell populations, the shade of each tiny color box represents the corresponding correlation value between two cell types, and the Pearson coefficient was used for the significance test.

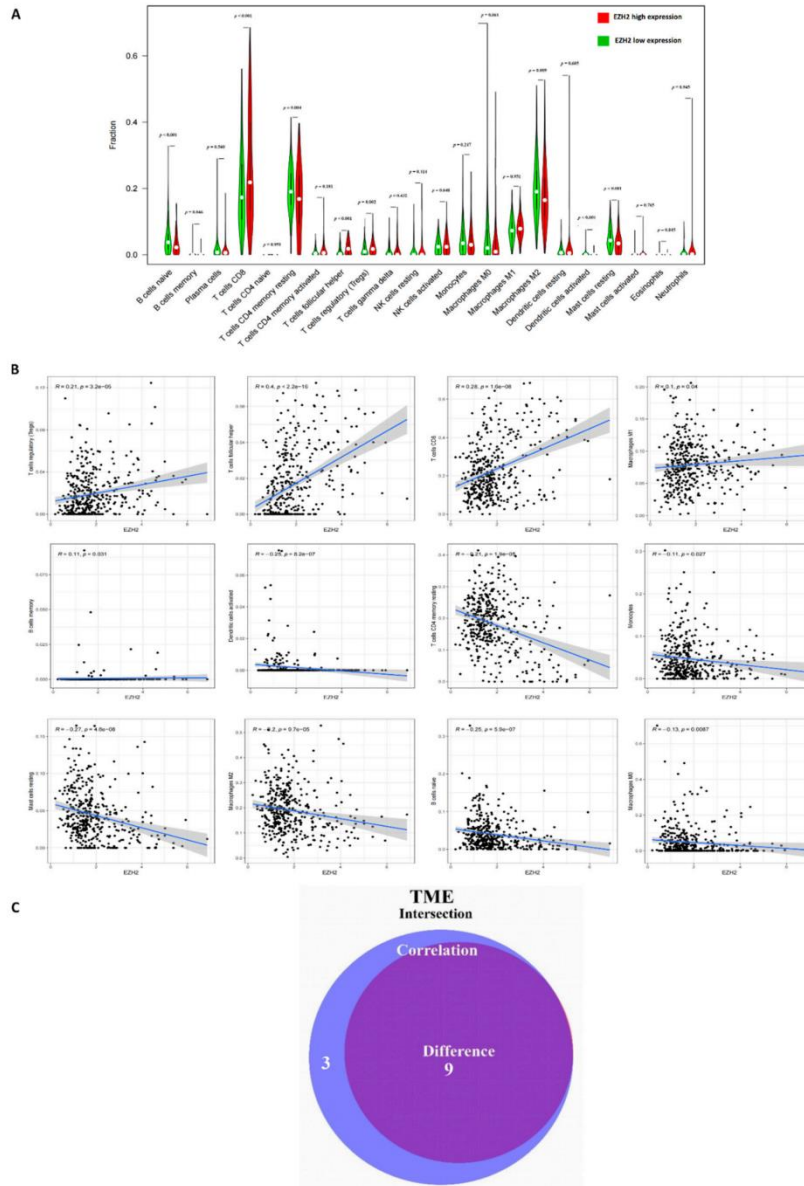
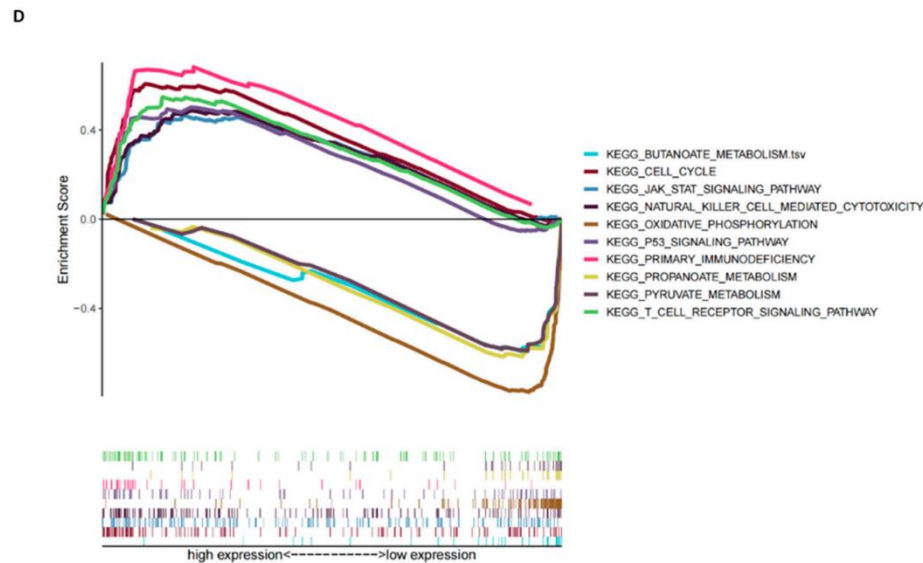


Figure 6. Cont.



**Figure 6.** The correlation of the TIC composition and signaling pathway with EZH2 expression. (A) Correlation of the TIC population with EZH2 expression, the Violin diagram shows the relationship between the different 22 TIC subpopulations and the KIRC tumor samples with low (green) or high (red) EZH2 expression, relative to the median of the EZH2 expression level, the Wilcoxon rank sum was used for the significance test. (B) The scatter plot shows the correlation of 12 TIC subpopulations to the EZH2 expression ( $p < 0.05$ ), the blue line in each plot shows the fitted linear model indicating the proportion tropism of the immune cell along with the EZH2 expression, and the Pearson coefficient was used for the correlation test. (C) The Venn plot displays nine TIC subpopulations correlated with the EZH2 expression codetermined by difference and correlation tests displayed in violin and scatter plots, respectively. (D) The gene set enrichment analysis for the enriched gene sets with high and low EZH2 expression in the KEGG collection, each line represents one particular gene set with a unique color, upregulated gene sets are located on the left near at the origin of the coordinates, in contrast, the downregulated gene sets are on the right of the  $x$ -axis. Only gene sets with NOM  $p < 0.05$  and FDR  $q < 0.06$  were considered as significant and only some of the leading pathways are displayed in the plot.

### 3.8. EGCG Inhibits Cell Viability and Induces Apoptosis in RCC-53 and SKRC-17 Cell Lines

To further investigate the anti-tumor effect of EGCG, we performed cell viability and apoptosis assays with the RCC-53 and SKRC-17 adherent cell lines and spheres. The results showed a dose-dependent tendency for inhibiting the viability and enhancing apoptosis among the different concentration groups ( $0.5 \times IC_{50}$ ,  $1 \times IC_{50}$ , and  $2 \times IC_{50}$ ) (Figure 8). The SKRC-17 sphere and RCC-53 sphere groups were less sensitive to EGCG than the adherent SKRC-17 and RCC-53 cells.

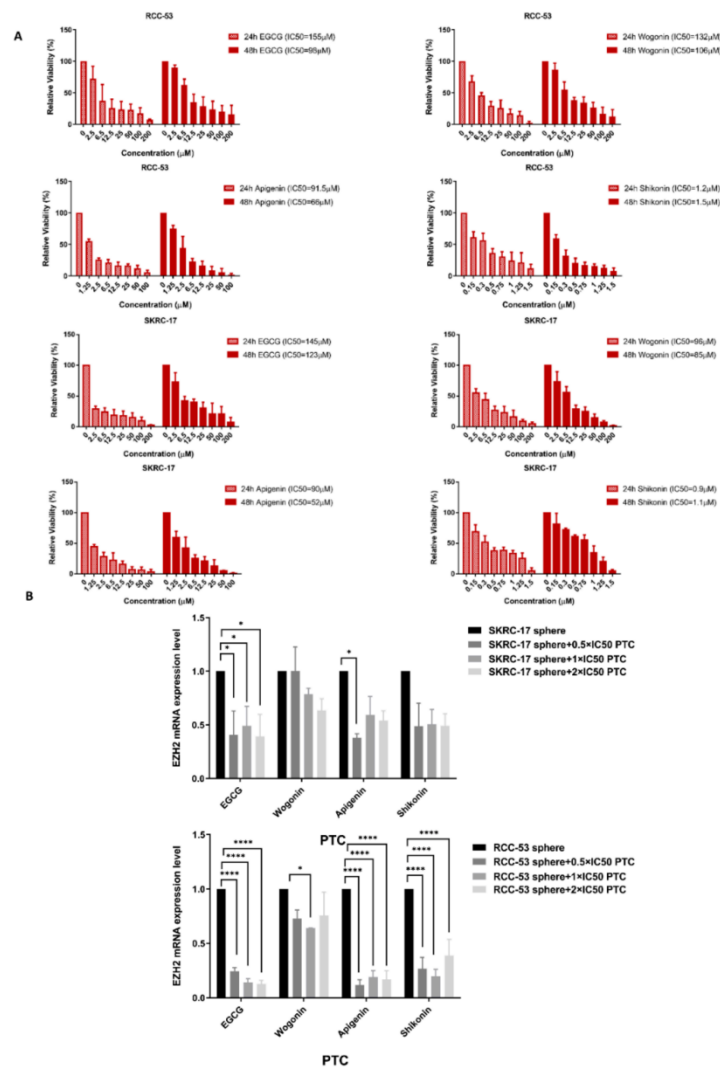


**Figure 7.** EGCG inhibited the expression of EZH2 in ccRCC CSCs. (A) CellTiter-Blue Cell Viability Assay: EGCG, wogonin, apigenin, and shikonin inhibited the viability of SKRC-17, RCC-53 in a dose-dependent manner, shown after 24 and 48 h. The half-maximal inhibitory concentration (IC50) was calculated by the logit regression model. (B) RT-qPCR analysis: EGCG, wogonin, apigenin, and shikonin reduced the expression of EZH2 in the sphere cells, normalized expression levels are displayed ( $n = 3$ , \*  $p < 0.05$ , \*\*\*\*  $p < 0.0001$ ).

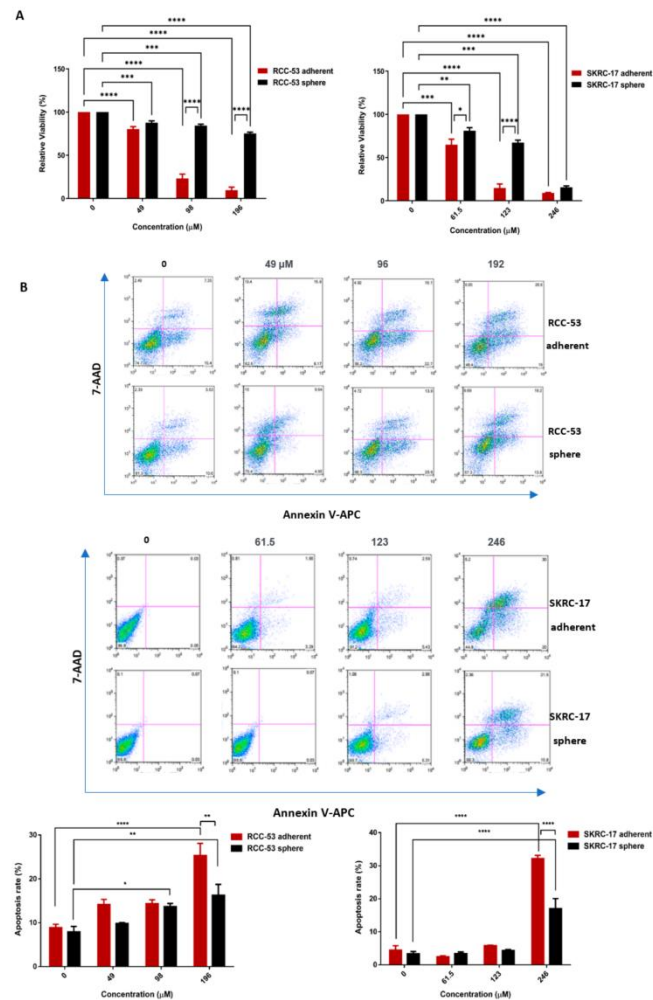


**Figure 8.** EGCG mediated the anti-tumor effect against SKRC-17, RCC-53, and their corresponding CSCs. (A) CellTiter-Blue Cell Viability Assay: EGCG suppressed the cell viability (shown for 48 h). (B) EGCG induced apoptosis, the apoptosis rate was calculated by Annexin V and 7-AAD positive staining using flow cytometry ( $n = 3$ , \*  $p < 0.05$ , \*\*  $p < 0.01$ , \*\*\*  $p < 0.001$ , \*\*\*\*  $p < 0.0001$ ).

### 3.9. EGCG Inhibits Migration and Invasion of RCC-53 and SKRC-17 Cell Lines

Migration and invasion are two essential biological characteristics for the metastatic process. Therefore, we evaluated the effect of EGCG on the migration and invasion of SKRC-17, the RCC-53 adherent cell lines, and their corresponding sphere cells. The invasion ability was determined using the Boyden chamber system and cells were treated with different concentrations of EGCG ( $0.5 \times IC_{50}$ ,  $1 \times IC_{50}$ , and  $2 \times IC_{50}$ ) for 48 h. The numbers of invaded cells decreased significantly in the adherent SKRC-17 and RCC-53 cell lines as well



as the corresponding spheres in the  $2 \times IC_{50}$  group (Figure 9A). Migration was evaluated using the scratch wound healing assay. After treatment with different concentrations of EGCG ( $0.25 \times IC_{50}$ ,  $0.5 \times IC_{50}$ , and  $1 \times IC_{50}$ ), images were taken at six time points every three hours apart. EGCG in the  $1 \times IC_{50}$  group inhibited the migration of both the adherent cells and sphere cells to the center of the gap, as shown in Figure 9B.

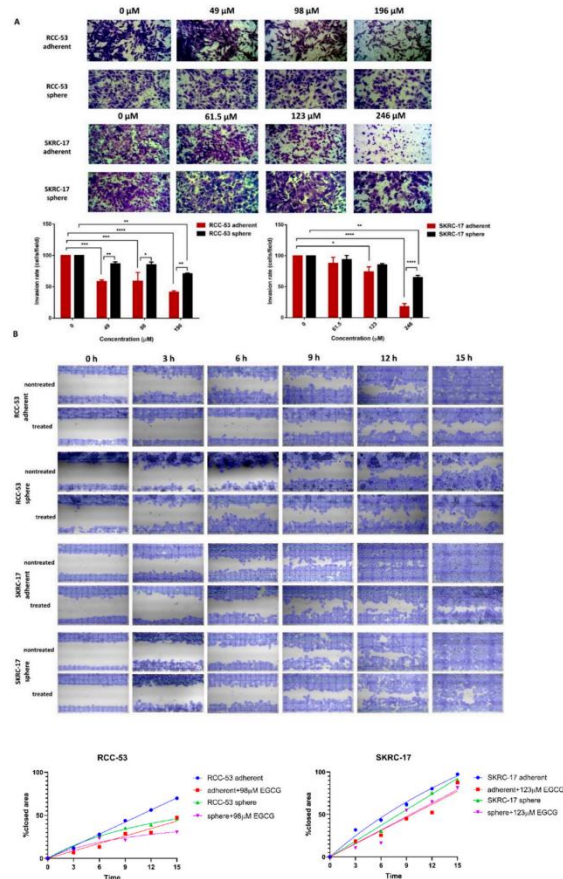


**Figure 9.** EGCG inhibited invasion and migration of the cCRCC cell lines and their corresponding CSCs. **(A)** For the invasion assay, the Boyden Chamber system was used with Transwell inserts in 24-well plates (8.0 μm pores), coated with growth factor reduced Matrigel Basement Matrix, from every insert a photo was taken at the magnification of 40× and the cells were counted (three fields per insert; Fiji ImageJ software). \*  $p < 0.05$ , \*\*  $p < 0.01$ , \*\*\*  $p < 0.001$ , \*\*\*\*  $p < 0.0001$ . **(B)** For the scratch wound healing, assay plates with a cell-free gap of 500 μm were used (ibidi GmbH), photos were taken under the microscope at different time points at the magnification of 40× (Bresser GmbH DE-46414 Rhede Germany). EGCG in the  $1 \times IC_{50}$  group is shown, and the data were analyzed with the web-based Automated Cellular Analysis System (ACAS, MetaVi Labs) using FastTrack AI image analysis algorithms.

### 3.10. Network of EGCG Target Genes and EZH2

To further uncover the potential pharmacological mechanisms of EGCG inhibiting CSC associated proteins, target genes of EGCG were analyzed in networks. A total of 71 genes were predicted to be direct targets of EGCG, and networks were constructed via the PPI network based on the STRING database. Interactions between the potential 71 target genes and *EZH2* are shown in Figure 10A. Subsequently, a network for EGCG, *EZH2* target genes, and *EZH2* was built using the String database and Cytoscape software. As shown in Figure 10B, *EZH2* is connected with the three EGCG potential target genes *VEGFA*, *KIF11*, and *MMP2*.

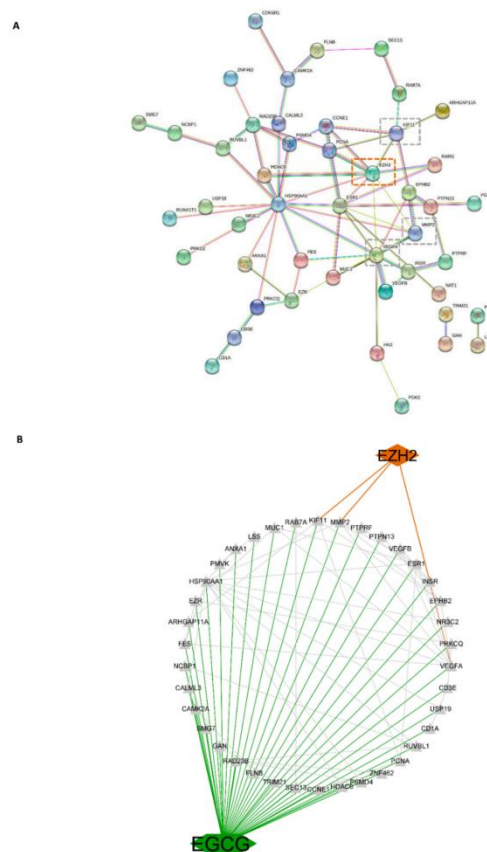
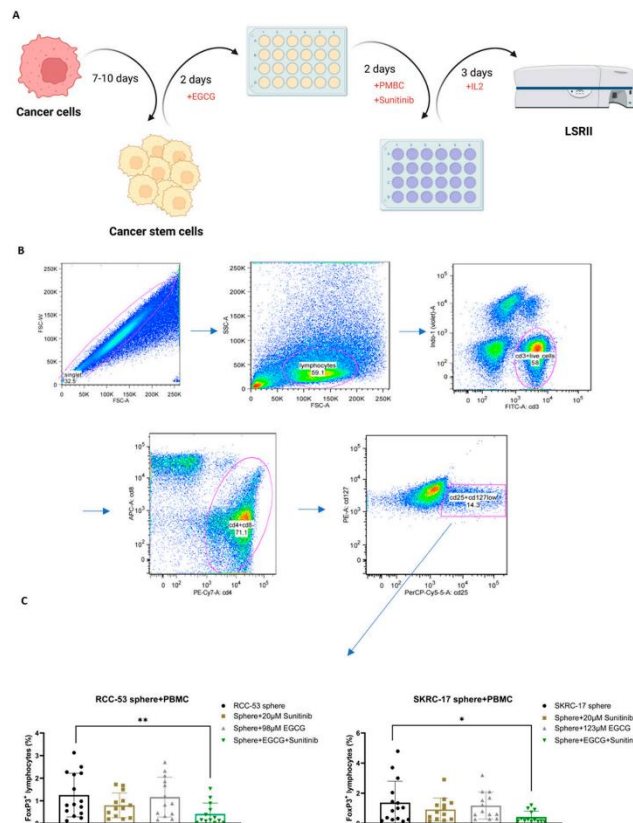


**Figure 10.** The interaction network based on the potential targets of EGCG. (A) The PPI network of potential target genes of EGCG and *EZH2*; the edges represent the predicted functional associations, green line: the neighborhood evidence, blue line: co-occurrence evidence, purple line: experimental evidence, yellow line: text mining evidence, black line: co-expression evidence, dotted lines: the potential target genes of EGCG and *EZH2*. (B) The network of EGCG, *EZH2* target genes, and *EZH2*, green lines represent the interaction between EGCG and its target genes, red lines represent interaction between *EZH2* and target genes, black lines represent interaction among target genes.



### 3.11. The Effect of EGCG Combined with Sunitinib on Immune Cells

To determine whether EGCG combined with the first line treatment agent sunitinib had an effect on immune cells, an immunophenotyping assay for the ccRCC patients' peripheral blood cells (PBMC) was conducted. For this, a co-culture system of CSCs and PBMC was established to study the influence of drug-treated CSCs on different PBMC subpopulations (Figure 11A). The main effect was observed in the Treg cell population. The gating strategy for the Treg cell population is shown in Figure 11B. The  $CD4^+$ ,  $CD25^+$ ,  $CD127^{low}$ ,  $FOXP3^+$  T cell subpopulation corresponded to the effector Treg cells. As shown in Figure 11C, the percentage of the  $FOXP3^+$  Treg subpopulation was significantly decreased in the combination group compared to the group without treatment, the EGCG group, or sunitinib group.



#### 4. Discussion

CSCs can evade cell death and can initiate metastasis of the tumor by possessing the capacity of self-renewal and multiple differentiation [50]. Studies have shown that 25–30% of ccRCC patients already had distant metastases at the time of initial diagnosis [51]. So far, angiogenesis inhibition with tyrosine kinase inhibitors (TKIs) combined with the inhibition of immune checkpoint proteins such as PD-1/PDL-1 and CTLA-4 have revolutionized the treatment landscape of ccRCC patients with metastases [52,53]. However, the responses are limited to a subgroup of patients and only approximately 5 to 30% of patients will primarily progress [54]. Therefore, additional therapies or promising additives to the current therapeutic landscape to those non-responders are needed. Recently, it was proposed that renal CSCs isolated from renal cell carcinomas can mediate tumor growth and be the cause for resistance to standard chemo- and radiotherapies, and even tyrosine kinase receptor inhibitors, mTOR inhibitors, VEGF antibodies, cytokines, checkpoint inhibitors, etc. [55–57]. Uncovering the molecular mechanisms of metastatic initiation and dynamics of ccRCC CSCs hold promise in improving the management of ccRCC. The key findings of this study can be summarized as follows. (1) a corrected-mRNAsi describing the stemness index of KIRC tumors of the TCGA atlas was significantly high in the KIRC tissue samples compared with normal tissue and positively correlated with the clinical stage and grade. (2) EZH2 was selected as the most promising CSC marker, which was expressed significantly higher in the tumor tissue and cell spheres of the cell lines than in the normal tissue or adherent cell lines, respectively. (3) The expression of EZH2 was statistically correlated with the clinical characteristics, nine types of TICs, immune-related signaling pathways as well as metabolic pathways. (4) Among the four tested PTCs, EGCG suppressed cell viability, migration and invasion, and enhanced apoptosis in adherent and sphere cell lines significantly and showed the highest inhibition of EZH2 expression. *KIF11*, *MMP2*, and *VEGFA* were predicted as target genes interacting with EZH2, and they may play a role and should be tested in future for co-expression. (5) The combination treatment of EGCG with sunitinib significantly decreased the frequency of CD4<sup>+</sup>, CD25<sup>+</sup>, CD127<sup>low</sup>, FOXP3<sup>+</sup>, Treg in the PBMC of the ccRCC patients compared to the group without treatment

Previously, in a pan-cancer stemness index study, the mRNAsi in the KIRC samples was shown to range between 0.2 and 0.5, indicating lower stemness ability than most other tumors such as chromophobe renal cell carcinoma, lymphoma, and uterine sarcoma. After correcting for tumor purity, the corrected-mRNAsi showed a strong prognostic value in KIRC tumors. Not all of the tested ccRCC cell lines possessed stemness capacity (see RCC-26 in Figure 3A), as also described in Gassenmaier et al. [19], and indicates that different ccRCC cells contain various amounts and types of CSC populations. A previous pan-cancer stemness index study identified high expression of EZH2 in ccRCC CSCs [20]. The high prognostic value of EZH2 expression and its association with immune related characteristics observed in this study confirms results from a previous study in which a correlation of high EZH2 expression with poor overall survival was identified in 373 RCC patients, especially in those with advanced disease [58]. The overexpression of EZH2 in RCC associated with lymphocytic infiltration and high CD8<sup>+</sup> density could navigate immune evasion and the poor patient outcome [16], supporting a treatment strategy aimed at downregulating EZH2. Modulating EZH2 expression or activity has been reported to suppress the phosphorylation of certain receptor tyrosine kinase inhibitors and restore the antitumor effects of sunitinib in models of acquired or intrinsically resistant ccRCC [59]. The proposed mechanism is that downregulated EZH2 expression unleashes pro-inflammatory functions in tumor-infiltrating Tregs cells, which promotes anti-cancer immunity as well as tumor elimination, boosts the recruitment and function of CD8<sup>+</sup> and CD4<sup>+</sup> effector T cells, and thus remodels the tumor microenvironment [60].

Several EZH2 inhibitors have been developed in recent years, for example, the 2-pyridone compounds GSK126, EPZ005687, and EI1 [61]. The studies have mostly addressed the EZH2-targeted treatments of lymphoma and melanoma or of tumor cell lines. Moreover, other drugs and compounds such as curcumin, omega-3 polyunsaturated fatty acids as

well as sorafenib have been reported to be able to downregulate EZH2 and this was critical for their anti-cancer activity, as shown for hepatoma cells, pancreatic tumor cells, and breast cancer cells, respectively [62–65]. Curcumin, which is another potential anti-tumor phytochemical, was also tested in our group using RCC spheres. An inhibiting effect on spheres was observed with only a slight downregulation of EZH2 (unpublished data). In addition, the inhibition of EZH2 also sensitizes cancer cells to various other anti-cancer drugs such as HDAC inhibitors, imatinib, gemcitabine, paclitaxel, and cisplatin [66–74]. In 2020, the Food and Drug Administration (FDA) approved the first EZH2 inhibitor tazemetostat (EPZ-6438) for the treatment of metastatic or locally advanced epithelioid sarcoma [75]. In the kidney, EZH2 plays a major role in maintaining normal kidney function. The overexpression of EZH2 has been demonstrated to be related to acute kidney injury (AKI). It can be speculated that the inhibition of EZH2 overexpression might help prevent the development of pathologies after acute kidney injury. In this regard, the substance zld1039, one of the EZH2 inhibitors, holds promise for the treatment of AKI [76]. Moreover, antibodies against other CSC markers (e.g., CXCR4 antibody, CD105 (endoglin) antibody) have been used in RCC clinical trials (NCT01391130: CXCR4 inhibitor plus sunitinib, NCT01727089: endoglin monoclonal antibody plus bevacizumab, and NCT01806064: endoglin monoclonal antibody plus axitinib). However, all trials failed to improve PFS when combined with TKI agents [77–79].

In this study, we hypothesize that EGCG may be a beneficial combination partner for sunitinib for the treatment of ccRCC patients due to its strong inhibitory effect on cancer stem cells (Figure 12). EGCG has been used in *in vivo* models of various cancers with promising therapeutic effects such as suppressing xenograft tumor growth and invasion, reducing tumor volume and size, inhibiting tumor angiogenesis, and increasing tumor cell apoptosis [31,34]. Our study confirms that EGCG combined with sunitinib showed a significant reduction in FoxP3<sup>+</sup> Treg cells in the PBMC of patients. Less Treg cells might allow, at least in part, an activation of the endogenous effector CD3<sup>+</sup>CD8<sup>+</sup> and CD3<sup>+</sup>CD4<sup>+</sup> T cells in response to the recognition of tumor specific antigens. We propose that the combination of EGCG and sunitinib could be a promising treatment strategy.

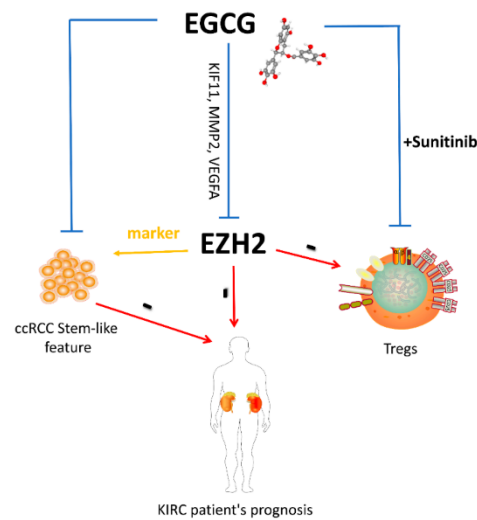


**Figure 12.** The proposed model for the correlation among EZH2, cancer stem cells, and EGCG for the KIRC patients.

This study aimed to identify a CSC marker in ccRCC that could be a potential prognostic marker modulating the microenvironment. Furthermore, we analyzed the mechanisms of the potential phytochemicals' network pharmacology using bioinformatics, cell biological, and immunological methods. We studied the potential mechanisms of a novel combination treatment strategy for ccRCC patients targeting cancer stem cells and the tumor microenvironment. These findings can help to optimize therapeutic strategies in the future.

## 5. Conclusions

We identified the CSC marker EZH2, which has the potential to be a prognostic and microenvironment-associated factor in ccRCC. Moreover, the novel treatment strategy—EGCG in combination with sunitinib—provides new insights into the treatment options of ccRCC based on targeting CSCs, and the related pharmacological mechanism was further explored in this study.

**Author Contributions:** C.L. and H.P. contributed to the conception and design of the study. C.L. and L.W. organized the database and performed the statistical analysis. C.L. and L.W. wrote the first draft of the manuscript. H.P., B.S., A.B. and E.N. offered technical or material support, critical reading, and text revisions. All authors have read and agreed to the published version of the manuscript.

**Funding:** The study was supported by the LMU clinic. The author Chen Lyu is funded by a China scholarship council (CSC No. 201908080121).

**Institutional Review Board Statement:** The study was conducted according to the guidelines of the Declaration of Helsinki and approved by the Ethics Committee of the Ludwig Maximilians University Munich (Project No. 003/02, 13 November 2003; Project No. 214/04, 22 October 2004).

**Informed Consent Statement:** Informed consent was obtained from all subjects involved in the study.

**Data Availability Statement:** Data are contained within the article from the corresponding author on reasonable request.

**Conflicts of Interest:** The authors declare no conflict of interest.

## References

- Capitaino, U.; Montorsi, F. Renal cancer. *Lancet* **2016**, *387*, 894–906. [[CrossRef](#)]
- Barata, P.C.; Rini, B.I. Treatment of renal cell carcinoma: Current status and future directions. *CA Cancer J. Clin.* **2017**, *67*, 507–524. [[CrossRef](#)] [[PubMed](#)]
- Motzer, R.J.; Jonasch, E.; Agarwal, N.; Beard, C.; Bhayani, S.; Bolger, G.B.; Chang, S.S.; Choueiri, T.K.; Costello, B.A.; Derweesh, I.H. Kidney cancer, version 3.2015. *J. Natl. Compr. Cancer Netw.* **2015**, *13*, 151–159. [[CrossRef](#)] [[PubMed](#)]
- Koren, E.; Fuchs, Y. The bad seed: Cancer stem cells in tumor development and resistance. *Drug Resist. Updates* **2016**, *28*, 1–12. [[CrossRef](#)]
- Pan, X.-W.; Zhang, H.; Xu, D.; Chen, J.-X.; Chen, W.-J.; Gan, S.-S.; Qu, F.-J.; Chu, C.-M.; Cao, J.-W.; Fan, Y.-H.; et al. Identification of a novel cancer stem cell subpopulation that promotes progression of human fatal renal cell carcinoma by single-cell RNA-seq analysis. *Int. J. Biol. Sci.* **2020**, *16*, 3149. [[CrossRef](#)]
- Bussolati, B.; Bruno, S.; Grange, C.; Ferrando, U.; Camussi, G. Identification of a tumor-initiating stem cell population in human renal carcinomas. *FASEB J.* **2008**, *22*, 3696–3705. [[CrossRef](#)]
- Hirata, A.; Hatano, Y.; Niwa, M.; Hara, A.; Tomita, H. Heterogeneity in colorectal cancer stem cells. *Cancer Prev. Res.* **2019**, *12*, 413–420. [[CrossRef](#)]
- Zhao, Y.; Ding, L.; Wang, D.; Ye, Z.; He, Y.; Ma, L.; Zhu, R.; Pan, Y.; Wu, Q.; Pang, K. EZH 2 cooperates with gain-of-function p53 mutants to promote cancer growth and metastasis. *EMBO J.* **2019**, *38*, e99599. [[CrossRef](#)]
- Wang, W.; Fang, F.; Ozes, A.; Nephew, K.P. Targeting Ovarian Cancer Stem Cells by Dual Inhibition of HOTAIR and DNA Methylation. *Mol. Cancer Ther.* **2021**, *20*, 1092–1101. [[CrossRef](#)]
- Wen, Y.; Hou, Y.; Yi, X.; Sun, S.; Guo, J.; He, X.; Li, T.; Cai, J.; Wang, Z. EZH2 activates CHK1 signaling to promote ovarian cancer chemoresistance by maintaining the properties of cancer stem cells. *Theranostics* **2021**, *11*, 1795. [[CrossRef](#)]
- Kempf, J.M.; Weser, S.; Bartoschek, M.D.; Metzeler, K.H.; Vick, B.; Herold, T.; Völse, K.; Mattes, R.; Scholz, M.; Wange, L.E. Loss-of-function mutations in the histone methyltransferase EZH2 promote chemotherapy resistance in AML. *Sci. Rep.* **2021**, *11*, 5838. [[CrossRef](#)] [[PubMed](#)]
- Suvà, M.-L.; Riggi, N.; Janiszewska, M.; Radovanovic, I.; Provero, P.; Stehle, J.-C.; Baumer, K.; Le Bitoux, M.-A.; Marino, D.; Cironi, L. EZH2 is essential for glioblastoma cancer stem cell maintenance. *Cancer Res.* **2009**, *69*, 9211–9218. [[CrossRef](#)] [[PubMed](#)]

13. Liu, H.; Sun, Q.; Sun, Y.; Zhang, J.; Yuan, H.; Pang, S.; Qi, X.; Wang, H.; Zhang, M.; Zhang, H. MELK and EZH2 Cooperate to Regulate Medulloblastoma Cancer Stem-like Cell Proliferation and Differentiation Interaction between MELK and EZH2 in Medulloblastoma. *Mol. Cancer Res.* **2017**, *15*, 1275–1286. [[CrossRef](#)] [[PubMed](#)]
14. van Vlerken, L.E.; Kiefer, C.M.; Morehouse, C.; Li, Y.; Groves, C.; Wilson, S.D.; Yao, Y.; Hollingsworth, R.E.; Hurt, E.M. EZH2 is required for breast and pancreatic cancer stem cell maintenance and can be used as a functional cancer stem cell reporter. *Stem Cells Transl. Med.* **2013**, *2*, 43–52. [[CrossRef](#)] [[PubMed](#)]
15. Singh, A.K.; Verma, A.; Singh, A.; Arya, R.K.; Maheshwari, S.; Chaturvedi, P.; Nengroo, M.A.; Saini, K.K.; Vishwakarma, A.L.; Singh, K. Salinomycin inhibits epigenetic modulator EZH2 to enhance death receptors in colon cancer stem cells. *Epigenetics* **2021**, *16*, 144–161. [[CrossRef](#)]
16. Eichenauer, T.; Simmendinger, L.; Fraune, C.; Mandelkow, T.; Blessin, N.C.; Kluth, M.; Hube-Magg, C.; Möller, K.; Clauditz, T.; Weidemann, S. High level of EZH2 expression is linked to high density of CD8-positive T-lymphocytes and an aggressive phenotype in renal cell carcinoma. *World J. Urol.* **2021**, *39*, 481–490. [[CrossRef](#)]
17. Zhang, Y.; Sun, B.; Zhao, X.; Liu, Z.; Wang, X.; Yao, X.; Dong, X.; Chi, J. Clinical significances and prognostic value of cancer stem-like cells markers and vasculogenic mimicry in renal cell carcinoma. *J. Surg. Oncol.* **2013**, *108*, 414–419. [[CrossRef](#)]
18. Ge, Y.; Weygant, N.; Qu, D.; May, R.; Berry, W.L.; Yao, J.; Chandrakesan, P.; Zheng, W.; Zhao, L.; Zhao, K.L. Alternative splice variants of DCLK1 mark cancer stem cells, promote self-renewal and drug-resistance, and can be targeted to inhibit tumorigenesis in kidney cancer. *Int. J. Cancer* **2018**, *143*, 1162–1175. [[CrossRef](#)]
19. Gassenmaier, M.; Chen, D.; Buchner, A.; Henkel, L.; Schiemann, M.; Mack, B.; Schendel, D.J.; Zimmermann, W.; Pohla, H. CXCL12 chemokine receptor 4 is essential for maintenance of renal cell carcinoma-initiating cells and predicts metastasis. *Stem Cells* **2013**, *31*, 1467–1476. [[CrossRef](#)]
20. Malta, T.M.; Sokolov, A.; Gentles, A.J.; Burzykowski, T.; Poisson, L.; Weinstein, J.N.; Kamińska, B.; Huelsken, J.; Omberg, L.; Gevaert, O. Machine learning identifies stemness features associated with oncogenic dedifferentiation. *Cell* **2018**, *173*, 338–354.e315. [[CrossRef](#)]
21. Tian, Y.; Wang, J.; Qin, C.; Zhu, G.; Chen, X.; Chen, Z.; Qin, Y.; Wei, M.; Li, Z.; Zhang, X. Identifying 8-mRNAsi based signature for predicting survival in patients with head and neck squamous cell carcinoma via machine learning. *Front. Genet.* **2020**, *11*, 1296. [[CrossRef](#)] [[PubMed](#)]
22. Ben-Porath, I.; Thomson, M.W.; Carey, V.J.; Ge, R.; Bell, G.W.; Regev, A.; Weinberg, R.A. An embryonic stem cell-like gene expression signature in poorly differentiated aggressive human tumors. *Nat. Genet.* **2008**, *40*, 499–507. [[CrossRef](#)] [[PubMed](#)]
23. Zhou, Q.-H.; Li, K.-W.; Chen, X.; He, H.-X.; Peng, S.-M.; Peng, S.-R.; Wang, Q.; Li, Z.-A.; Tao, Y.-R.; Cai, W.-L. HHLA2 and PD-L1 co-expression predicts poor prognosis in patients with clear cell renal cell carcinoma. *J. Immunother. Cancer* **2020**, *8*, e000157. [[CrossRef](#)]
24. Zhou, F.; Shen, D.; Xiong, Y.; Cheng, S.; Xu, H.; Wang, G.; Qian, K.; Ju, L.; Zhang, X. CTHRC1 is a prognostic biomarker and correlated with immune infiltrates in kidney renal papillary cell carcinoma and kidney renal clear cell carcinoma. *Front. Oncol.* **2020**, *10*, 3389. [[CrossRef](#)]
25. Gomez, K.E.; Wu, F.; Keysar, S.B.; Morton, J.J.; Miller, B.; Chimed, T.-S.; Le, P.N.; Nieto, C.; Chowdhury, F.N.; Tyagi, A. Cancer Cell CD44 Mediates Macrophage/Monocyte-Driven Regulation of Head and Neck Cancer Stem Cells. *Cancer Res.* **2020**, *80*, 4185–4198. [[CrossRef](#)]
26. Linette, G.P.; Carreno, B.M. Tumor-infiltrating lymphocytes in the checkpoint inhibitor era. *Curr. Hematol. Malig. Rep.* **2019**, *14*, 286–291. [[CrossRef](#)]
27. Huang, Z.; Yu, H.; Zhang, J.; Jing, H.; Zhu, W.; Li, X.; Kong, L.; Xing, L.; Yu, J.; Meng, X. Correlation of cancer stem cell markers and immune cell markers in resected non-small cell lung cancer. *J. Cancer* **2017**, *8*, 3190. [[CrossRef](#)] [[PubMed](#)]
28. Ghatalia, P.; Gordetsky, J.; Kuo, F.; Dulaimi, E.; Cai, K.Q.; Devarajan, K.; Bae, S.; Naik, G.; Chan, T.A.; Uzzo, R. Prognostic impact of immune gene expression signature and tumor infiltrating immune cells in localized clear cell renal cell carcinoma. *J. Immunother. Cancer* **2019**, *7*, 139. [[CrossRef](#)]
29. Bromwich, E.; McArdle, P.; Canna, K.; McMillan, D.; McNicol, A.; Brown, M.; Aitchison, M. The relationship between T-lymphocyte infiltration, stage, tumour grade and survival in patients undergoing curative surgery for renal cell cancer. *Br. J. Cancer* **2003**, *89*, 1906–1908. [[CrossRef](#)]
30. Dandawate, P.R.; Subramaniam, D.; Jensen, R.A.; Anant, S. Targeting cancer stem cells and signaling pathways by phytochemicals: Novel approach for breast cancer therapy. *Semin. Cancer Biol.* **2016**, *40–41*, 192–208. [[CrossRef](#)]
31. Naujokat, C.; McKee, D.L. The “Big Five” phytochemicals targeting cancer stem cells: Curcumin, EGCG, sulforaphane, resveratrol, and genistein. *Curr. Med. Chem.* **2020**, *28*, 4321–4342. [[CrossRef](#)] [[PubMed](#)]
32. Namiki, K.; Wongsirisin, P.; Yokoyama, S.; Sato, M.; Rawangkan, A.; Sakai, R.; Iida, K.; Sukanuma, M. (–)-Epigallocatechin gallate inhibits stemness and tumorigenicity stimulated by AXL receptor tyrosine kinase in human lung cancer cells. *Sci. Rep.* **2020**, *10*, 2444. [[CrossRef](#)] [[PubMed](#)]
33. Sun, X.; Song, J.; Li, E.; Geng, H.; Li, Y.; Yu, D.; Zhong, C. (–)-Epigallocatechin-3-gallate inhibits bladder cancer stem cells via suppression of sonic hedgehog pathway. *Oncol. Rep.* **2019**, *42*, 425–435. [[CrossRef](#)]
34. Jiang, P.; Xu, C.; Chen, L.; Chen, A.; Wu, X.; Zhou, M.; ul Haq, I.; Mariyam, Z.; Feng, Q. EGCG inhibits CSC-like properties through targeting miR-485/CD44 axis in A549-cisplatin resistant cells. *Mol. Carcinog.* **2018**, *57*, 1835–1844. [[CrossRef](#)] [[PubMed](#)]



35. Tang, S.N.; Fu, J.; Nall, D.; Rodova, M.; Shankar, S.; Srivastava, R.K. Inhibition of sonic hedgehog pathway and pluripotency maintaining factors regulate human pancreatic cancer stem cell characteristics. *Int. J. Cancer* **2012**, *131*, 30–40. [[CrossRef](#)] [[PubMed](#)]
36. Jiang, P.; Xu, C.; Zhang, P.; Ren, J.; Mageed, F.; Wu, X.; Chen, L.; Zeb, F.; Feng, Q.; Li, S. Epigallocatechin-3-gallate inhibits self-renewal ability of lung cancer stem-like cells through inhibition of CLOCK. *Int. J. Mol. Med.* **2020**, *46*, 2216–2224. [[CrossRef](#)] [[PubMed](#)]
37. Li, Y.-W.; Xu, J.; Zhu, G.-Y.; Huang, Z.-J.; Lu, Y.; Li, X.-Q.; Wang, N.; Zhang, F.-X. Apigenin suppresses the stem cell-like properties of triple-negative breast cancer cells by inhibiting YAP/TAZ activity. *Cell Death Discov.* **2018**, *4*, 105. [[CrossRef](#)]
38. Chan, M.M.; Chen, R.; Fong, D. Targeting cancer stem cells with dietary phytochemical-repositioned drug combinations. *Cancer Lett.* **2018**, *433*, 53–64. [[CrossRef](#)]
39. Wang, L.; Stadlbauer, B.; Lyu, C.; Buchner, A.; Pohla, H. Shikonin enhances the antitumor effect of cabazitaxel in prostate cancer stem cells and reverses cabazitaxel resistance by inhibiting ABCG2 and ALDH3A1. *Am. J. Cancer Res.* **2020**, *10*, 3784.
40. Schendel, D.J.; Gansbacher, B.; Oberneder, R.; Kriegmair, M.; Hofstetter, A.; Riethmüller, G.; Segurado, O. Tumor-specific lysis of human renal cell carcinomas by tumor-infiltrating lymphocytes. I. HLA-A2-restricted recognition of autologous and allogeneic tumor lines. *J. Immunol.* **1993**, *151*, 4209–4220.
41. Schindelin, J.; Arganda-Carreras, I.; Frise, E.; Kaynig, V.; Longair, M.; Pietzsch, T.; Preibisch, S.; Rueden, C.; Saalfeld, S.; Schmid, B. Fiji: An open-source platform for biological-image analysis. *Nat. Methods* **2012**, *9*, 676–682. [[CrossRef](#)] [[PubMed](#)]
42. Shannon, P.; Markiel, A.; Ozier, O.; Baliga, N.S.; Wang, J.T.; Ramage, D.; Amin, N.; Schwikowski, B.; Ideker, T. Cytoscape: A software environment for integrated models of biomolecular interaction networks. *Genome Res.* **2003**, *13*, 2498–2504. [[CrossRef](#)] [[PubMed](#)]
43. Pan, S.; Zhan, Y.; Chen, X.; Wu, B.; Liu, B. Identification of biomarkers for controlling cancer stem cell characteristics in bladder cancer by network analysis of transcriptome data stemness indices. *Front. Oncol.* **2019**, *9*, 613. [[CrossRef](#)]
44. Pei, J.; Wang, Y.; Li, Y. Identification of key genes controlling breast cancer stem cell characteristics via stemness indices analysis. *J. Transl. Med.* **2020**, *18*, 74. [[CrossRef](#)] [[PubMed](#)]
45. Butte, A.; Aran, D.; Sirota, M.; Butte, A. Systematic pan-cancer analysis of tumour purity. *Nat. Commun.* **2015**, *6*, 8971.
46. Corro, C.; Moch, H. Biomarker discovery for renal cancer stem cells. *J. Pathol. Clin. Res.* **2018**, *4*, 3–18. [[CrossRef](#)]
47. Rasti, A.; Mehrazma, M.; Madjd, Z.; Abolhasani, M.; Saeednejad Zanjani, L.; Asgari, M. Co-expression of cancer stem cell markers OCT4 and NANOG predicts poor prognosis in renal cell carcinomas. *Sci. Rep.* **2018**, *8*, 11739. [[CrossRef](#)]
48. Shi, D.; Che, J.; Yan, Y.; Peng, B.; Yao, X.; Guo, C. Expression and clinical value of CD105 in renal cell carcinoma based on data mining in The Cancer Genome Atlas. *Exp. Ther. Med.* **2019**, *17*, 4499–4505. [[CrossRef](#)]
49. Abbaszadegan, M.R.; Bagheri, V.; Razavi, M.S.; Momtazi, A.A.; Sahebkar, A.; Gholamin, M. Isolation, identification, and characterization of cancer stem cells: A review. *J. Cell. Physiol.* **2017**, *232*, 2008–2018. [[CrossRef](#)]
50. Plaks, V.; Kong, N.; Werb, Z. The cancer stem cell niche: How essential is the niche in regulating stemness of tumor cells? *Cell Stem Cell* **2015**, *16*, 225–238. [[CrossRef](#)]
51. Koh, W.-J.; Abu-Rustum, N.R.; Bean, S.; Bradley, K.; Campos, S.M.; Cho, K.R.; Chon, H.S.; Chu, C.; Clark, R.; Cohn, D. Cervical cancer, version 3.2019, NCCN clinical practice guidelines in oncology. *J. Natl. Compr. Cancer Netw.* **2019**, *17*, 64–84. [[CrossRef](#)] [[PubMed](#)]
52. Anker, J.; Miller, J.; Taylor, N.; Kyprianou, N.; Tsao, C.-K. From bench to bedside: How the tumor microenvironment is impacting the future of immunotherapy for renal cell carcinoma. *Cells* **2021**, *10*, 3231. [[CrossRef](#)] [[PubMed](#)]
53. Lin, E.; Liu, X.; Liu, Y.; Zhang, Z.; Xie, L.; Tian, K.; Liu, J.; Yu, Y. Roles of the dynamic tumor immune microenvironment in the individualized treatment of advanced clear cell renal cell carcinoma. *Front. Immunol.* **2021**, *12*, 653358. [[CrossRef](#)] [[PubMed](#)]
54. Ballesteros, P.Á.; Chamorro, J.; Román-Gil, M.S.; Pozas, J.; Gómez Dos Santos, V.; Granados, Á.R.; Grande, E.; Alonso-Gordoa, T.; Molina-Cerrillo, J. Molecular Mechanisms of Resistance to Immunotherapy and Antiangiogenic Treatments in Clear Cell Renal Cell Carcinoma. *Cancers* **2021**, *13*, 5981. [[CrossRef](#)] [[PubMed](#)]
55. Yuan, Z.-X.; Mo, J.; Zhao, G.; Shu, G.; Fu, H.-L.; Zhao, W. Targeting strategies for renal cell carcinoma: From renal cancer cells to renal cancer stem cells. *Front. Pharmacol.* **2016**, *7*, 423. [[CrossRef](#)]
56. Fang, P.; Zhou, L.; Lim, L.Y.; Fu, H.; Yuan, Z.-X.; Lin, J. Targeting strategies for renal cancer stem cell therapy. *Curr. Pharm. Des.* **2020**, *26*, 1964–1978. [[CrossRef](#)]
57. Singh, D. Current updates and future perspectives on the management of renal cell carcinoma. *Life Sci.* **2021**, *264*, 118632. [[CrossRef](#)]
58. Liu, L.; Xu, Z.; Zhong, L.; Wang, H.; Jiang, S.; Long, Q.; Xu, J.; Guo, J. Prognostic value of EZH2 expression and activity in renal cell carcinoma: A prospective study. *PLoS ONE* **2013**, *8*, e81484. [[CrossRef](#)]
59. Adelaiye-Ogala, R.; Budka, J.; Damayanti, N.P.; Arrington, J.; Ferris, M.; Hsu, C.-C.; Chintala, S.; Orillion, A.; Miles, K.M.; Shen, L. EZH2 modifies sunitinib resistance in renal cell carcinoma by kinome reprogramming. *Cancer Res.* **2017**, *77*, 6651–6666. [[CrossRef](#)]
60. Wang, D.; Quiros, J.; Mahuron, K.; Pai, C.-C.; Ranzani, V.; Young, A.; Silveria, S.; Harwin, T.; Abnousian, A.; Pagani, M. Targeting EZH2 reprograms intratumoral regulatory T cells to enhance cancer immunity. *Cell Rep.* **2018**, *23*, 3262–3274. [[CrossRef](#)]
61. Fioravanti, R.; Stazi, G.; Zwergel, C.; Valente, S.; Mai, A. Six years (2012–2018) of researches on catalytic ezh2 inhibitors: The boom of the 2-pyridone compounds. *Chem. Rec.* **2018**, *18*, 1818–1832. [[CrossRef](#)] [[PubMed](#)]
62. Wang, S.; Zhu, Y.; He, H.; Liu, J.; Xu, L.; Zhang, H.; Liu, H.; Liu, W.; Liu, Y.; Pan, D. Sorafenib suppresses growth and survival of hepatoma cells by accelerating degradation of enhancer of zeste homolog 2. *Cancer Sci.* **2013**, *104*, 750–759. [[CrossRef](#)] [[PubMed](#)]

63. Bao, B.; Ali, S.; Banerjee, S.; Wang, Z.; Logna, F.; Azmi, A.S.; Kong, D.; Ahmad, A.; Li, Y.; Padhye, S. Curcumin Analogue CDF Inhibits Pancreatic Tumor Growth by Switching on Suppressor microRNAs and Attenuating EZH2 Expression Targeting miRNA-Mediated Inactivation of EZH2 by CDF. *Cancer Res.* **2012**, *72*, 335–345. [\[CrossRef\]](#)
64. Hua, W.-F.; Fu, Y.-S.; Liao, Y.-J.; Xia, W.-J.; Chen, Y.-C.; Zeng, Y.-X.; Kung, H.-F.; Xie, D. Curcumin induces down-regulation of EZH2 expression through the MAPK pathway in MDA-MB-435 human breast cancer cells. *Eur. J. Pharmacol.* **2010**, *637*, 16–21. [\[CrossRef\]](#)
65. Dimri, M.; Bommi, P.V.; Sahasrabudhe, A.A.; Khandekar, J.D.; Dimri, G.P. Dietary omega-3 polyunsaturated fatty acids suppress expression of EZH2 in breast cancer cells. *Carcinogenesis* **2010**, *31*, 489–495. [\[CrossRef\]](#) [\[PubMed\]](#)
66. Zhang, J.-G.; Guo, J.-F.; Liu, D.-L.; Liu, Q.; Wang, J.-J. MicroRNA-101 exerts tumor-suppressive functions in non-small cell lung cancer through directly targeting enhancer of zeste homolog 2. *J. Thorac. Oncol.* **2011**, *6*, 671–678. [\[CrossRef\]](#) [\[PubMed\]](#)
67. Ougolkov, A.V.; Bilim, V.N.; Billadeau, D.D. Regulation of pancreatic tumor cell proliferation and chemoresistance by the histone methyltransferase enhancer of zeste homologue 2. *Clin. Cancer Res.* **2008**, *14*, 6790–6796. [\[CrossRef\]](#)
68. De Carvalho, D.; Binato, R.; Pereira, W.D.O.; Leroy, J.M.G.; Colassanti, M.; Proto-Siqueira, R.; Bueno-Da-Silva, A.; Zago, M.A.; Zanichelli, M.; Abdelhay, E. BCR–ABL-mediated upregulation of PRAME is responsible for knocking down TRAIL in CML patients. *Oncogene* **2011**, *30*, 223–233. [\[CrossRef\]](#)
69. Avan, A.; Crea, F.; Paolicchi, E.; Funel, N.; Galvani, E.; Marquez, V.E.; Honeywell, R.J.; Danesi, R.; Peters, G.J.; Giovannetti, E. Molecular Mechanisms Involved in the Synergistic Interaction of the EZH2 Inhibitor 3-Deazaneplanocin A with Gemcitabine in Pancreatic Cancer Cells DZNeP/Gemcitabine Combination in Pancreatic Cancer. *Mol. Cancer Ther.* **2012**, *11*, 1735–1746. [\[CrossRef\]](#)
70. Fiskus, W.; Rao, R.; Balusu, R.; Ganguly, S.; Tao, J.; Sotomayor, E.; Mudunuru, U.; Smith, J.E.; Hembruff, S.L.; Atadja, P. Superior Efficacy of a Combined Epigenetic Therapy against Human Mantle Cell Lymphoma Cells Combined Epigenetic Therapy against Human MCL Cells. *Clin. Cancer Res.* **2012**, *18*, 6227–6238. [\[CrossRef\]](#)
71. Hayden, A.; Johnson, P.W.; Packham, G.; Crabb, S.J. S-adenosylhomocysteine hydrolase inhibition by 3-deazaneplanocin A analogues induces anti-cancer effects in breast cancer cell lines and synergy with both histone deacetylase and HER2 inhibition. *Breast Cancer Res. Treat.* **2011**, *127*, 109–119. [\[CrossRef\]](#) [\[PubMed\]](#)
72. Sun, F.; Chan, E.; Wu, Z.; Yang, X.; Marquez, V.E.; Yu, Q. Combinatorial pharmacologic approaches target EZH2-mediated gene repression in breast cancer cells. *Mol. Cancer Ther.* **2009**, *8*, 3191–3202. [\[CrossRef\]](#)
73. Lv, Y.; Yuan, C.; Xiao, X.; Wang, X.; Ji, X.; Yu, H.; Wu, Z.; Zhang, J. The expression and significance of the enhancer of zeste homolog 2 in lung adenocarcinoma. *Oncol. Rep.* **2012**, *28*, 147–154.
74. Hu, S.; Yu, L.; Li, Z.; Shen, Y.; Wang, J.; Cai, J.; Xiao, L.; Wang, Z. Overexpression of EZH2 contributes to acquired cisplatin resistance in ovarian cancer cells in vitro and in vivo. *Cancer Biol. Ther.* **2010**, *10*, 788–795. [\[CrossRef\]](#) [\[PubMed\]](#)
75. Straining, R.; Eighmy, W. Tazemetostat: EZH2 Inhibitor. *J. Adv. Pract. Oncol.* **2022**, *13*, 158. [\[CrossRef\]](#)
76. Wen, L.; Tao, S.-H.; Guo, F.; Li, L.-Z.; Yang, H.-L.; Liang, Y.; Zhang, L.-D.; Ma, L.; Fu, P. Selective EZH2 inhibitor zld1039 alleviates inflammation in cisplatin-induced acute kidney injury partially by enhancing RKIP and suppressing NF- $\kappa$ B p65 pathway. *Acta Pharmacol. Sin.* **2021**, *43*, 2067–2080. [\[CrossRef\]](#) [\[PubMed\]](#)
77. Dorff, T.B.; Longmate, J.A.; Pal, S.K.; Stadler, W.M.; Fishman, M.N.; Vaishampayan, U.N.; Rao, A.; Pinski, J.K.; Hu, J.S.; Quinn, D.I. Bevacizumab alone or in combination with TRC105 for patients with refractory metastatic renal cell cancer. *Cancer* **2017**, *123*, 4566–4573. [\[CrossRef\]](#) [\[PubMed\]](#)
78. Hainsworth, J.D.; Reeves, J.A.; Mace, J.R.; Crane, E.J.; Hamid, O.; Stille, J.R.; Flynt, A.; Roberson, S.; Polzer, J.; Arrowsmith, E.R. A randomized, open-label phase 2 study of the CXCR4 inhibitor LY2510924 in combination with sunitinib versus sunitinib alone in patients with metastatic renal cell carcinoma (RCC). *Target Oncol.* **2016**, *11*, 643–653. [\[CrossRef\]](#)
79. Choueiri, T.; Kocsis, J.; Pachynski, R.; Poprach, A.; Deshazo, M.; Zakharia, Y.; Lara, P.; Pal, S.; Gecci, L.; Ho, T. Results of the phase II TRAXAR study: A randomized phase II trial of axitinib and TRC105 (TRAX) versus axitinib (AX) alone in patients with advanced or metastatic renal cell carcinoma (mRCC). *Ann. Oncol.* **2019**, *30*, v362–v363. [\[CrossRef\]](#)



## 5. Paper III




International Journal of  
Molecular Sciences



Article

### A Pan-Cancer Landscape of ABCG2 across Human Cancers: Friend or Foe?

Chen Lyu <sup>1</sup>, Lili Wang <sup>1</sup>, Birgit Stadlbauer <sup>1,2</sup>, Alexander Buchner <sup>1,2</sup>  and Heike Pohla <sup>1,2,\*</sup>

<sup>1</sup> Tumor Immunology Laboratory, LIFE Center, LMU Klinikum, University Munich, 82152 Planegg, Germany

<sup>2</sup> Department of Urology, LMU Klinikum, University Munich, 81377 Munich, Germany

\* Correspondence: heike.pohla@med.uni-muenchen.de

**Abstract:** Emerging evidence from research or clinical studies reported that ABCG2 (ATP-binding cassette sub-family G member 2) interrelates with multidrug resistance (MDR) development in cancers. However, no comprehensive pan-cancer analysis is available at present. Therefore, we explore multiple databases, such as TCGA to investigate the potential therapeutic roles of ABCG2 across 33 different tumors. ABCG2 is expressed on a lower level in most cancers and shows a protective effect. For example, a lower expression level of ABCG2 was detrimental to the survival of adrenocortical carcinoma (TCGA-ACC), glioblastoma multiforme (GBM), and kidney renal clear cell carcinoma (KIRC) patients. Distinct associations exist between ABCG2 expression and stemness scores, microenvironmental scores, microsatellite instability (MSI), and tumor mutational burden (TMB) of tumor patients. We observed a significant positive correlation between the ABCG2 mutation site and prognosis in uterine corpus endometrial carcinoma (UCEC) patients. Moreover, transmembrane transporter activity and hormone biosynthetic-associated functions were found to be involved in the functionality of ABCG2 and its related genes. The cDNAs of cancer cell lines were collected to detect exon mutation sequences and to analyze ABCG2 mRNA expression. The mRNA expression level of ABCG2 showed a significant difference among spheres and drug-resistant cancer cell lines compared with their corresponding adherent cancer cell lines in six types of cancer. This pan-cancer study provides, for the first time, a comprehensive understanding of the multifunctionality of ABCG2 and unveils further details of the potential therapeutic role of ABCG2 in pan-cancer.

**Keywords:** ABCG2; pan-cancer; prognosis; cancer stem cell; genetic alteration



**Citation:** Lyu, C.; Wang, L.; Stadlbauer, B.; Buchner, A.; Pohla, H. A Pan-Cancer Landscape of ABCG2 across Human Cancers: Friend or Foe? *Int. J. Mol. Sci.* **2022**, *23*, 15955. <https://doi.org/10.3390/ijms232415955>

Academic Editor: Antonella Zannetti

Received: 24 October 2022

Accepted: 6 December 2022

Published: 15 December 2022

**Publisher's Note:** MDPI stays neutral with regard to jurisdictional claims in published maps and institutional affiliations.



**Copyright:** © 2022 by the authors. Licensee MDPI, Basel, Switzerland. This article is an open access article distributed under the terms and conditions of the Creative Commons Attribution (CC BY) license (<https://creativecommons.org/licenses/by/4.0/>).

#### 1. Introduction

ABCG2, known as breast cancer resistance protein (BCRP), was described as the second member of the G subfamily and a subfamily in the ATP-binding cassette (ABC) family proteins, which are expressed in many tissues, such as intestine, liver, kidney, and cancerous tissue [1]. Several studies have revealed that ABCG2 as a biomarker of cancer stem-like cell (CSC) populations can limit the efficacy of chemotherapy and is a target for clinical interventions during the period of tumor relapse [2,3]. In cancer therapy, inhibition of ABCG2 has emerged as a new treatment strategy that is believed to increase chemotherapeutic drug bioavailability and to overcome drug resistance [4].

The structural feature of ABCG2 helps us to further understand drug efflux independent contributions of ABCG2 concerning polydrug recognition and transport.

ABCG2 domain structure is a dimer of two protein chains each consisting of a catalytic nucleotide binding domain (NBD) and a transmembrane domain with at least six membrane spanning  $\alpha$ -helices (TMD) [5]. TMD carries the substrate binding site and represents the translocation pathway for substrate, while NBD is responsible for ATP binding and ATP hydrolysis [6]. If a physiological substrate, for example, the molecule estrone-3-sulfate (E1S), is bound in the cavity of the TMD, NBDs can face away from each other and help to identify key residues contributing to substrate recognition. Then, two ATP molecules

bind and induce a conformational change of the dimerization of the NBDs that stimulates the sign to close the cavity, thereby leaving no space for other substrate binding. On the extracellular side, the extracellular loop has rotated away from TMD, opening up a smaller cavity so that endogenous substrates can be transported. When the second molecule of ATP is hydrolyzed, the conformational change will be reset, and substrate and ATP can bind again allowing the process to repeat [6]. Moreover, ABCG2 can also remove exogenous substrates, such as a variety of xenobiotics and pharmaceuticals, to limit drug delivery to the brain, thereby strongly influencing drug resistance and chemotherapeutic intervention [7]. Binding of drugs can induce a conformational switch of the transporter, which is observed for several anticancer drugs (imatinib, mitoxantrone, or SN38) with different effects [8].

While the role of ABCG2 in multidrug resistance is widely recognized, the dysfunction of ABCG2 gene can be induced by other factors, such as genetic polymorphisms, which have been proven in several diseases, such as hyperuricemia and hypertension in humans [9]. For example, the common ABCG2 variant-Q141K impairs the stability of NBD, which may affect the pharmacokinetic profile of several drugs in the clinic [10,11]. Several other variants (G406R, F431L, S441N, P480L, F489L, M515R, L525R, A528T, and T542A) located within the transmembrane region of ABCG2 have been shown to affect the activity of the protein in vitro [12]. For non-small cell lung cancer (NSCLC), variant genotypes of ABCG2 rs3114020 were found to be associated with a significantly increased risk of death ( $p < 0.001$ ), and the rs1871744 genotype was significantly associated with poor response, suggesting that ABCG2 mutation patterns can be an independent risk factor for the prognosis of NSCLC [13]. However, it remains unclear, which of the ABCG2 mutation sites are found in different types of cancers and how it might influence the drug-ABCG2 interactions. Therefore, a detailed understanding of the mechanism and genetic polymorphisms of ABCG2 could drive the development of the bioavailability of the desired drug, minimize multidrug resistance, and promote more effective therapeutic strategies.

Our study carried out, for the first time, a pan-cancer analysis of ABCG2 based on The Cancer Genome Atlas (TCGA) (<https://www.cancer.gov/tcga>) to explore the multifunctional role of ABCG2 in different types of cancer. We also investigated gene expression, genetic alteration, stemness scores, microenvironmental scores, relevant immune checkpoint genes, and cellular function of ABCG2 to reveal the potential molecular pathogenesis of multiple cancers, challenging the pathogenic role of ABCG2 as a reference gene for cancers and presenting a potential prognosis biomarker and immunotherapeutic target.

## 2. Results

### 2.1. ABCG2 Expression in Human Cancers

To determine the effects of ABCG2 on cancer in humans, we used TIMER2.0 to explore ABCG2 expression in various types of cancer from the TCGA database. As demonstrated in (Figure 1A), expression differences of ABCG2 between tumor and normal tissues were found in bladder urothelial carcinoma (BLCA), breast invasive carcinoma (BRCA), cervical squamous cell carcinoma and endocervical adenocarcinoma (CESC), cholangiocarcinoma (CHOL), colon adenocarcinoma (COAD), kidney chromophobe (KICH), kidney renal clear cell carcinoma (KIRC), kidney renal papillary cell carcinoma (KIRP), liver hepatocellular carcinoma (LIHC), lung adenocarcinoma (LUAD), lung squamous cell carcinoma (LUSC), prostate adenocarcinoma (PRAD), rectum adenocarcinoma (READ), skin cutaneous melanoma (SKCM), stomach adenocarcinoma (STAD), and uterine corpus endometrial carcinoma (UCEC) ( $p < 0.05$ ). The expression analysis via TIMER2.0 indicates that different cancers and specific cancer subtypes affect the ABCG2 gene expression status. For some tumors, not enough normal tissue sample was available in the TCGA database (those tumors are shown with a white background in Figure 1A). Then, GTEx dataset was used as control for the normal tissues, and we evaluated the ABCG2 expression differences between tumor and normal tissues of CESC, CHOL, brain lower grade glioma (LGG), ovarian serous cystadenocarcinoma (OV), UCEC, and uterine carcinosarcoma (UCS) ( $p < 0.05$ , Figure 1B).

The Clinical Proteomic Tumor Analysis Consortium (CPTAC) integrates genomic and proteomic data to identify and describe all proteins within tumor and normal tissues and explores candidate proteins that can be used as tumor biomarkers. Available data from the CPTAC dataset indicate that ABCG2 protein expression was lower in UCEC and LUAD than in normal tissues; Figure 1C and the opposite was shown in RCC.

The ABCG2 protein expression level between normal samples and breast, lung, testis, and prostate cancer samples was validated using The Human Protein Atlas. The results indicate that the expression level of ABCG2 was markedly increased in normal prostate tissue compared with other normal tissues. For testis, tumor tissue revealed a higher ABCG2 expression compared to the normal tissue (Figure 2).

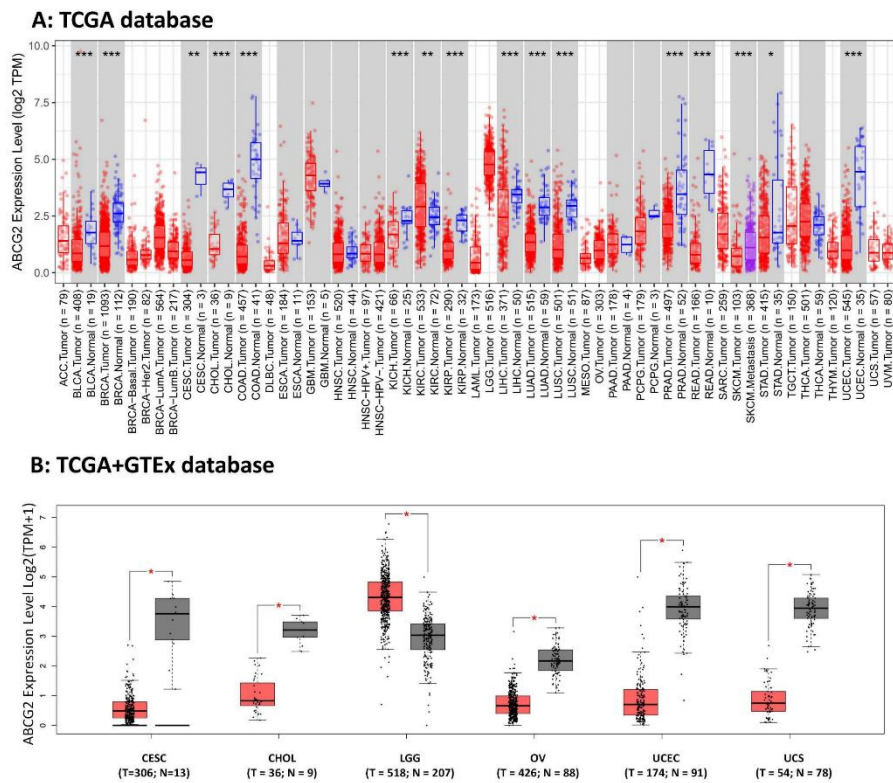
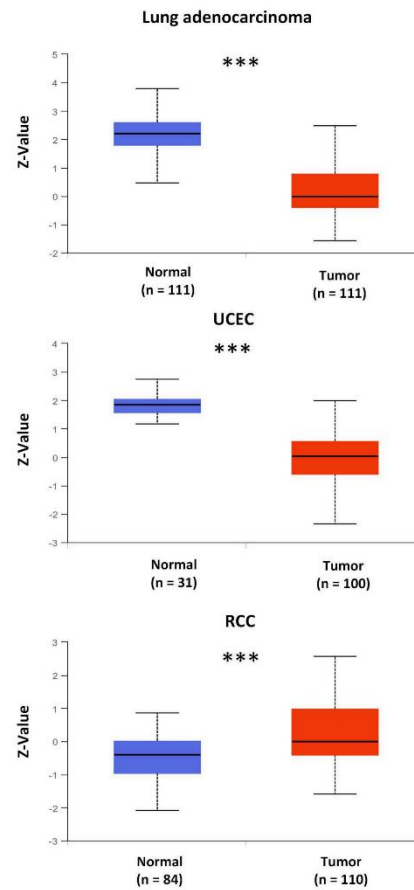


Figure 1. Cont.

## C: CPTAC database



**Figure 1.** The ABCG2 expression data were obtained from various databases: (A) Data collected from TCGA database and analyzed by the TIMER2.0 database. Samples with gray backgrounds represent both tumor (red) and normal tissue (blue) samples and one metastasis (purple), which can be compared statistically. Samples with white backgrounds represent only tumor samples, which cannot be compared statistically because other types of tissue samples were not available (\*  $p < 0.05$ ; \*\*  $p < 0.01$ ; \*\*\*  $p < 0.001$ ). (B) We used normal tissue data from the Genotype-Tissue Expression (GTEx) database as controls for comparisons with the corresponding data from The Cancer Genome Atlas (TCGA) project. The results are presented as a box plot (\*  $p < 0.05$ ). Tumor samples in red and normal samples in black. (C) Expression levels of ABCG2 protein were also compared between tumor tissue (red) and normal tissue (blue) in LUAD (lung adenocarcinoma), UCEC (uterine corpus endometrial carcinoma), and RCC (clear cell renal cell carcinoma (RCC)) based on the CPTAC dataset (\*\*\*  $p < 0.001$ ).



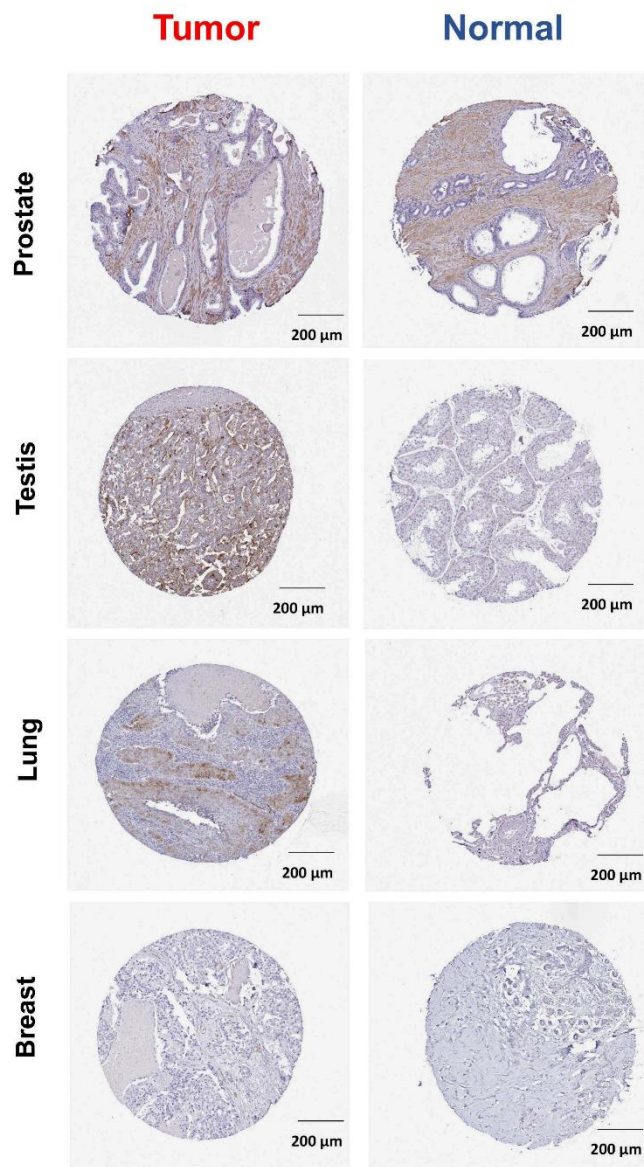


**Figure 2.** ABCG2 protein expression was shown in immunohistological sections of breast (T: HPA054719 antibody; N: HPA054719 antibody), lung (T: HPA054719 antibody; N: HPA054719 antibody), testis (T: HPA054719 antibody; N: HPA054719 antibody), and prostate (T: HPA054719 antibody; N: HPA054719 antibody), obtained from the Human Protein Atlas database.

2.2. ABCG2 as a Prognostic Factor in Human Cancers

We divided the cancer types into high-expression and low-expression groups according to the expression levels of ABCG2 and investigated the correlation of ABCG2 expression with the prognosis of patients within different tumors. As shown in Figure 3A, analysis of overall survival (OS) demonstrates that a low expression level of ABCG2 was linked to poor prognosis for the cancer types of adrenocortical carcinoma (ACC) ( $p = 0.030$ ), glioblastoma multiforme (GBM) ( $p = 0.048$ ), and KIRC ( $p < 0.001$ ) within the TCGA project. Analysis of disease-free survival (DFS) (Figure 3B) shows a correlation between low ABCG2 expression and poor prognosis for CESC ( $p = 0.029$ ), LUAED ( $p = 0.010$ ), sarcoma (SARC) ( $p = 0.047$ ), and thyroid carcinoma (THCA) ( $p = 0.009$ ).

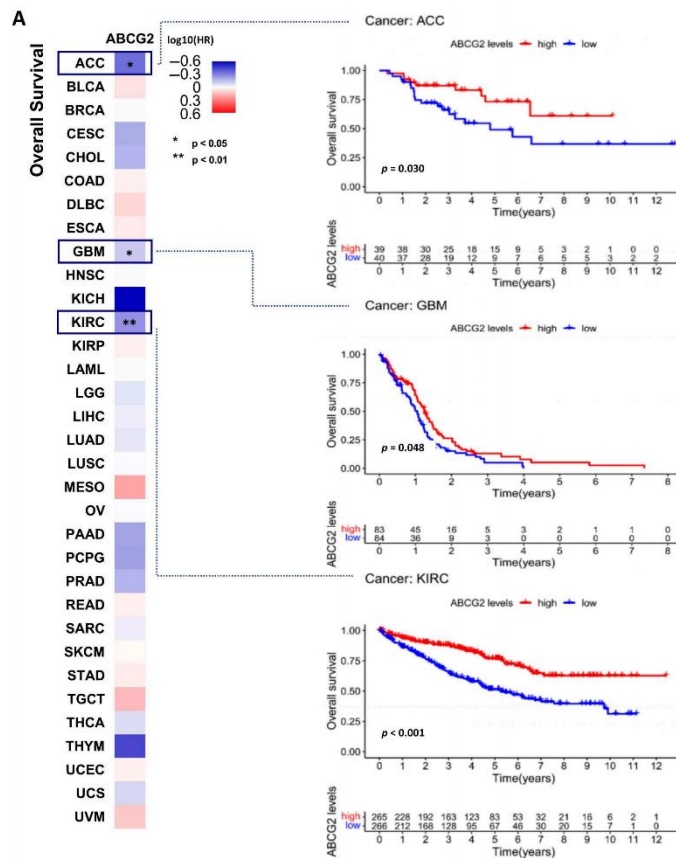
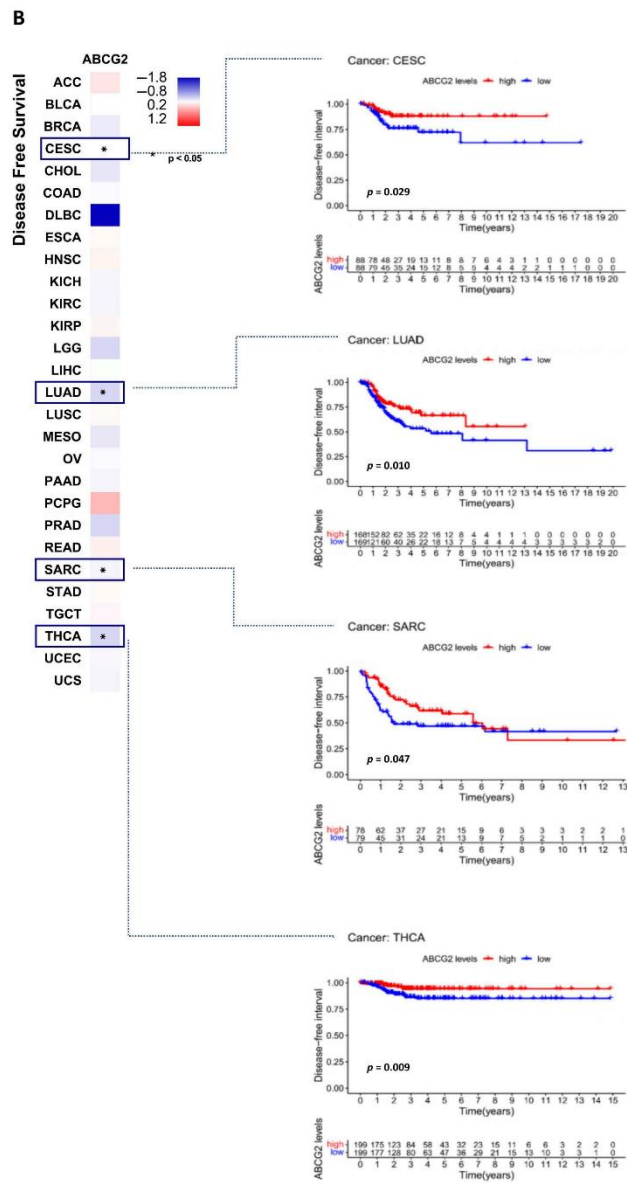


Figure 3. Cont.



**Figure 3.** Correlation between ABCG2 gene expression, overall survival, and disease-free survival for different cancer types: (A,B) The pan-cancer survival maps with significant results are given. For the Kaplan–Meier survival analysis, patients were grouped into high and low ABCG2 expression scores determined by the comparison with the median by log-rank test.



Moreover, significant correlations between pathological stages, age, gender, and ABCG2 expression are shown in Figures 4 and 5A,B. For the pathological stage, significant correlations emerge among KICH, KIRC, testicular germ cell tumors (TGCT), and THCA (Figure 4), of which KIRC, THCA, and KICH show ascending tendency with increasing expression of ABCG2, and TGCT shows the opposite trend. Higher expression of ABCG2 was observed in the patient group  $\leq 65$  years for LUSC, SARC, SKCM, and BLCA, whereas for thymoma (THYM), KIRP, and LIHC in the group  $> 65$  years (Figure 5A). There are also clear differences between the gender groups. For KIRC and SARC, female patients show higher ABCG2 expression, in contrast to mesothelioma (MESO) and LIHC, where male patients show higher ABCG2 expression (Figure 5B).

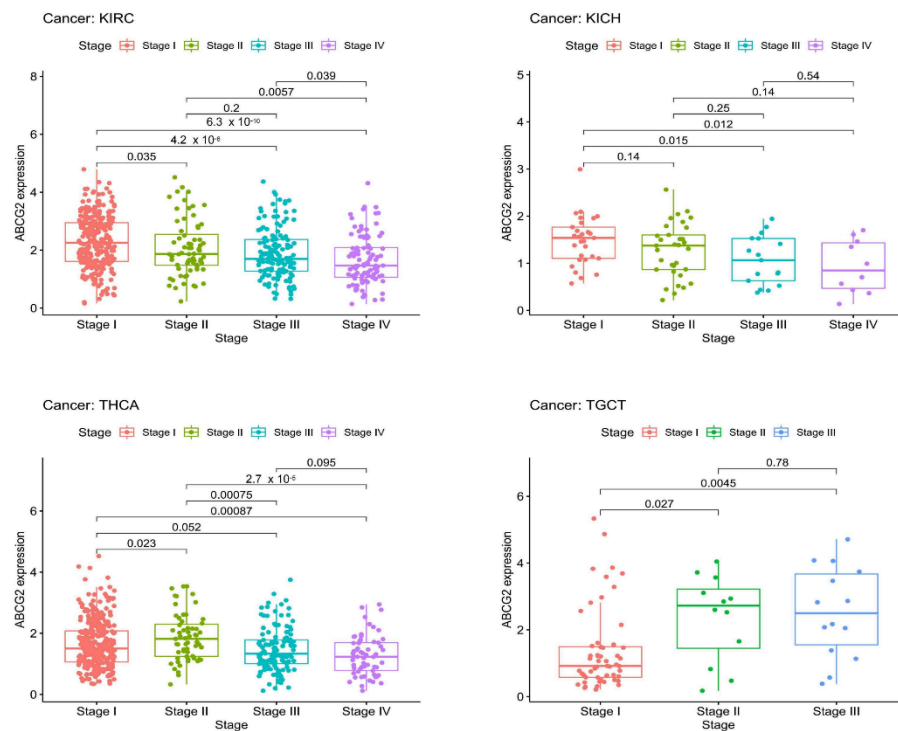


**Figure 4.** Correlation between ABCG2 gene expression and the pathological stages of different cancer types. The pathological stages (stages I to IV) with significant results are shown.

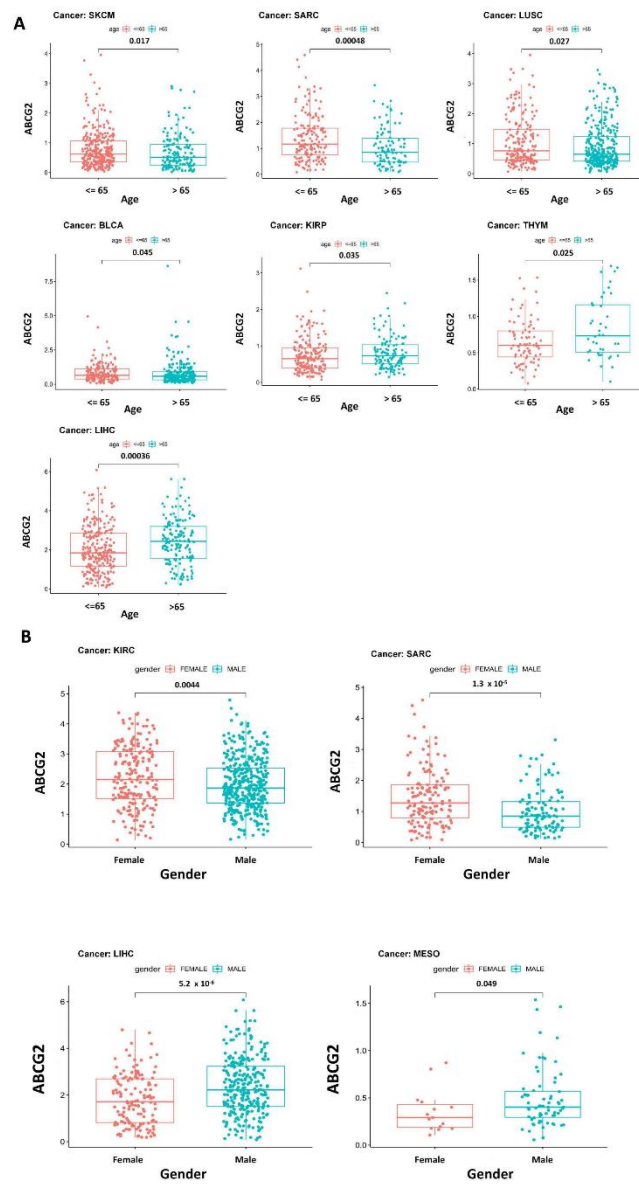


**Figure 5.** Correlation between ABCG2 gene expression and the clinicopathological characteristics of different cancer types: (A) age ( $\leq 65$  and  $> 65$ ) and (B) gender (female and male) with significant results are shown.

### 2.3. The Correlation between ABCG2 Expression and RNAss, DNAss, ImmuneScore, and StromalScore

ABCG2 correlates with drug resistance in several types of cancer possibly due to its expression in CSCs. Tumor stemness can be measured using the RNA stemness score (RNAss) based on mRNA expression and using the DNA stemness score (DNAss) based on DNA methylation pattern. The correlation between ABCG2 expression and tumor stemness measured by RNAss and DNAss was investigated. Interestingly, the results show that ABCG2 is negatively correlated to most types of cancer concerning RNAss and DNAss. Notably, ABCG2 expression shows positive correlation with DNAss but a negative correlation with RNAss in THYM, KIRC, and SKCM, and the opposite tendency is shown in TGCT (Figure 6A). These contradictory results suggest that RNAss and DNAss may identify distinct cancerous cell populations characterized by different features or degrees of stemness in different cancers. ImmuneScore and StromalScore represent newly developed algorithms that take advantage of the unique properties of the transcriptional profiles of cancerous tissues to infer tumor cellularity as well as the various infiltrating normal cells. For this, the ESTIMATE scores can be applied to predict tumor purity, which was calculated by the StromalScore and the ImmuneScore [14]. Specific gene expression signatures of stromal and immune cells can be used to develop a prognosis stratification in cancer. In this study, ABCG2 expression shows a positive correlation with the ImmuneScore and the StromalScore in most types of cancer (Figure 6B). For TGCT, THCA, and THYM, a stronger negative correlation was observed for the expression of ABCG2 and the ImmuneScore and StromalScore ( $p < 0.001$ ). For KIRC patients, ABCG2 expression shows an opposite trend between the ImmuneScore and the StromalScore ( $p < 0.001$ ), of which a positive correlation is observed with the StromalScore and a negative correlation with the ImmuneScore. These results confirm the important role of ABCG2 in the microenvironmental processes.

### 2.4. The Correlation between ABCG2 Expression and TMB, MSI, Genetic Alteration Analysis

TMB (tumor mutational burden) and MSI (microsatellite instability) are important biomarkers for immunotherapy and are of clinical practical value, which can evaluate the efficacy of immune checkpoint inhibition therapy in diverse types of cancer [15–17]. Therefore, we analyzed the correlation between ABCG2 expression and TMB/MSI across all tumors of the TCGA database using Spearman rank correlation test. As shown in Figure 7C, the expression of ABCG2 in 19 different cancers is significantly correlated with TMB, of which ABCG2 gene expression is positively correlated with a high mutation status in LIHC, LAML, and HNSC, and with a low mutation status in lymphoid neoplasm diffuse large B-cell lymphoma (DLBC), KICH, LUAD, pancreatic adenocarcinoma (PAAD), pheochromocytoma and paraganglioma (PCPG), PRAD, READ, ACC, uveal melanoma (UVM), UCEC, THCA, STAD, SKCM, SARC, BRCA, and CESC. In addition, there are significant correlations between the expression of ABCG2 with MSI in 10 cancer types, including esophageal carcinoma (ESCA), UCEC, THCA, STAD, SARC, LUSC, LUAD, KIRP, DLBC, and BRCA, of which ESCA patients are positively correlated to the expression of ABCG2, and the other cancer types show the opposite trend. Furthermore, we investigated the genetic alteration status of ABCG2 in the different tumor samples of the TCGA cohorts. The types, sites, and case numbers of the ABCG2 genetic alterations are presented in Figure 7A. We found that a missense mutation of ABCG2 was the main type of genetic alteration. For example, the K653E/Y654Ifs\*21/K653Nfs\*11 alteration in the exon 16 domain was detected in one case of COAD and four cases of UCEC and is displayed in the 3D structure of the ABCG2 protein (Figure 7B). Additionally, we analyzed the potential association between ABCG2 genetic alteration and the clinical survival prognosis in UCEC patients. The data of Figure 8 indicate that UCEC patients with altered ABCG2 show a better prognosis in overall ( $p = 2.452 \times 10^{-3}$ ), disease-specific survival ( $p = 0.0481$ ), progression-free survival ( $p = 0.0283$ ), and disease-free survival ( $p = 0.0703$ ) compared with patients without ABCG2 alteration.

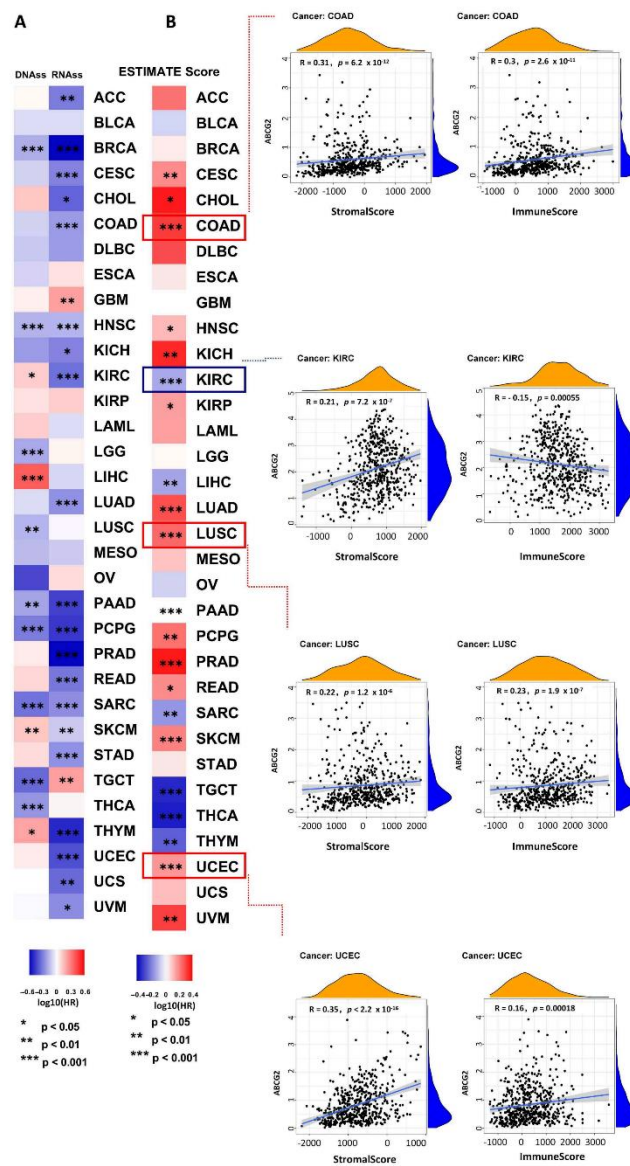


**Figure 6.** Correlation between ABCG2 gene expression, stemness scores, and microenvironmental scores based on the TCGA database: (A) Correlation of ABCG2 expression with the RNA and DNA stemness scores; (B) the ESTIMATE score map was analyzed and the StromalScore and the ImmuneScore for COAD, KIRC, LUSC, and UCEC with  $p < 0.001$  are shown \*  $p < 0.05$ , \*\*  $p < 0.01$ , \*\*\*  $p < 0.001$ . Blue box (downregulation), red box (upregulation).

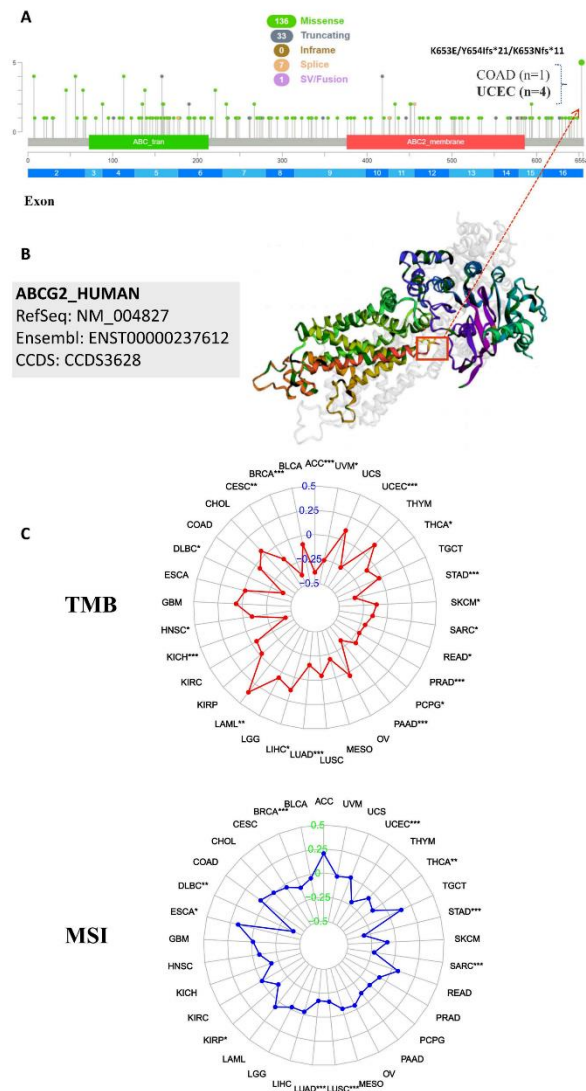


**Figure 7.** Mutation features of ABCG2 in different tumors: **(A,B)** The mutation features of ABCG2 for the TCGA tumors were analyzed using the cBioPortal tool. The altered mutation sites, the mutation site with the highest frequency (K653E/Y654Ifs\*21/K653Nfs\*11) (four cases for UCEC and one case for COAD), and the 3D structure of ABCG2 are displayed. **(C)** The radar charts illustrated the association between TMB or MSI and ABCG2 gene expression in different cancers. The red and blue curve represent the correlation coefficient, and the blue and green value represent the range. \*  $p < 0.05$ , \*\*  $p < 0.01$ , \*\*\*  $p < 0.001$ .

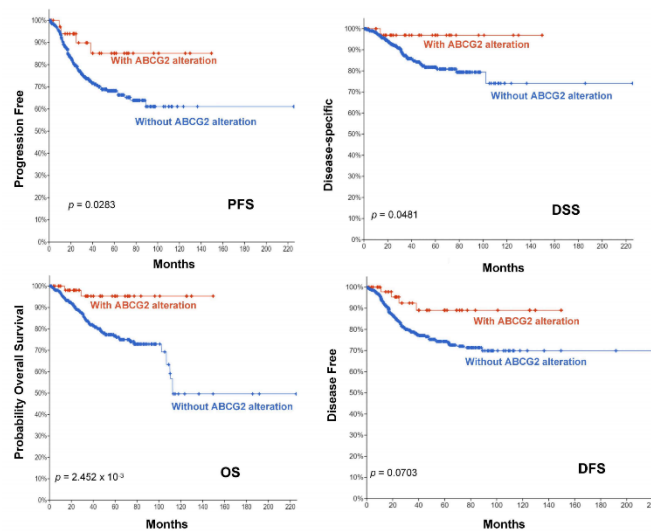


**Figure 8.** The potential correlation between the mutation site and the survival patterns. The potential correlation between this mutation site and progression-free survival (PFS) (n = 528), overall survival (OS) (n = 1602), disease-specific survival (DSS) (n = 526), and disease-free survival (DFS) (n = 1346) of UCEC is shown.

### 2.5. Analysis of ABCG2-Related Genes and the Correlation between ABCG2 Expression, GSEA, and Checkpoint Gene Expression

The relationship between ABCG2 gene expression and a total of 47 immune checkpoint genes in tumor immune responses was further analyzed. We found that ABCG2 expression shows a close link with T lymphocyte-related immune genes (CD28), T follicular helper cell associated immune genes (CD200 and CD200R1), and cancer-related genes, such as neuropilin-1 (NRP1), tumor necrosis factor receptor superfamily member 25 (TNFRSF25), and galectin-9 (LGALS9), in several different cancer types. Additionally, ABCG2 is significantly co-expressed along with more than 20 immune checkpoint genes in BRCA, CESC, COAD, HNSC, KIRC, KIRP, LAML, LIHC, LUAD, LUSC, PAAD, PRAD, SKCM, TGCT, THCA, THYM, UCEC, and UVM (Figure 9A). These results suggest that the positive association between the expression of ABCG2 and the immune checkpoint genes in various tumors have a function in regulating tumor immune responses.

The corresponding heatmap data among pan-cancer show a positive correlation between ABCG2 and EPAS1, and GLC in most cancer types (Figure 9B). The top 20 ABCG2-related genes from the GeneMANIA online tool were analyzed by the protein-protein interaction (PPI) network in Figure 10A. Based on the genes set provided by the GeneMANIA online tool, the ontology (GO) enrichment analysis was used to gather the corresponding pathways among ABCG2 and its 20 related genes, which are vascular transport, primary active transmembrane transporter activity, ATPase-coupled transmembrane transporter activity, transport across the blood-brain barrier, and hormone biosynthetic process (Figure 10B). Furthermore, based on the normalized enrichment scores, we used gene set enrichment analysis (GSEA) that included related genes in humans to find general enrichment trends and to identify GO functional enrichment of different expression levels of ABCG2 among pan-cancer. The most significantly enriched signal transduction pathways were selected, and six types of cancers show the strongest potential connection with the ABCG2 gene expression. The mRNA binding pathway was differentially enriched in





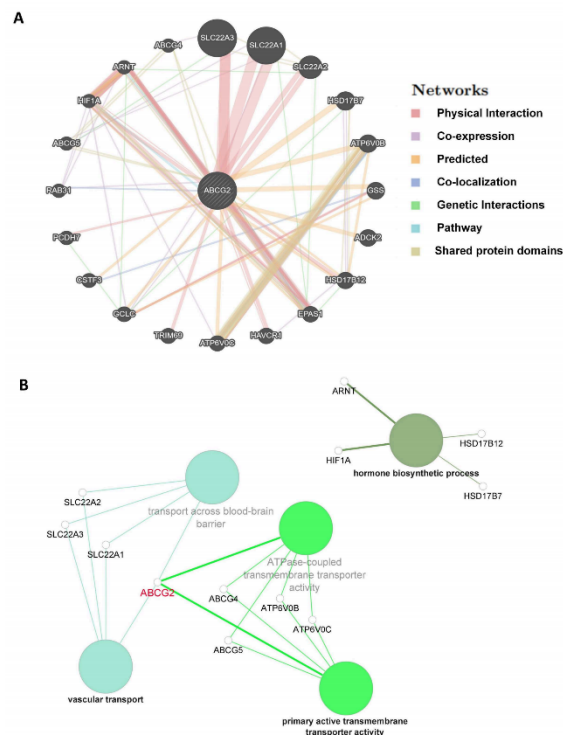


**Figure 10.** ABCG2-related genes enrichment analysis: (A) Protein–protein interaction (PPI) network for the top 20 ABCG2-related proteins based on the GeneMANIA online tool. Different colors of the network edges indicate the bioinformatic methods applied: physical interaction, co-expression, predicted, colocalization, pathway, genetic interaction, and shared protein domains. (B) ABCG2 gene and its top 20 related genes were associated to some biological process pathways in GO analysis using Cytoscape. Functionally correlated groups partially overlap and are arbitrarily colored. The node size represents the pathway enrichment significance.

#### 2.6. ABCG2 mRNA Expression among Six Types of Cancer in Cancer Cells, Cancer Stem Cells, and Corresponding Drug Resistant Cells

The observed correlation between ABCG2 gene alteration and clinical prognosis in this study and multi-drug resistance function of cancer stem cells inspired us to perform exon sequencing and to analyze the mRNA expression level of ABCG2 among different cancer cells, cancer stem cells, and corresponding drug resistant cells. The cancer cell lines were selected as follows. First, adherent normal cell line, derived sphere-forming cancer stem cells, and sunitinib-resistant cell lines were from the RCC cell lines SKRC-17 and RCC-53 [18]. Sunitinib is the widely used first-line treatment medication for RCC. Second, the prostate cancer cell line-derived spheres [19] and cabazitaxel-resistant cell line are from DU-145 [20]. Cabazitaxel is the second-line treatment option for metastatic castration-resistant prostate cancer. Third, the glioblastoma cell line-derived spheres and temozolomide-resistant cell line are from U87-MG. Temozolomide is the first-line chemotherapeutic drug for glioblastoma. Fourth, adherent and sphere forming cells from the two UCEC cell lines EN (primary endometrial carcinoma, stage IIIC) [21] and MFE-319 (established from the primary

adenosquamous endometrium carcinoma, grading G1–G2) were used [22] (Figure 12A). Unfortunately, we could not find any ABCG2 mutations in the exons. For the RT-qPCR analyses (Figure 12B), we used the sphere and drug-resistant cell lines in comparison to the corresponding adherent cell lines. Spheres of all cell lines except MTE-319 express higher levels of ABCG2 mRNA than the adherent cell lines. Drug-resistant cell lines of SKRC-17, DU145, and U87 showed a significantly lower expression level. Only the sunitinib-resistant cell line of RCC-53 showed a significantly higher expression level in comparison to the corresponding sphere and adherent cell lines.

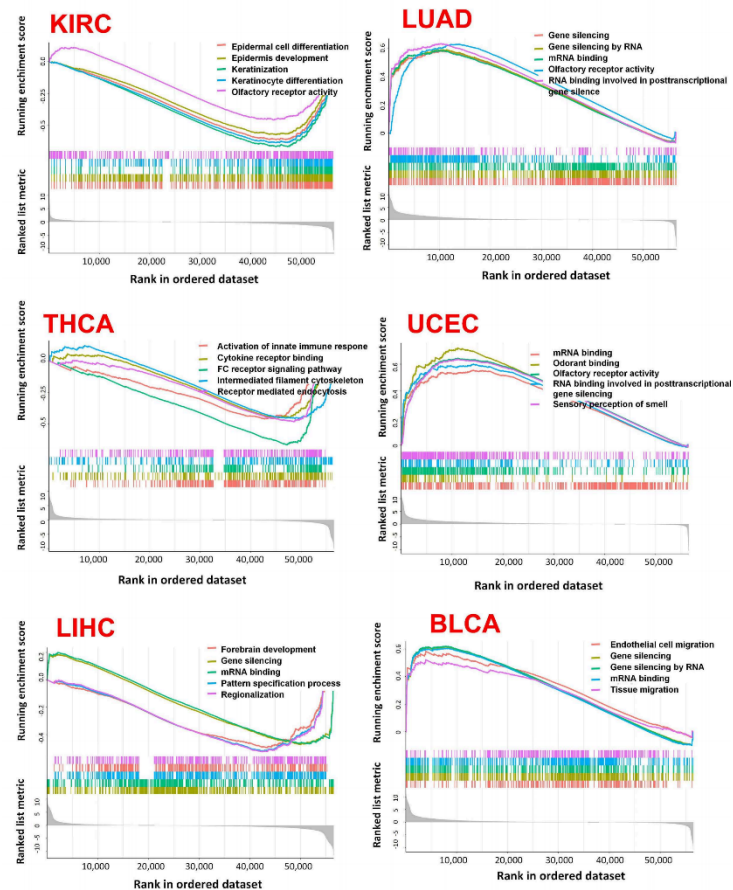


**Figure 11.** GSEA analysis in six types of cancers. GO functional annotation of the ABCG2 gene in different cancers were displayed. Differently colored curves indicate that the ABCG2 gene regulates different functions or pathways in different cancers. Peaks of curves upward indicate positive regulation and peaks of curves downward represents negative regulation.

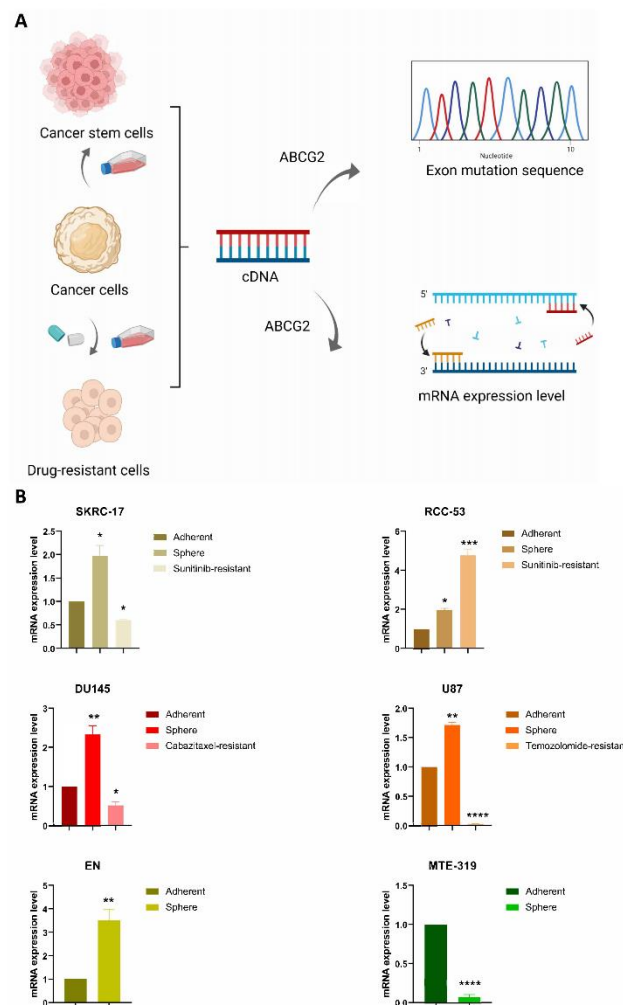


**Figure 12.** The detection of ABCG2 gene in cancer cells, cancer stem cells, and corresponding drug resistant cells: (A) Workflow of cell line preparation and exon sequencing of the ABCG2 gene; (B) RT-qPCR analysis representing relative mRNA expression levels of ABCG2 in various cancer cell lines and their corresponding sphere and drug-resistant cell lines. \*  $p < 0.05$ , \*\*  $p < 0.01$ , \*\*\*  $p < 0.001$ , \*\*\*\*  $p < 0.0001$ .

### 3. Discussion

It has been reported that ABCG2 plays multifunctional roles in human diseases, such as inducing multidrug resistance in cancer treatment, contributing to the risk for hyperuricemia and gout, and overexpressing in resistant acute myeloid leukemia phenotype [23–28]. Emerging publications have reported a functional link between ABCG2 as well as its genetic alterations and the clinical relevance in tumors [29,30]. Whether

ABCG2 participates in the pathogenesis or pharmacokinetics in all types of cancer through certain common molecular mechanisms remains to be clarified. A literature search failed to retrieve any publication with a pan-cancer analysis for ABCG2. Thus, we comprehensively examined the ABCG2 gene expression in a total of 33 different tumors based on the TCGA, CPTAC, and GEO databases and analyzed the molecular features of gene expression, prognosis, tumor microenvironment, tumor stemness, and genetic alteration to further explore the multifunctional role of ABCG2 gene in different cancer types.

Based on the results, ABCG2 was differentially expressed in tumors, of which a lower expression was found in most cancer types but a significantly higher expression in KIRC and LGG patients, which illustrated the flexible function of ABCG2 among pan-cancer. For normal healthy tissue expression groups, the ABCG2 can be regarded as an essential protector from xenobiotics as an oral bioavailability regulator, part of component of the blood–brain barrier, the blood–testis barrier, and the maternal–fetal barrier [31]. In contrast, in ABCG2 high expressing cancer tissues, ABCG2 contributes to drug resistance in cancer treatments. Moreover, previous research showed that two SNPs in ABCG2 have a significant correlation with mRNA expression in ccRCC tissues in univariate analyses (mRNA: rs76212402, rs2231164), but no significant association was found for BCRP/ABCG2 protein expression [32]. Thus, the potential of ABCG2 as therapeutic target to overcome multi-drug resistance strategies by ABC drug transporter inhibitors to increase the efficiency of chemotherapy should be further discussed.

ABCG2 is considered as a biomarker of cancer stem-like cells (CSCs), which can arise from various sources, including long-lived stem or progenitor cells or via dedifferentiation from non-stem cancer cells. The capacity for self-renewal and invasion of CSCs can promote cancer progression, which is the main cause for treatment-induced drug resistance [33–35]. In the present study, we investigated the association of ABCG2 with stem cell-like features using the RNAss and DNAss scores [36]. Unexpectedly, we found that ABCG2 expression was negatively associated with cancer stem-like features, RNAss among most types of cancers. We assume that the reason for this trend could be related to the tumor purity among pan-cancer samples. Apart from the tumor cells, the tumor tissues in the TCGA database also consist of other cell types, such as stromal and immune cells, which means that tumor purity could be a potential influencing factor on ABCG2 expression and the stemness scores. By contrast, we can see from the results of evaluating the stromal and immune scores in KIRC samples, ABCG2 expression significantly shows an opposite tendency, suggesting that ABCG2 plays a role in the KIRC tumor microenvironment and can be used as a therapeutic target to aid drug sensitivity.

Several studies have reported a role of ABCG2 in the progression or prognosis of renal cell carcinoma [13,32,37]. In 2017, Wang et al. reported that stronger ABCG2 expression correlates with poorer overall survival. The median overall survival was 93.2, 85.8, and 17.0 months in ABCG2(–), (+), and (++) subgroups, respectively, and the five-year survival rate was 95%, 77%, and 27% in ABCG2(–), (+), and (++) subgroups, respectively [13]. However, we found that low expression of ABCG2 was associated with poorer overall survival and higher grades of RCC. The reason for this discrepancy is as follows: First, it should be noted that no more than 60 cases of RCC patients were included in either ABCG2(–), (+), and (++) subgroups in Wang's study; thus, the different sample sizes perhaps are warranted for verification of the above conclusion. Second, the significant associations for ccRCC patients with survival were found for the ABCG2 SNPs rs2622621 and rs3109823 in univariate analyses [32], so that the additional patients' features should be fully considered as well. Third, 101 patients without metastasis were treated for one year with interferon-alpha in Wang's study, and 19 patients with metastatic RCC received Sorafenib or Sunitinib. However, because of the tremendous data of the pan-cancer study, we did not include the treatment features of patients yet; thus, more clinical details of the patients should be considered in the following investigations for RCC.

In addition, more interesting results were found for the correlation between ABCG2 gene alteration and prognosis in this study. First, we discovered a significant difference



between ABCG2 gene alterations and ABCG2 wild type regarding OS, PFS, and DSS in UCEC patients. As we mentioned before, ABCG2 mutations can also alter the survival progress in renal cell carcinoma patients [32]. Moreover, investigations of the correlation of ABCG2 gene mutations with ABCG2 transport activities and further clinical pharmacogenetic studies have also been carried out in various types of cancer [38–42]. One of the main reasons for the association between gene alteration and clinical features may lie in the nature of the substrate transport process. ABCG2 is a symmetrical homodimer consisting of two proteins, each with a nucleotide binding domain (NBD) and a transmembrane domain (TMD) building the substrate binding site. When a substrate binds to the binding pocket, NBDs face away from each other and ATP binds, thus inducing a conformational change. The substrate is released from the protein. When the second ATP molecule is hydrolyzed, the conformation is reset and substrate and ATP can rebind, allowing the process to repeat. The study from Manolaridis et al. found that the human ABCG2 gene with the mutation E211Q can drastically reduce the catalytic activity for ATP hydrolysis within the NBD. This mutation was helpful to trap the protein conformation in the respective state [43]. Thus, the mutations can change the transport efficiency and, therefore, the pharmacokinetics, which may be reflected in the patient's clinic. The development of an endometrial carcinoma starts with preinvasive intraepithelial lesions and estrogen stimulation and then penetrates into the myometrium to reach lymphatic capillaries and the regional lymph nodes from where metastases reach other organs through vascular channels [44]. Using the GO enrichment analysis (Figure 10B), we know which of the ABCG2-related genes are associated with the "vascular transport" and "hormone biosynthetic process". Thus, we can speculate that the ABCG2 gene plays an essential role in the pathogenesis and the pharmacokinetics in UCEC patients. More in-depth molecular experiments are needed to verify these results.

The observed correlation between ABCG2 gene alteration and clinical prognosis in this study and the emerging publications of the resulting multi-drug resistance inspired us to analyze the correlation of ABCG2 gene alteration and mRNA expression level among different cancer cells, cancer stem cells, and corresponding drug resistant cells. Based on the sequencing results, we could not find any ABCG2 mutations in the exons. Further experiments, such as intron sequencing and protein structure analysis, will follow in order to be able to analyze correlations between ABCG2 gene mutations and therapy resistance. For the qPCR result, sphere groups had a higher expression level of ABCG2 compared to the adherent group in DU145 cell lines, which were similar to the results from the former research's results [20]. The significantly different expression levels of the ABCG2 gene between drug-resistance groups and the adherent groups were explored in this article for the first time, which implied that ABCG2 acts multi-functionally in the different types of drug-resistant cancer cells. Moreover, the higher expression of ABCG2 in spheres and sunitinib-resistant cell lines of RCC-53 compared to the adherent cell line, showed that further in-depth research, such as analyzing tumorigenicity of different ABCG2 expressing sub-phenotypes in RCC-53 cell lines, can be organized in the future. Furthermore, endometrial carcinoma cell lines were selected in this part of the experiments not only because of impressive results observed in our study but also because ABCG2, as one of ATP-binding cassette genes, is involved in estrogen transport; meanwhile the increased estrogen action is closely associated with endometrial carcinoma [45]. Based on our result, the different expression levels observed between adherent and sphere cell lines from endometrial carcinoma can be the result of the category of cancer type. MTE-319 is established from primary adenosquamous endometrial carcinoma containing both malignant glandular and malignant squamous components [46], and EN is established from stage IIIC of primary endometrium carcinoma, showing that ABCG2 gene expression probably displays various stemness capacity in different types of endometrial carcinoma.

In this study, for the first time, a pan-cancer analysis of ABCG2 expression and its correlation with clinical prognosis, stemness score, tumor microenvironmental score, TMB, and MSI was performed, aiming to understand the role of ABCG2 in tumorigenesis. Furthermore, the results from the correlation between ABCG2 mutations and clinical



prognosis helps to realize personalized medicine. More clinically relevant mutations in membrane proteins on tumor cells should be analyzed in the future.

#### 4. Materials and Methods

##### 4.1. Gene Expression Analysis

We loaded ABCG2 into the “Gene\_DE” module of TIMER2.0 (tumor immune estimation resource, version 2; (<http://timer.cistrome.org/>) (accessed on 19 June 2022), which can provide four modules for investigating the correlations between immune infiltrates and genetic or clinical features and four modules for exploring cancer-related associations in the TCGA cohorts [47] and analyze the expression patterns of ABCG2 between tumor and adjacent normal tissues for the different tumors or specific tumor subtypes of the TCGA project.

For certain tumors without normal or with highly limited normal tissues, we used the “expression analysis-box plots” module of the GEPIA2 (Gene Expression Profiling Interactive Analysis, version 2) web server (<http://gepia2.cancer-pku.cn/#analysis>) (accessed on 19 June 2022) to obtain box plots of the expression difference between these tumor tissues and the corresponding normal tissues of the GTEx (Genotype-Tissue Expression) database [48], under the settings p-value cutoff = 0.01, log2FC (fold change) cutoff = 1, and “Match TCGA normal and GTEx data”.

The UALCAN portal (<http://ualcan.path.uab.edu/analysis-prot.html>), an interactive web resource for analyzing cancer omics data, allowed us to conduct protein expression analysis of the CPTAC (clinical proteomic tumor analysis consortium) dataset [49] (accessed on 19 June 2022). Herein, we explored the expression level of the total protein of ABCG2 between primary tumor and normal tissues, respectively, by entering “ABCG2”. The available datasets of three tumors were selected, namely, clear cell RCC (renal cell carcinoma), UCEC (uterine corpus endometrial carcinoma), and LUAD (lung adenocarcinoma).

Immunohistochemistry (IHC)-based protein expression images of ABCG2 protein expression in clinical specimens of cancer patients were obtained from the Human Protein Atlas database (<https://www.proteinatlas.org/>) (accessed on 6 September 2022) [50].

##### 4.2. Prognosis Analysis

To investigate the prognostic value of ABCG2 in pan-cancer, we extracted patient data, including OS (overall survival), DFS (disease-free survival), and other clinical features with detailed follow-up and survival information from the TCGA database. The data were first analyzed by “survival” R package (<https://www.r-project.org/>) (accessed on 17 May 2021), and then the survival maps were displayed in GraphPad Prism 7.0. The Kaplan–Meier curve of ABCG2 in the different cancers were plotted using the “ggplot2” package, where  $p < 0.05$  was shown. Moreover, the correlation between patient stage, age, gender, and ABCG2 expression among the different cancer types were analyzed by the R packages “ggpubr” and “limma”.

##### 4.3. Tumor Stemness Indices and Tumor Microenvironment Scores

According to the transcriptome and to the epigenetic characteristics of TCGA tumor samples, the stem cell-like features of tumor cells were detected. The correlation of cancer stemness with ABCG2 expression was evaluated using Spearman correlation test. Furthermore, the degree of infiltration of immune and stromal cells in the distinct tumor tissues was analyzed based on the RNA-seq data from the TCGA database (accessed on 18 March 2021) in the “estimate” and “limma” R package and displayed in “ggplot2”, “ggpubr”, and “ggExtra” R packages. The score maps were performed using GraphPad Prism 7.0.

##### 4.4. Genetic Alteration Analysis

Tumor mutational burden (TMB) was evaluated based on Perl scripts, and this value was corrected by dividing by the exon length. Microsatellite instability (MSI) scores were extracted using TCGA (accessed on 3 May 2021). The correlation between ABCG2

expression and either TMB or MSI was analyzed using the “cor.test” command based on Spearman’s method. The two metrics were visualized using radar plots, which were generated using the R package “fmsb”.

The cBioPortal web (<https://www.cbioportal.org/>) (accessed on 10 January 2022) was used to analyze the ABCG2 gene alteration analysis. The results of the alteration frequency across all TCGA tumors were analyzed in the “Cancer Types Summary” module in the “TCGA Pan-Cancer Atlas Studies”. The schematic diagram of the protein structure and the mutated sites in the 3D (three-dimensional) structure of ABCG2 can be operated via the “Mutations” module. Then, we selected the three studies: Uterine Corpus Endometrial Carcinoma (TCGA, Firehose Legacy) (549 samples), (TCGA, Nature 2013) (373 samples), and (TCGA, Pan-cancer Atlas) (529 samples) to generate the clinical data. The “Comparison” module was used to obtain the data for overall survival (OS), progression-free survival (PFS), disease-free survival (DFS), and disease-specific survival (DSS) differences with or without ABCG2 genetic alterations, and Kaplan–Meier plots with log-rank *p*-values were generated as well.

#### 4.5. Co-Expression of ABCG2 with Immune-Related Genes, ABCG2-Related Genes, and Pathways in Tumors

The R packages “limma”, “reshape2”, and “RColorBrewer” were used for analyzing the co-expression with immune-related genes.

GeneMANIA online database tool (<http://www.genemania.org>) (accessed on 10 January 2022) was applied for ABCG2-related gene analysis and its protein–protein interaction (PPI) analysis, which includes physical interaction, co-expression, co-localization, gene enrichment analysis, genetic interaction, and website prediction [51].

The software Cytoscape (version 3.8.2) (<https://cytoscape.org/>) (accessed on 17 April 2022) and its plug-in ClueGO were used to perform the ABCG2-related genes’ pathway enrichment analysis in gene ontology (GO)-biological process. *p* < 0.05 and minimum gene numbers, which must be more than four, were set up [52,53].

The “Gene\_Corr” module of TIMER2.0 (accessed on 10 January 2022) was used to supply the heatmap data of the selected genes, which contains the partial correlation (cor) and *p*-value in the purity-adjusted Spearman’s rank correlation test.

Gene ontology (GO) gene sets were obtained from the Gene Set Enrichment Analysis website (GSEA, <https://www.gsea-msigdb.org/gsea/downloads.jsp>) (accessed on 1 April 2020). GO functional annotations and enriched pathways associated with ABCG2 expression were analyzed using the R packages “limma”, “org.Hs.eg.db”, “clusterProfiler”, and “enrichplot”.

#### 4.6. Cell Culture

SKRC-17 (kind gift from J. Vissers, Nijmegen), RCC-53 (derived from a patient with stage IV disease (pT2N1MxG2-3)), sunitinib-resistant SKRC-17 and RCC-53 [18], DU145, cabacitaxel-resistant DU-145 [19,20], U87-MG (from European Collection of Authenticated Cell Cultures), temozolomide-resistant U87-MG, and MFE-319 (established from the primary adenosquamous endometrium carcinoma, grading G1–G2) [22] were cultured in RPMI 1640 medium, and EN (primary endometrial carcinoma, stage IIIC) [21] was cultured in DMEM GlutaMAX medium, both supplemented with 10% fetal calf serum (FCS “Gold Plus”, Bio & Sell GmbH, Feucht, Germany), 2 mM L-glutamine, 1 mM sodium pyruvate, and 1% minimal essential medium (Invitrogen, Life Technologies GmbH, Darmstadt, Germany) at 37 °C in humidified incubator with 5% CO<sub>2</sub>. CSCs were cultured in DMEM/F12 culture medium, containing 2% B-27 (Invitrogen, Life Technologies, Darmstadt, Germany) 10 ng/mL human recombinant basic fibroblast growth factor (bFGF, Sigma Aldrich Chemie GmbH, Taufkirchen, Germany), and 10 ng/mL epidermal growth factor (EGF, Sigma Aldrich).

#### 4.7. Sphere Formation Assay

SKRC-17, RCC-53, DU145, U87-MG, EN, and MFE-319 adherent cell lines were collected by StemPro<sup>®</sup> Accutase<sup>®</sup> (Life Technologies, Thermo Fisher Scientific, Waltham, MA, USA). Then, harvested adherent cells were filtered through a cell strainer with 40  $\mu$ M nylon mesh (BD Biosciences, Heidelberg, Germany) and seeded in 75 cm<sup>2</sup> ultra-low attachment flasks (Corning, New York, NY, USA) with 10 mL serum-free CSC medium. After seven days, the spheres were harvested and dissociated by Accutase for 10 min at 37 °C. After being centrifuged at 500  $\times$  g for 4 min at room temperature, cells were collected and used for the following assays.

#### 4.8. RNA Extraction, Reverse Transcription, and Sequencing

Total RNA was extracted from cells using the RNeasy Mini-Kit (Qiagen, Hilden, Germany) based on the manufacturer's instructions. The cDNA was synthesized according to kit instructions (GoScript<sup>™</sup> Reverse Transcriptase System, Promega GmbH, Walldorf, Germany). ABCG2 mRNA sequencing was performed by the company Eurofins Genomics (Ebersberg, Germany).

#### 4.9. Quantitative Reverse Transcription PCR (RT-qPCR)

RT-qPCR was performed using the FastStart Essential DNA Green Master kit (Roche, Penzberg, Germany) and the LightCycler<sup>®</sup> 96 (Roche). Data were analyzed by the LightCycler<sup>®</sup> 96 software version 1.1. The relative expression analysis was carried out by the 2<sup>- $\Delta\Delta$ Ct</sup> method. The annealing temperature was 60 °C for all primers, listed in Table 1, and the transcription level of GAPDH and ACTB was used as an internal control.

**Table 1.** Primers used for RT-qPCR.

Transcript	Primer	Sequence (5'-3')	Product Size (bp)
GAPDH	GAPDH-F	CATGGGTGTGAACCATGA	104
	GAPDH-R	TGTCATGGATGACCTTGG	
ACTB	ACTB-F	CTGCCCTGAGGCACIC	197
	ACTB-R	GTGCCAGGGCAGTGAT	
ABCG2	ABCG2-f	CATCAACTTTCGGGGGTGA	266
	ABCG2-r	CACTGGTGGTCGTCAGGAA	

**Author Contributions:** C.L. and H.P. contributed to conception and design of the study. C.L. and L.W. organized the database and performed the statistical analysis. C.L. and L.W. wrote the first draft of the manuscript. B.S., H.P. and A.B. offered technical or material support, critical reading, and text revisions. All authors contributed to manuscript revision, read, and approved the submitted version. All authors have read and agreed to the published version of the manuscript.

**Funding:** The study was supported by the LMU clinic. The author Chen Lyu is funded by the China scholarship council (ID:201908080121).

**Data Availability Statement:** The raw data supporting the conclusions of this article will be made available by the authors, without undue reservation.

**Conflicts of Interest:** The authors declare that the research was conducted in the absence of any commercial or financial relationships that could be construed as potential conflict of interest.

## References

- Fetsch, P.A.; Abati, A.; Litman, T.; Morisaki, K.; Honjo, Y.; Mittal, K.; Bates, S.E. Localization of the ABCG2 mitoxantrone resistance-associated protein in normal tissues. *Cancer Lett.* **2006**, *235*, 84–92. [[CrossRef](#)] [[PubMed](#)]
- Noguchi, K.; Katayama, K.; Sugimoto, Y. Human ABC transporter ABCG2/BCRP expression in chemoresistance: Basic and clinical perspectives for molecular cancer therapeutics. *Pharm. Pers. Med.* **2014**, *7*, 53. [[CrossRef](#)] [[PubMed](#)]
- de Gooijer, M.C.; de Vries, N.A.; Buckle, T.; Buil, L.C.; Beijnen, J.H.; Boogerd, W.; van Tellingen, O.J.N. Improved brain penetration and antitumor efficacy of temozolomide by inhibition of ABCB1 and ABCG2. *Neoplasia* **2018**, *20*, 710–720. [[CrossRef](#)] [[PubMed](#)]

4. Fletcher, J.I.; Williams, R.T.; Henderson, M.J.; Norris, M.D.; Haber, M. ABC transporters as mediators of drug resistance and contributors to cancer cell biology. *Drug Resist. Updates* **2016**, *26*, 1–9. [[CrossRef](#)] [[PubMed](#)]
5. Polgar, O.; Robey, R.W.; Bates, S.E. ABCG2: Structure, function and role in drug response. *Expert Opin. Drug Metab. Toxicol.* **2008**, *4*, 1–15. [[CrossRef](#)]
6. Eckenstaler, R.; Benndorf, R.A. 3D structure of the transporter ABCG2—What’s new? *Br. J. Pharmacol.* **2020**, *177*, 1485–1496. [[CrossRef](#)]
7. Mo, W.; Zhang, J.-T. Human ABCG2: Structure, function, and its role in multidrug resistance. *Int. J. Biochem. Mol. Biol.* **2012**, *3*, 1.
8. Orlando, B.J.; Liao, M. ABCG2 transports anticancer drugs via a closed-to-open switch. *Nat. Commun.* **2020**, *11*, 2264. [[CrossRef](#)]
9. Zámbo, B.; Bartos, Z.; Móznér, O.; Szabó, E.; Várady, G.; Poór, G.; Pálkás, M.; Andrikovics, H.; Hegedűs, T.; Homolya, L. Clinically relevant mutations in the ABCG2 transporter uncovered by genetic analysis linked to erythrocyte membrane protein expression. *Sci. Rep.* **2018**, *8*, 7487. [[CrossRef](#)]
10. Hira, D.; Terada, T. BCRP/ABCG2 and high-alert medications: Biochemical, pharmacokinetic, pharmacogenetic, and clinical implications. *Biochem. Pharmacol.* **2018**, *147*, 201–210. [[CrossRef](#)]
11. Khunweearaphong, N.; Stockner, T.; Kuchler, K. The structure of the human ABC transporter ABCG2 reveals a novel mechanism for drug extrusion. *Sci. Rep.* **2017**, *7*, 13767. [[CrossRef](#)] [[PubMed](#)]
12. Sjöstedt, N.; van den Heuvel, J.J.; Koenderink, J.B.; Kidron, H. Transmembrane domain single-nucleotide polymorphisms impair expression and transport activity of ABC transporter ABCG2. *Pharm. Res.* **2017**, *34*, 1626–1636. [[CrossRef](#)]
13. Wang, H.; Luo, F.; Zhu, Z.; Xu, Z.; Huang, X.; Ma, R.; He, H.; Zhu, Y.; Shao, K.; Zhao, J. ABCG2 is a potential prognostic marker of overall survival in patients with clear cell renal cell carcinoma. *BMC Cancer* **2017**, *17*, 222. [[CrossRef](#)]
14. Yoshihara, K.; Shahmoradgoli, M.; Martínez, E.; Vegesna, R.; Kim, H.; Torres-García, W.; Treviño, V.; Shen, H.; Laird, P.W.; Levine, D.A. Inferring tumour purity and stromal and immune cell admixture from expression data. *Nat. Commun.* **2013**, *4*, 2612. [[CrossRef](#)]
15. Li, Y.; Ma, Y.; Wu, Z.; Zeng, F.; Song, B.; Zhang, Y.; Li, J.; Lui, S.; Wu, M. Tumor Mutational Burden Predicting the Efficacy of Immune Checkpoint Inhibitors in Colorectal Cancer: A Systematic Review and Meta-Analysis. *Front. Immunol.* **2021**, *12*, 751407. [[CrossRef](#)] [[PubMed](#)]
16. Khan, S.A.; Kurian, P.; Mobley, B.; Burks, T.; Beg, M.S.; Ross, J.S.; Ali, S.M.; Bowles, D.W. Relationship of anaplastic thyroid cancer high tumor mutation burden and MSI-H status with response to anti-PD1 monotherapy. *J. Clin. Oncol.* **2018**, *36* (Suppl. 15), e18114. [[CrossRef](#)]
17. Rizzo, A.; Ricci, A.D.; Brandi, G. PD-L1, TMB, MSI, and other predictors of response to immune checkpoint inhibitors in biliary tract cancer. *Cancers* **2021**, *13*, 558. [[CrossRef](#)]
18. Gassenmaier, M.; Chen, D.; Buchner, A.; Henkel, L.; Schiemann, M.; Mack, B.; Schendel, D.J.; Zimmermann, W.; Pohla, H. CXC chemokine receptor 4 is essential for maintenance of renal cell carcinoma-initiating cells and predicts metastasis. *Stem Cells* **2013**, *31*, 1467–1476. [[CrossRef](#)]
19. Mickey, D.; Stone, K.; Wunderli, H.; Mickey, G.; Paulson, D. Characterization of a human prostate adenocarcinoma cell line (DU 145) as a monolayer culture and as a solid tumor in athymic mice. *Prog. Clin. Biol. Res.* **1980**, *37*, 67–84.
20. Wang, L.; Stadlbauer, B.; Lyu, C.; Buchner, A.; Pohla, H. Shikonin enhances the antitumor effect of cabazitaxel in prostate cancer stem cells and reverses cabazitaxel resistance by inhibiting ABCG2 and ALDH3A1. *Am. J. Cancer Res.* **2020**, *10*, 3784.
21. Isaka, K.; Nishi, H.; Sagawa, Y.; Nakada, T.; Osakabe, Y.; Serizawa, H.; Ebihara, Y.; Takayama, M. Establishment of a new human cell line (EN) with TP53 mutation derived from endometrial carcinoma. *Cancer Genet. Cytogenet.* **2003**, *141*, 20–25. [[CrossRef](#)] [[PubMed](#)]
22. Hackenberg, R.; Hawighorst, T.; Hild, F.; Schulz, K.-D. Establishment of new epithelial carcinoma cell lines by blocking monolayer formation. *J. Cancer Res. Clin. Oncol.* **1997**, *123*, 669–673. [[CrossRef](#)] [[PubMed](#)]
23. Robey, R.W.; Pluchino, K.M.; Hall, M.D.; Fojo, A.T.; Bates, S.E.; Gottesman, M.M. Revisiting the role of ABC transporters in multidrug-resistant cancer. *Nat. Rev. Cancer* **2018**, *18*, 452–464. [[CrossRef](#)] [[PubMed](#)]
24. Kukal, S.; Guin, D.; Rawat, C.; Bora, S.; Mishra, M.K.; Sharma, P.; Paul, P.R.; Kanojia, N.; Grewal, G.K.; Kukreti, S. Multidrug efflux transporter ABCG2: Expression and regulation. *Cell. Mol. Life Sci.* **2021**, *78*, 6887–6939. [[CrossRef](#)]
25. Hoque, K.M.; Dixon, E.E.; Lewis, R.M.; Allan, J.; Gamble, G.D.; Phipps-Green, A.J.; Kuhns, V.L.H.; Horne, A.M.; Stamp, L.K.; Merriman, T.R. The ABCG2 Q141K hyperuricemia and gout associated variant illuminates the physiology of human urate excretion. *Nat. Commun.* **2020**, *11*, 2767. [[CrossRef](#)]
26. Fujita, K.; Ichida, K. ABCG2 as a therapeutic target candidate for gout. *Expert Opin. Ther. Targets* **2018**, *22*, 123–129. [[CrossRef](#)]
27. Sorf, A.; Sucha, S.; Morell, A.; Novotna, E.; Staud, F.; Zavrlova, A.; Visek, B.; Wsol, V.; Ceckova, M. Targeting Pharmacokinetic Drug Resistance in Acute Myeloid Leukemia Cells with CDK4/6 Inhibitors. *Cancers* **2020**, *12*, 1596. [[CrossRef](#)]
28. Megias-Vericat, J.E.; Martínez-Cuadron, D.; Herrero, M.J.; Alino, S.F.; Poveda, J.L.; Sanz, M.A.; Montesinos, P. Pharmacogenetics of metabolic genes of anthracyclines in acute myeloid leukemia. *Curr. Drug Metab.* **2018**, *19*, 55–74. [[CrossRef](#)]
29. Zhang, W.; Sun, S.; Zhang, W.; Shi, Z. Polymorphisms of ABCG2 and its impact on clinical relevance. *Biochem. Biophys. Res. Commun.* **2018**, *503*, 408–413. [[CrossRef](#)]
30. Okubo, H.; Ando, H.; Ishizuka, K.; Morishige, J.-i.; Ikejima, K.; Shiina, S.; Nagahara, A. Impact of genetic polymorphisms on the pharmacokinetics and pharmacodynamics of lenvatinib in patients with hepatocellular carcinoma. *J. Pharmacol. Sci.* **2022**, *148*, 6–13. [[CrossRef](#)]



31. Robey, R.W.; To, K.K.; Polgar, O.; Dohse, M.; Fetsch, P.; Dean, M.; Bates, S.E. ABCG2: A perspective. *Adv. Drug Deliv. Rev.* **2009**, *61*, 3–13. [[CrossRef](#)]
32. Reustle, A.; Fisel, P.; Renner, O.; Büttner, F.; Winter, S.; Rausch, S.; Kruck, S.; Nies, A.T.; Hennenlotter, J.; Scharpf, M. Characterization of the breast cancer resistance protein (BCRP/ABCG2) in clear cell renal cell carcinoma. *Int. J. Cancer* **2018**, *143*, 3181–3193. [[CrossRef](#)] [[PubMed](#)]
33. Ding, X.-W.; Wu, J.-H.; Jiang, C.-P. ABCG2: A potential marker of stem cells and novel target in stem cell and cancer therapy. *Life Sci.* **2010**, *86*, 631–637. [[CrossRef](#)] [[PubMed](#)]
34. An, Y.; Ongkeko, W.M. ABCG2: The key to chemoresistance in cancer stem cells? *Expert Opin. Drug Metab. Toxicol.* **2009**, *5*, 1529–1542. [[CrossRef](#)] [[PubMed](#)]
35. Clevers, H. The cancer stem cell: Premises, promises and challenges. *Nat. Med.* **2011**, *17*, 313–319. [[CrossRef](#)] [[PubMed](#)]
36. Malta, T.M.; Sokolov, A.; Gentles, A.J.; Burzykowski, T.; Poisson, L.; Weinstein, J.N.; Kamińska, B.; Huelsken, J.; Omberg, L.; Gevaert, O. Machine learning identifies stemness features associated with oncogenic dedifferentiation. *Cell* **2018**, *173*, 338–354.e15. [[CrossRef](#)]
37. Howley, R.; Mansi, M.; Shinde, J.; Restrepo, J.; Chen, B. Evaluation of aminolevulinic acid-mediated protoporphyrin IX fluorescence and enhancement by ABCG2 inhibitors in renal cell carcinoma cells. *J. Photochem. Photobiol. B Biol.* **2020**, *211*, 112017. [[CrossRef](#)]
38. Poller, B.; Iusuf, D.; Sparidans, R.W.; Wagenaar, E.; Beijnen, J.H.; Schinkel, A.H. Differential impact of P-glycoprotein (ABCB1) and breast cancer resistance protein (ABCG2) on axitinib brain accumulation and oral plasma pharmacokinetics. *Drug Metab. Dispos.* **2011**, *39*, 729–735. [[CrossRef](#)]
39. Li, J.; Cusatis, G.; Brahmner, J.; Sparreboom, A.; Robey, R.W.; Bates, S.E.; Hidalgo, M.; Baker, S. Association of variant ABCG2 and the pharmacokinetics of epidermal growth factor receptor tyrosine kinase inhibitors in cancer patients. *Cancer Biol. Ther.* **2007**, *6*, 432–438. [[CrossRef](#)]
40. Elmeliegy, M.A.; Carcaboso, A.M.; Tagen, M.; Bai, F.; Stewart, C.F. Role of ATP-binding cassette and solute carrier transporters in erlotinib CNS penetration and intracellular accumulation. *Clin. Cancer Res.* **2011**, *17*, 89–99. [[CrossRef](#)]
41. Brendel, C.; Scharenberg, C.; Dohse, M.; Robey, R.; Bates, S.; Shukla, S.; Ambudkar, S.; Wang, Y.; Wennemuth, G.; Burchert, A. Imatinib mesylate and nilotinib (AMN107) exhibit high-affinity interaction with ABCG2 on primitive hematopoietic stem cells. *Leukemia* **2007**, *21*, 1267–1275. [[CrossRef](#)] [[PubMed](#)]
42. Tanaka, Y.; Kitamura, Y.; Maeda, K.; Sugiyama, Y. Quantitative analysis of the ABCG2 c. 421C>A polymorphism effect on in vivo transport activity of breast cancer resistance protein (BCRP) using an intestinal absorption model. *J. Pharm. Sci.* **2015**, *104*, 3039–3048. [[CrossRef](#)] [[PubMed](#)]
43. Manolaridis, I.; Jackson, S.M.; Taylor, N.M.; Kowal, J.; Stahlberg, H.; Locher, K.P. Cryo-EM structures of a human ABCG2 mutant trapped in ATP-bound and substrate-bound states. *Nature* **2018**, *563*, 426–430. [[CrossRef](#)] [[PubMed](#)]
44. Amant, F.; Moerman, P.; Neven, P.; Timmerman, D.; Van Limbergen, E.; Vergote, I. Endometrial cancer. *Lancet* **2005**, *366*, 491–505. [[CrossRef](#)]
45. Lakhani, N.J.; Venitz, J.; Figg, W.D.; Sparreboom, A. Pharmacogenetics of estrogen metabolism and transport in relation to cancer. *Curr. Drug Metab.* **2003**, *4*, 505–513. [[CrossRef](#)]
46. Haqqani, M.; Fox, H. Adenosquamous carcinoma of the endometrium. *J. Clin. Pathol.* **1976**, *29*, 959–966. [[CrossRef](#)]
47. Li, T.; Fu, J.; Zeng, Z.; Cohen, D.; Li, J.; Chen, Q.; Li, B.; Liu, X.S. TIMER2. 0 for analysis of tumor-infiltrating immune cells. *Nucleic Acids Res.* **2020**, *48*, W509–W514. [[CrossRef](#)]
48. Lonsdale, J.; Thomas, J.; Salvatore, M.; Phillips, R.; Lo, E.; Shad, S.; Hasz, R.; Walters, G.; Garcia, F.; Young, N. The genotype-tissue expression (GTEx) project. *Nat. Genet.* **2013**, *45*, 580–585. [[CrossRef](#)]
49. Edwards, N.J.; Oberti, M.; Thangudu, R.R.; Cai, S.; McGarvey, P.B.; Jacob, S.; Madhavan, S.; Ketchum, K.A. The CPTAC data portal: A resource for cancer proteomics research. *J. Proteome Res.* **2015**, *14*, 2707–2713. [[CrossRef](#)]
50. Pontén, F.; Jirstrom, K.; Uhlen, M. The Human Protein Atlas—A tool for pathology. *J. Pathol. J. Pathol. Soc. Great Br. Reland* **2008**, *216*, 387–393. [[CrossRef](#)]
51. Warde-Farley, D.; Donaldson, S.L.; Comes, O.; Zuberi, K.; Badrawi, R.; Chao, P.; Franz, M.; Grouios, C.; Kazi, F.; Lopes, C.T. The GeneMANIA prediction server: Biological network integration for gene prioritization and predicting gene function. *Nucleic Acids Res.* **2010**, *38*, W214–W220. [[CrossRef](#)] [[PubMed](#)]
52. Kohl, M.; Wiese, S.; Warscheid, B. Cytoscape: Software for visualization and analysis of biological networks. In *Data Mining in Proteomics*; Springer: Berlin/Heidelberg, Germany, 2011; pp. 291–303.
53. Shannon, P.; Markiel, A.; Ozier, O.; Baliga, N.S.; Wang, J.T.; Ramage, D.; Amin, N.; Schwikowski, B.; Ideker, T. Cytoscape: A software environment for integrated models of biomolecular interaction networks. *Genome Res.* **2003**, *13*, 2498–2504. [[CrossRef](#)] [[PubMed](#)]

## References

1. Vento JA, Rini BI. Treatment of refractory metastatic renal cell carcinoma. *Cancers*. 2022;14(20):5005.
2. Le Guevelou J, Sargos P, Siva S, Ploussard G, Ost P, Gillessen S, et al. The emerging role of extracranial stereotactic ablative radiotherapy for metastatic renal cell carcinoma: a systematic review. *European Urology Focus*. 2023;9(1):114-24.
3. Bray F, Ferlay J, Soerjomataram I, Siegel RL, Torre LA, Jemal A. Global cancer statistics 2018: GLOBOCAN estimates of incidence and mortality worldwide for 36 cancers in 185 countries. *CA: a cancer journal for clinicians*. 2018;68(6):394-424.
4. PeaceHealth M, a Bill P, Go G. Renal Cell Cancer Treatment (PDQ®): Treatment-Health Professional Information [NCI].
5. Escudier B, Porta C, Schmidinger M, Algaba F, Patard J, Khoo V, et al. Renal cell carcinoma: ESMO Clinical Practice Guidelines for diagnosis, treatment and follow-up. *Annals of oncology*. 2014;25:iii49-iii56.
6. Kwan JT, Marsh FP. Bilateral Nephrocalcinosis. *New England Journal of Medicine*. 1996;334(17):1105-.
7. Ljungberg B, Albiges L, Abu-Ghanem Y, Bedke J, Capitanio U, Dabestani S, et al. European Association of Urology guidelines on renal cell carcinoma: the 2022 update. *European urology*. 2022.
8. Campbell S, Uzzo RG, Allaf ME, Bass EB, Cadeddu JA, Chang A, et al. Renal mass and localized renal cancer: AUA guideline. *The Journal of urology*. 2017;198(3):520-9.
9. Kim SP, Thompson RH, Boorjian SA, Weight CJ, Han LC, Murad MH, et al. Comparative effectiveness for survival and renal function of partial and radical nephrectomy for localized renal tumors: a systematic review and meta-analysis. *The Journal of urology*. 2012;188(1):51-7.
10. Kaushik D, Kim SP, Childs MA, Lohse CM, Costello BA, Cheville JC, et al. Overall survival and development of stage IV chronic kidney disease in patients undergoing partial and radical nephrectomy for benign renal tumors. *European urology*. 2013;64(4):600-6.
11. Rini BI. Vascular endothelial growth factor–targeted therapy in renal cell carcinoma: current status and future directions. *Clinical Cancer Research*. 2007;13(4):1098-106.
12. Jonasch E, Walker CL, Rathmell WK. Clear cell renal cell carcinoma ontogeny and mechanisms of lethality. *Nature Reviews Nephrology*. 2021;17(4):245-61.
13. Ravaud A, Gross-Goupil M. Overcoming resistance to tyrosine kinase inhibitors in renal cell carcinoma. *Cancer treatment reviews*. 2012;38(8):996-1003.
14. Motzer RJ, Hutson TE, Tomczak P, Michaelson MD, Bukowski RM, Rixe O, et al. Sunitinib versus interferon alfa in metastatic renal-cell carcinoma. *New England Journal of Medicine*. 2007;356(2):115-24.
15. Hudes G, Carducci M, Tomczak P, Dutcher J, Figlin R, Kapoor A, et al. Temsirolimus, interferon alfa, or both for advanced renal-cell carcinoma. *New England Journal of Medicine*. 2007;356(22):2271-81.
16. Motzer RJ, Jonasch E, Michaelson MD, Nandagopal L, Gore JL, George S, et al. NCCN guidelines insights: kidney cancer, version 2.2020: featured updates to the NCCN guidelines. *Journal of the National Comprehensive Cancer Network*. 2019;17(11):1278-85.
17. Borghaei H, Paz-Ares L, Horn L, Spigel DR, Steins M, Ready NE, et al. Nivolumab versus docetaxel in advanced nonsquamous non–small-cell lung cancer. *New England Journal of Medicine*. 2015;373(17):1627-39.
18. Ribas A, Wolchok JD. Cancer immunotherapy using checkpoint blockade. *Science*. 2018;359(6382):1350-5.



19. Motzer RJ, Rini BI, McDermott DF, Redman BG, Kuzel TM, Harrison MR, et al. Nivolumab for metastatic renal cell carcinoma: results of a randomized phase II trial. *Journal of clinical oncology*. 2015;33(13):1430.
20. Powles T, Eder JP, Fine GD, Braiteh FS, Loriot Y, Cruz C, et al. MPDL3280A (anti-PD-L1) treatment leads to clinical activity in metastatic bladder cancer. *Nature Reviews Nephrology*. 2014;515(7528):558-62.
21. Kaufman HL, Russell J, Hamid O, Bhatia S, Terheyden P, D'Angelo SP, et al. Avelumab in patients with chemotherapy-refractory metastatic Merkel cell carcinoma: a multicentre, single-group, open-label, phase 2 trial. *The lancet oncology*. 2016;17(10):1374-85.
22. Hadjimichael C, Chanoumidou K, Papadopoulou N, Arampatzi P, Papamatheakis J, Kretsovali A. Common stemness regulators of embryonic and cancer stem cells. *World journal of stem cells*. 2015;7(9):1150.
23. Al-Hajj M, Wicha MS, Benito-Hernandez A, Morrison SJ, Clarke MF. Prospective identification of tumorigenic breast cancer cells. *Proceedings of the National Academy of Sciences*. 2003;100(7):3983-8.
24. Clarke MF, Dick JE, Dirks PB, Eaves CJ, Jamieson CH, Jones DL, et al. Cancer stem cells—perspectives on current status and future directions: AACR Workshop on cancer stem cells. *Cancer research*. 2006;66(19):9339-44.
25. Lapidot T, Sirard C, Vormoor J, Murdoch B, Hoang T, Caceres-Cortes J, et al. A cell initiating human acute myeloid leukaemia after transplantation into SCID mice. *Nature Reviews Nephrology*. 1994;367(6464):645-8.
26. Bonnet D, Dick JE. Human acute myeloid leukemia is organized as a hierarchy that originates from a primitive hematopoietic cell. *Nature medicine*. 1997;3(7):730-7.
27. Hope KJ, Jin L, Dick JE. Acute myeloid leukemia originates from a hierarchy of leukemic stem cell classes that differ in self-renewal capacity. *Nature immunology*. 2004;5(7):738-43.
28. O'Brien CA, Pollett A, Gallinger S, Dick JE. A human colon cancer cell capable of initiating tumour growth in immunodeficient mice. *Nature immunology*. 2007;445(7123):106-10.
29. Bellam N, Pasche B. TGF- $\beta$  signaling alterations and colon cancer. *Cancer genetics*. 2010;85-103.
30. Núñez FJ, Mendez FM, Kadiyala P, Alghamri MS, Savelieff MG, Garcia-Fabiani MB, et al. IDH1-R132H acts as a tumor suppressor in glioma via epigenetic up-regulation of the DNA damage response. *Science translational medicine*. 2019;11(479):eaaq1427.
31. Wang L, Stadlbauer B, Lyu C, Buchner A, Pohla H. Shikonin enhances the antitumor effect of cabazitaxel in prostate cancer stem cells and reverses cabazitaxel resistance by inhibiting ABCG2 and ALDH3A1. *American journal of cancer research*. 2020;10(11):3784.
32. Gassenmaier M, Chen D, Buchner A, Henkel L, Schiemann M, Mack B, et al. CXC chemokine receptor 4 is essential for maintenance of renal cell carcinoma-initiating cells and predicts metastasis. *Stem Cells*. 2013;31(8):1467-76.
33. Clevers H. The cancer stem cell: premises, promises and challenges. *Nature medicine*. 2011;17(3):313-9.
34. Reya T, Morrison SJ, Clarke MF, Weissman IL. Stem cells, cancer, and cancer stem cells. *nature immunology*. 2001;414(6859):105-11.
35. Bao B, Ahmad A, Azmi AS, Ali S, Sarkar FH. Overview of cancer stem cells (CSCs) and mechanisms of their regulation: implications for cancer therapy. *Current protocols in pharmacology*. 2013;61(1):14.25. 1-14.25. 14.
36. Gottesman MM. Mechanisms of cancer drug resistance. *Annual review of medicine*. 2002;53(1):615-27.
37. Wu C-P, Calcagno AM, Ambudkar SV. Reversal of ABC drug transporter-mediated multidrug resistance in cancer cells: evaluation of current strategies. *Current molecular pharmacology*. 2008;1(2):93-105.
38. Di C, Zhao Y. Multiple drug resistance due to resistance to stem cells and stem cell treatment progress in cancer. *Experimental therapeutic medicine*. 2015;9(2):289-93.

39. Paul R, Dorsey JF, Fan Y. Cell plasticity, senescence, and quiescence in cancer stem cells: biological and therapeutic implications. *Pharmacology therapeutics*. 2022;231:107985.
40. Tang DG. Understanding cancer stem cell heterogeneity and plasticity. *Cell research*. 2012;22(3):457-72.
41. Zhou C, Yi C, Yi Y, Qin W, Yan Y, Dong X, et al. LncRNA PVT1 promotes gemcitabine resistance of pancreatic cancer via activating Wnt/ $\beta$ -catenin and autophagy pathway through modulating the miR-619-5p/Pygo2 and miR-619-5p/ATG14 axes. *Molecular cancer*. 2020;19:1-24.
42. Simon JA, Lange CA. Roles of the EZH2 histone methyltransferase in cancer epigenetics. *Mutation Research/Fundamental Molecular Mechanisms of Mutagenesis*. 2008;647(1-2):21-9.
43. Kathawala RJ, Gupta P, Ashby Jr CR, Chen Z-S. The modulation of ABC transporter-mediated multidrug resistance in cancer: a review of the past decade. *Drug resistance updates*. 2015;18:1-17.
44. Chen ZS, Tiwari AK. Multidrug resistance proteins (MRPs/ABCCs) in cancer chemotherapy and genetic diseases. *The FEBS journal*. 2011;278(18):3226-45.
45. Bao B, Ahmad A, Li Y, Azmi AS, Ali S, Banerjee S, et al. Targeting CSCs within the tumor microenvironment for cancer therapy: a potential role of mesenchymal stem cells. *Expert Opinion on Therapeutic Targets*. 2012;16(10):1041-54.
46. Kang YW, Lee JE, Jung KH, Son MK, Shin S-M, Kim SJ, et al. KRAS targeting antibody synergizes anti-cancer activity of gemcitabine against pancreatic cancer. *Cancer letters*. 2018;438:174-86.
47. Singh A, Settleman J. EMT, cancer stem cells and drug resistance: an emerging axis of evil in the war on cancer. *Oncogene*. 2010;29(34):4741-51.
48. Lu C, Han HD, Mangala LS, Ali-Fehmi R, Newton CS, Ozbun L, et al. Regulation of tumor angiogenesis by EZH2. *Cancer cell*. 2010;18(2):185-97.
49. Alves IR, Lima-Noronha MA, Silva LG, Fernández-Silva FS, Freitas ALD, Marques MV, et al. Effect of SOS-induced levels of imuABC on spontaneous and damage-induced mutagenesis in *Caulobacter crescentus*. *DNA repair*. 2017;59:20-6.
50. Xu K WZ, Groner AC. EZH2 oncogenic activity in castration-resistant prostate cancer cells is Polycomb-independent. *science*. 2012;1227604(1465):338.
51. Edmund L, Rotker KL, Lakis NS, Brito III JM, Lepe M, Lombardo KA, et al. Upgrading and upstaging at radical prostatectomy in the post-prostate-specific antigen screening era: an effect of delayed diagnosis or a shift in patient selection? *Human pathology*. 2017;59:87-93.
52. Huang X, Wang Z, Hou S, Yue C, Li Z, Hu W, et al. Long non-coding RNA DSCAM-AS1 promotes pancreatic cancer progression via regulating the miR-136-5p/PBX3 axis. *Bioengineered*. 2022;13(2):4153-65.
53. Kreso A, Dick JE. Evolution of the cancer stem cell model. *Cell stem cell*. 2014;14(3):275-91.
54. Li K, Liu C, Zhou B, Bi L, Huang H, Lin T, et al. Role of EZH2 in the growth of prostate cancer stem cells isolated from LNCaP cells. *International journal of molecular sciences*. 2013;14(6):11981-93.
55. Li J, Hart RP, Mallimo EM, Swerdel MR, Kusnecov AW, Herrup K. EZH2-mediated H3K27 trimethylation mediates neurodegeneration in ataxia-telangiectasia. *Nature neuroscience*. 2013;16(12):1745-53.
56. Liu L, Xu Z, Zhong L, Wang H, Jiang S, Long Q, et al. Enhancer of zeste homolog 2 (EZH2) promotes tumour cell migration and invasion via epigenetic repression of E-cadherin in renal cell carcinoma. *BJU international*. 2016;117(2):351-62.
57. Chen S, Pu J, Bai J, Yin Y, Wu K, Wang J, et al. EZH2 promotes hepatocellular carcinoma progression through modulating miR-22/galectin-9 axis. *Journal of Experimental Clinical Cancer Research*. 2018;37(1):1-12.

58. Guo J, Cai J, Yu L, Tang H, Chen C, Wang Z. EZH2 regulates expression of p57 and contributes to progression of ovarian cancer in vitro and in vivo. *Cancer science*. 2011;102(3):530-9.
59. Chang C-J, Yang J-Y, Xia W, Chen C-T, Xie X, Chao C-H, et al. EZH2 promotes expansion of breast tumor initiating cells through activation of RAF1- $\beta$ -catenin signaling. *Cancer cell*. 2011;19(1):86-100.
60. Adelaiye-Ogala RM, Chintala S, Shen L, Orillion A, Ciamporcerio E, Elbanna M, et al. Inhibition of EZH2 overcomes resistance to sunitinib in clear cell renal cell carcinoma models. *Cancer Research*. 2015;75(15\_Supplement):3508-.
61. Wei D, Ricketts CJ, Schmidt LS, Yang Y, Vocke CD, Linehan WMJCR. Investigating the role of EZH2 as a therapeutic target in clear cell renal cell carcinoma (ccRCC). 2016;76(14\_Supplement):4707-.
62. Wagener N, Macher-Goeppinger S, Pritsch M, Hüsing J, Hoppe-Seyler K, Schirmacher P, et al. Enhancer of zeste homolog 2 (EZH2) expression is an independent prognostic factor in renal cell carcinoma. *BMC cancer*. 2010;10:1-10.
63. Lee HW, Choe M. Expression of EZH2 in renal cell carcinoma as a novel prognostic marker. *Pathology international*. 2012;62(11):735-41.
64. Hinz S, Weikert S, Magheli A, Hoffmann M, Engers R, Miller K, et al. Expression profile of the polycomb group protein enhancer of Zeste homologue 2 and its prognostic relevance in renal cell carcinoma. *The Journal of urology*. 2009;182(6):2920-5.
65. Banumathy G, Cairns P. Signaling pathways in renal cell carcinoma. *Cancer biology therapy*. 2010;10(7):658-64.
66. Lyu C, Wang L, Stadlbauer B, Noessner E, Buchner A, Pohla H. Identification of EZH2 as Cancer Stem Cell Marker in Clear Cell Renal Cell Carcinoma and the Anti-Tumor Effect of Epigallocatechin-3-Gallate (EGCG). *Cancers*. 2022;14(17):4200.
67. Krishnamurthy P, Schuetz J. Role of ABCG2/BCRP in biology and medicine. *Annu Rev Pharmacol Toxicol*. 2006;46:381-410.
68. Reustle A, Fisel P, Renner O, Büttner F, Winter S, Rausch S, et al. Characterization of the breast cancer resistance protein (BCRP/ABCG2) in clear cell renal cell carcinoma. *International Journal of Cancer*. 2018;143(12):3181-93.
69. Khunweeraphong N, Stockner T, Kuchler K. The structure of the human ABC transporter ABCG2 reveals a novel mechanism for drug extrusion. *Scientific reports*. 2017;7(1):13767.
70. Rasouli A, Yu Q, Dehghani-Ghahnaviyeh S, Wen P-C, Kowal J, Locher KP, et al. Differential dynamics and direct interaction of bound ligands with lipids in multidrug transporter ABCG2. *Proceedings of the National Academy of Sciences*. 2023;120(1):e2213437120.
71. Robey RW, To KK, Polgar O, Dohse M, Fetsch P, Dean M, et al. ABCG2: a perspective. *Advanced drug delivery reviews*. 2009;61(1):3-13.
72. Polgar O, Robey RW, Bates SE. ABCG2: structure, function and role in drug response. *Expert opinion on drug metabolism toxicology*. 2008;4(1):1-15.
73. Sui H, Zhou LH, Zhang YL, Huang JP, Liu X, Ji Q, et al. Evodiamine suppresses ABCG2 mediated drug resistance by inhibiting p50/p65 NF- $\kappa$ B pathway in colorectal cancer. *Journal of cellular biochemistry*. 2016;117(6):1471-81.
74. An G, Gallegos J, Morris ME. The bioflavonoid kaempferol is an Abcg2 substrate and inhibits Abcg2-mediated quercetin efflux. *Drug metabolism disposition*. 2011;39(3):426-32.
75. Miyata H, Takada T, Toyoda Y, Matsuo H, Ichida K, Suzuki H. Identification of febusostat as a new strong ABCG2 inhibitor: potential applications and risks in clinical situations. *Frontiers in pharmacology*. 2016;7:518.
76. Ding X-w, Wu J-h, Jiang C-p. ABCG2: a potential marker of stem cells and novel target in stem cell and cancer therapy. *Life sciences*. 2010;86(17-18):631-7.

77. Arrigoni E, Galimberti S, Petrini M, Danesi R, Di Paolo A. ATP-binding cassette transmembrane transporters and their epigenetic control in cancer: an overview. *Expert opinion on drug metabolism toxicology*. 2016;12(12):1419-32.
78. Huang B, Huang YJ, Yao ZJ, Chen X, Guo SJ, Mao XP, et al. Cancer stem cell-like side population cells in clear cell renal cell carcinoma cell line 769P. *PloS one*. 2013;8(7):e68293.
79. Khan MI, Czarnecka AM, Helbrecht I, Bartnik E, Lian F, Szczylik C, et al. Current approaches in identification and isolation of human renal cell carcinoma cancer stem cells. *Stem cell research*. 2015;6(1):1-11.
80. Mowla M, Hashemi A. Functional roles of exosomal miRNAs in multi-drug resistance in cancer chemotherapeutics. *Experimental Molecular Pathology*. 2021;118:104592.
81. Moitra K, Lou H, Dean M. Multidrug efflux pumps and cancer stem cells: insights into multidrug resistance and therapeutic development. *Clinical Pharmacology Therapeutics*. 2011;89(4):491-502.
82. Howley R, Mansi M, Shinde J, Restrepo J, Chen B. Evaluation of aminolevulinic acid-mediated protoporphyrin IX fluorescence and enhancement by ABCG2 inhibitors in renal cell carcinoma cells. *Journal of Photochemistry Photobiology B: Biology*. 2020;211:112017.
83. Hu J, Li J, Yue X, Wang J, Liu J, Sun L, et al. Expression of the cancer stem cell markers ABCG2 and OCT-4 in right-sided colon cancer predicts recurrence and poor outcomes. *Oncotarget*. 2017;8(17):28463.
84. Mizuno T, Fukudo M, Fukuda T, Terada T, Dong M, Kamba T, et al. The effect of ABCG2 genotype on the population pharmacokinetics of sunitinib in patients with renal cell carcinoma. *Therapeutic drug monitoring*. 2014;36(3):310-6.
85. Wang H, Luo F, Zhu Z, Xu Z, Huang X, Ma R, et al. ABCG2 is a potential prognostic marker of overall survival in patients with clear cell renal cell carcinoma. *BMC cancer*. 2017;17:1-7.
86. Lyu C, Wang L, Stadlbauer B, Buchner A, Pohla H. A Pan-Cancer Landscape of ABCG2 across Human Cancers: Friend or Foe? *International Journal of Molecular Sciences*. 2022;23(24):15955.
87. Cybulsky MI, Iiyama K, Li H, Zhu S, Chen M, Iiyama M, et al. A major role for VCAM-1, but not ICAM-1, in early atherosclerosis. *The Journal of clinical investigation*. 2001;107(10):1255-62.
88. Kong D-H, Kim YK, Kim MR, Jang JH, Lee S. Emerging roles of vascular cell adhesion molecule-1 (VCAM-1) in immunological disorders and cancer. *International journal of molecular sciences*. 2018;19(4):1057.
89. Ding Y-B, Chen G-Y, Xia J-G, Zang X-W, Yang H-Y, Yang L. Association of VCAM-1 overexpression with oncogenesis, tumor angiogenesis and metastasis of gastric carcinoma. *World journal of gastroenterology: WJG*. 2003;9(7):1409.
90. Byrne GJ, Ghellal A, Iddon J, Blann AD, Venizelos V, Kumar S, et al. Serum soluble vascular cell adhesion molecule-1: role as a surrogate marker of angiogenesis. *Journal of the national cancer institute*. 2000;92(16):1329-36.
91. Chuang MJ, Sun KH, Tang SJ, Deng MW, Wu YH, Sung JS, et al. Tumor-derived tumor necrosis factor- $\alpha$  promotes progression and epithelial-mesenchymal transition in renal cell carcinoma cells. *Cancer science*. 2008;99(5):905-13.
92. Schlesinger M, Bendas G. Vascular cell adhesion molecule-1 (VCAM-1)—an increasing insight into its role in tumorigenicity and metastasis. *International journal of cancer*. 2015;136(11):2504-14.
93. Wu TC. The role of vascular cell adhesion molecule-1 in tumor immune evasion. *Cancer research*. 2007;67(13):6003-6.
94. De Wolf K, Vermaelen K, De Meerleer G, Lambrecht BN, Ost P. The potential of radiotherapy to enhance the efficacy of renal cell carcinoma therapy. *Oncoimmunology*. 2015;4(10):e1042198.
95. Wuthrich RP. Intercellular adhesion molecules and vascular cell adhesion molecule-1 and the kidney. *Journal of the American Society of Nephrology*. 1992;3(6):1201-11.

96. Zhong L, Simard MJ, Huot J. Endothelial microRNAs regulating the NF- $\kappa$ B pathway and cell adhesion molecules during inflammation. *The FASEB Journal*. 2018;32(8):4070-84.
97. Zhao S, Liang M, Wang Y, Hu J, Zhong Y, Li J, et al. Chrysin suppresses vascular endothelial inflammation via inhibiting the NF- $\kappa$ B signaling pathway. *Journal of Cardiovascular Pharmacology Therapeutics*. 2019;24(3):278-87.
98. Angelo LS, Kurzrock R. Vascular endothelial growth factor and its relationship to inflammatory mediators. *Clinical cancer research*. 2007;13(10):2825-30.
99. Zeng X, Li H, Jiang W, Li Q, Xi Y, Wang X, et al. Phytochemical compositions, health-promoting properties and food applications of crabapples: A review. *Food Chemistry*. 2022:132789.
100. Mohapatra P, Singh P, Singh D, Sahoo S, Sahoo SK. Phytochemical based nanomedicine: a panacea for cancer treatment, present status and future prospective. *OpenNano*. 2022:100055.
101. Zheng Z, Zhang L, Hou X. Potential roles and molecular mechanisms of phytochemicals against cancer. *Food Function*. 2022;13(18):9208-25.
102. Prajapati KS, Gupta S, Kumar S. Targeting breast cancer-derived stem cells by dietary phytochemicals: a strategy for cancer prevention and treatment. *Cancers*. 2022;14(12):2864.
103. Almatroodi SA, Almatroudi A, Khan AA, Alhumaydhi FA, Alsahli MA, Rahmani AH. Potential therapeutic targets of epigallocatechin gallate (EGCG), the most abundant catechin in green tea, and its role in the therapy of various types of cancer. *Molecules*. 2020;25(14):3146.
104. Zhou H, Chen JX, Yang CS, Yang MQ, Deng Y, Wang H. Gene regulation mediated by microRNAs in response to green tea polyphenol EGCG in mouse lung cancer. *BMC genomics*. 2014;15:1-10.
105. Manohar M, Fatima I, Saxena R, Chandra V, Sankhwar PL, Dwivedi A. (-)-Epigallocatechin-3-gallate induces apoptosis in human endometrial adenocarcinoma cells via ROS generation and p38 MAP kinase activation. *The Journal of nutritional biochemistry*. 2013;24(6):940-7.
106. Na H-K, Surh Y-J. Modulation of Nrf2-mediated antioxidant and detoxifying enzyme induction by the green tea polyphenol EGCG. *Food Chemical Toxicology*. 2008;46(4):1271-8.
107. Novilla A, Djamhuri DS, Nurhayati B, Rihibiha DD, Afifah E, Widowati W. Anti-inflammatory properties of oolong tea (*Camellia sinensis*) ethanol extract and epigallocatechin gallate in LPS-induced RAW 264.7 cells. *Asian pacific journal of tropical biomedicine*. 2017;7(11):1005-9.
108. Alam M, Ali S, Ashraf GM, Bilgrami AL, Yadav DK, Hassan MI. Epigallocatechin 3-gallate: From green tea to cancer therapeutics. *Food Chemistry*. 2022:132135.
109. Chen SJ, Yao XD, Peng B, Xu YF, Wang GC, Huang J, et al. Epigallocatechin-3-gallate inhibits migration and invasion of human renal carcinoma cells by downregulating matrix metalloproteinase-2 and matrix metalloproteinase-9. *Experimental therapeutic medicine*. 2016;11(4):1243-8.
110. Carvalho M, Jerónimo C, Valentão P, Andrade PB, Silva BM. Green tea: A promising anticancer agent for renal cell carcinoma. *Food Chemistry*. 2010;122(1):49-54.
111. Kang TH, Lee JH, Song CK, Han HD, Shin BC, Pai SI, et al. Epigallocatechin-3-gallate enhances CD8+ T cell-mediated antitumor immunity induced by DNA vaccination. *Cancer research*. 2007;67(2):802-11.
112. Yongvongsoontorn N, Chung JE, Gao SJ, Bae KH, Yamashita A, Tan M-H, et al. Carrier-enhanced anticancer efficacy of sunitinib-loaded green tea-based micellar nanocomplex beyond tumor-targeted delivery. *Acs Nano*. 2019;13(7):7591-602.
113. Andújar I, Ríos JL, Giner RM, Recio MC. Pharmacological properties of shikonin—a review of literature since 2002. *Planta medica*. 2013;79(18):1685-97.
114. Boulos JC, Rahama M, Hegazy M-EF, Efferth T. Shikonin derivatives for cancer prevention and therapy. *Cancer letters*. 2019;459:248-67.

115. Shilnikova K, Piao MJ, Kang KA, Fernando PDSM, Herath HMUL, Cho SJ, et al. Natural compound Shikonin induces apoptosis and attenuates epithelial to mesenchymal transition in radiation-resistant human colon cancer cells. *Biomolecules Therapeutics*. 2022;30(2):137.
116. Zhang Z, Shen C, Zhou F, Zhang Y. Shikonin potentiates therapeutic efficacy of oxaliplatin through reactive oxygen species-mediated intrinsic apoptosis and endoplasmic reticulum stress in oxaliplatin-resistant colorectal cancer cells. *Drug Development Research*. 2023.
117. Werner M, Lyu C, Stadlbauer B, Schrader I, Buchner A, Stepp H, et al. The role of Shikonin in improving 5-aminolevulinic acid-based photodynamic therapy and chemotherapy on glioblastoma stem cells. *Photodiagnosis Photodynamic Therapy*. 2022;39:102987.
118. Markowitsch SD, Vakhrusheva O, Schupp P, Akele Y, Kitanovic J, Slade KS, et al. Shikonin inhibits cell growth of sunitinib-resistant renal cell carcinoma by activating the necrosome complex and inhibiting the AKT/mTOR signaling pathway. *Cancers*. 2022;14(5):1114.
119. Tsai M-F, Chen S-M, Ong A-Z, Chung Y-H, Chen P-N, Hsieh Y-H, et al. Shikonin induced program cell death through generation of reactive oxygen species in renal cancer cells. *Antioxidants*. 2021;10(11):1831.
120. Salehi B, Venditti A, Sharifi-Rad M, Kręgiel D, Sharifi-Rad J, Durazzo A, et al. The therapeutic potential of apigenin. *International journal of molecular sciences*. 2019;20(6):1305.
121. Shukla S, Gupta S. Apigenin: a promising molecule for cancer prevention. *Pharmaceutical research*. 2010;27:962-78.
122. Yan X, Qi M, Li P, Zhan Y, Shao H. Apigenin in cancer therapy: Anti-cancer effects and mechanisms of action. *Cell bioscience reports*. 2017;7(1):1-16.
123. Shukla S, Fu P, Gupta S. Apigenin induces apoptosis by targeting inhibitor of apoptosis proteins and Ku70–Bax interaction in prostate cancer. *Apoptosis*. 2014;19:883-94.
124. Seo H-S, Jo JK, Ku JM, Choi H-S, Choi YK, Woo J-K, et al. Induction of caspase-dependent extrinsic apoptosis by apigenin through inhibition of signal transducer and activator of transcription 3 (STAT3) signalling in HER2-overexpressing BT-474 breast cancer cells. *Bioscience reports*. 2015;35(6):e00276.
125. Coombs MRP, Harrison ME, Hoskin DW. Apigenin inhibits the inducible expression of programmed death ligand 1 by human and mouse mammary carcinoma cells. *Cancer letters*. 2016;380(2):424-33.
126. Lee Y-M, Lee G, Oh T-I, Kim BM, Shim D-W, Lee K-H, et al. Inhibition of glutamine utilization sensitizes lung cancer cells to apigenin-induced apoptosis resulting from metabolic and oxidative stress. *International journal of oncology*. 2016;48(1):399-408.
127. Dai J, Van Wie PG, Fai LY, Kim D, Wang L, Poyil P, et al. Downregulation of NEDD9 by apigenin suppresses migration, invasion, and metastasis of colorectal cancer cells. *Toxicology applied pharmacology*. 2016;311:106-12.
128. Shukla S, Gupta S. Apigenin-induced cell cycle arrest is mediated by modulation of MAPK, PI3K-Akt, and loss of cyclin D1 associated retinoblastoma dephosphorylation in human prostate cancer cells. *Cell cycle*. 2007;6(9):1102-14.
129. Meng S, Zhu Y, Li J-F, Wang X, Liang Z, Li S-Q, et al. Apigenin inhibits renal cell carcinoma cell proliferation. *Oncotarget*. 2017;8(12):19834.
130. Bao Y, Wu X, Jin X, Kanematsu A, Nojima M, Kakehi Y, et al. Apigenin inhibits renal cell carcinoma cell proliferation through G2/M phase cell cycle arrest. *Oncology Reports*. 2022;47(3):1-7.
131. Li J, Tan G, Cai Y, Liu R, Xiong X, Gu B, et al. A novel Apigenin derivative suppresses renal cell carcinoma via directly inhibiting wild-type and mutant MET. *Biochemical Pharmacology*. 2021;190:114620.
132. Tai MC, Tsang SY, Chang LY, Xue H. Therapeutic potential of wogonin: a naturally occurring flavonoid. *CNS drug reviews*. 2005;11(2):141-50.



133. Gharari Z, Bagheri K, Khodaeiaminjan M, Sharafi A. Potential therapeutic effects and bioavailability of wogonin, the flavone of Baikal skullcap. *J Nutri Med Diet Care*. 2019;5(039).
134. Yeh CH, Yang ML, Lee CY, Yang CP, Li YC, Chen CJ, et al. Wogonin attenuates endotoxin-induced prostaglandin E2 and nitric oxide production via Src-ERK1/2-NFκB pathway in BV-2 microglial cells. *Environmental toxicology*. 2014;29(10):1162-70.
135. Lim BO. Effects of wogonin, wogonoside, and 3, 5, 7, 2', 6'-pentahydroxyflavone on chemical mediator production in peritoneal exudate cells and immunoglobulin E of rat mesenteric lymph node lymphocytes. *Journal of ethnopharmacology*. 2003;84(1):23-9.
136. Gao Z, Huang K, Yang X, Xu H. Free radical scavenging and antioxidant activities of flavonoids extracted from the radix of *Scutellaria baicalensis* Georgi. *Biochimica et Biophysica Acta -General Subjects*. 1999;1472(3):643-50.
137. Feng Q, Wang H, Pang J, Ji L, Han J, Wang Y, et al. Prevention of wogonin on colorectal cancer tumorigenesis by regulating p53 nuclear translocation. *Frontiers in pharmacology*. 2018;9:1356.
138. Huang K, Huang Y, Diao Y. Wogonin induces apoptosis and down-regulates survivin in human breast cancer MCF-7 cells by modulating PI3K-AKT pathway. *International immunopharmacology*. 2012;12(2):334-41.
139. Yu JS, Kim AK. Wogonin induces apoptosis by activation of ERK and p38 MAPKs signaling pathways and generation of reactive oxygen species in human breast cancer cells. *Molecules cells*. 2011;31:327-35.
140. Wang W, Guo Q-L, You Q-D, Zhang K, Yang Y, Yu J, et al. The anticancer activities of wogonin in murine sarcoma S180 both in vitro and in vivo. *Biological Pharmaceutical Bulletin*. 2006;29(6):1132-7.
141. Parajuli P, Joshee N, Rimando AM, Mittal S, Yadav AK. In vitro antitumor mechanisms of various *Scutellaria* extracts and constituent flavonoids. *Planta medica*. 2009;75(01):41-8.
142. Dandawate S, Williams L, Joshee N, Rimando AM, Mittal S, Thakur A, et al. *Scutellaria* extract and wogonin inhibit tumor-mediated induction of T reg cells via inhibition of TGF-β1 activity. *Cancer Immunology, Immunotherapy*. 2012;61:701-11.
143. Wang Y, Chen S, Sun S, Liu G, Chen L, Xia Y, et al. Wogonin induces apoptosis and reverses sunitinib resistance of renal cell carcinoma cells via inhibiting CDK4-RB pathway. *Frontiers in Pharmacology*. 2020;11:1152.

## Acknowledgements

I would like to take this opportunity to express my heartfelt gratitude to the individuals who have contributed to the successful completion of my doctoral study and thesis.

First and foremost, I am immensely grateful to PD Dr. Heike Pohla, my supervisor, for offering me the opportunity to work in her lab. She did not only provide me with valuable academic guidance and research experience, but also extended her support in my personal life. The friendly atmosphere in our group made my time in the lab enjoyable and comfortable. Her patience and meticulousness in reviewing my papers, reports, and other documents were deeply appreciated. Then, I would also like to thank Prof. Dr. Alexander Buchner, my co-supervisor, for his exceptional support and guidance throughout my research work, particularly in the field of statistics. His patience and kindness in assisting me with daily life issues and computer problems were greatly appreciated. Moreover, I would like to extend my gratitude to Prof. Dr. Elfriede Nössner, one of my TAC members, for granting me the opportunity to complete my doctoral degree. Lastly, I am grateful to Birgit Stadlbauer for her kindness and assistance during my work. She taught me a lot about my research and served as an excellent role model in both life and work. Her impeccable experiment records were truly inspiring, and I deeply respect her work ethic.

Furthermore, I would like to thank my teammate - Lili Wang. Working with you has been an incredible experience, and I will miss our teamwork dearly. Also, I appreciate the help of the other members in our institute: Sarah Hubschneider, Isabel Schrader, Maxim Werner, Linglin Zhang, Lei Shi, Yuhan Liu, Bingsheng Li, Ru Huang, Sheng Hu, Siwei Qian, Maximilian Christian Aumiller, Christian Heckl, Max Eisel, Prof. Dr. Ronald Sroka, Prof. em. Wolfgang Zimmermann and everyone who helped me during my stay in Munich. Their kindness and support meant a lot to me, and I am grateful to have had the opportunity to work with such amazing people.

During my study in Munich, I have had the opportunity to live through many unique experiences. I have witnessed ER doctors rushing to me late at night and cannot forget the warmth of blankets to prepare for in sight. So, I want to express my gratitude to the people, who help me through these experiences: Wenyue Li, Qingyan Wu, and PD Dr. Kong Bo. Most importantly, a huge thank you to Dr. Dingyi Yang. Without your accompany, I am not sure I would have made it through those challenging moments.

Finally, I would like to express my heartfelt appreciation to my parents for their unwavering support and understanding of my academic pursuits. I am also grateful to the China Scholarship Council (CSC) for their financial support, which has enabled me to pursue my studies, work at the Ludwig-Maximilians-Universität (LMU), and explore the world.